Reply to Referee 1

Comments on

> From climatological to small scale applications: Simulating water isotopologues with ICON-ART-Iso (version 2.1)

Under revision at Geosci. Model Dev. Discuss., https://doi.org/10.5194/gmd-2017-280

Dear referee,

thank you for taking the time to review the manuscript. Your exact reading and recalculation of the microphysics algebra have greatly improved the model and subsequently also the manuscript. The physics have been corrected and as a consequence, we redid all the simulations. After analyzing the results of the parameterization by Blossey, we decided to no longer compare the two parameterizations in the current manuscript. This is the biggest change to our original submission.

Below, you will find a point by point reply to all your comments. We have attached a manuscript highlighting all the differences between the original and the current version of the manuscript. This includes the changes from all three referees. For completeness, we have also attached the updated version of the manuscript.

On behalf of all coauthors,

Johannes Eckstein

Major comment:

1.

> *Why perform the sensitivity study on the parameterizations for isotopic exchange during evaporation from rain on water vapor in the upper troposphere? Also, since rain evaporation predominantly happens in the lower troposphere, I would argue that this sensitivity study be performed either for precipitation or for near-surface/lower-tropospheric vapor. Since rain evaporation is a non-equilibrium process, I would expect differing parameterizations to have the strongest impact on deuterium excess rather than deltaD or delta18O.*
>
> *In this paper, measurements of deuterium excess are only available for the GNIP data, so that this would argue for the evaporation test to be applied on that data. Alternately, a recent dataset of isoptopic measurements in water vapor (Benetti et al, 2017, Scientific Data, https://doi.org/10.1038/sdata.2016.128) might provide a reasonable constraint on isotopic values over the ocean surface. I would suggest that the authors try out the evaporation scheme sensitivity study for the GNIP data and possibly also for this vapor dataset (perhaps using climatological monthly values for the appropriate locations). If they help differentiate between the performance of the two evaporation parameterizations, I would suggest that the CARIBIC comparison only apply to the standard model and the evaporation test applied to lower-tropospheric vapor or precipitation.*
>
> As stated above, we no longer compare the two parameterizations in the manuscript. After analyzing results of the decadal simulation in comparison with the GNIP dataset, we decided that a discussion of the results would inflate the manuscript. Instead, we now focus solely on the parameterization by Stewart. The implementation of the parameterization by Blossey is noted and the physics are compared in a short appendix. The comparison in terms of results is postponed to a future study.

Minor comments:

2/30:

I think that this statement should be qualified as "isotopologue enabled _global_models", since COSMOiso (Pfahl et al, 2012) and SAM (Blossey et al, 2010) are non-hydrostatic.

As suggested, we have included “global”.

3/15-20:

Might it be useful to specify a few sample grid resolutions here for the different applications of ICON?

Following your suggestion, we now state the resolution of DWD’s operational forecast. The paragraph now ends with:
“At DWD, ICON is used operationally for global numerical weather prediction (currently 13 km horizontal resolution, with a nest of 6.5 km resolution), it already proved successful as a Large Eddy Simulation (LES) model (Heinze et al., 2017), and is currently prepared for climate prediction studies at MPI-M. More details on ICON are given by Zängl et al. (2015).”

5/eqn 2:

I find the choice of alpha_eq < 1 to be surprising, but if this is carried consistently throughout the code, I suppose it fine. If one looks at Majoube (1971), for example, one finds log(alpha_18O) = 1.137e3/T^2 - 0.4156/T - 2.0667e-3, which if my computations are correct yields 0.0117. This suggests alpha itself is greater than one.

Still, as I said, if this interpretation of alpha is applied consistently through the code, that seems okay, but be careful to comment things well so that the next coder who is accustomed to alpha > 1 is not confused. I would suggest that the variable might be renamed to something other than alpha to avoid confusion in the future. Checking these equations against those in Blossey and Stewart required a lot of careful attention, with the alpha switching meaning between those papers and this one.

We admit that your concern is justified. The definition of alpha was taken over from the code of COSMOiso. It is consistently used this way in the code and we therefore decided to also use it this way in the manuscript.

6/eqn 6:

First, I am a bit worried by equation 6 with the saturation vapor deficit in the denominator since this will go to zero in the cloud Of course, the evaporation rate of the standard isotope will also go to zero, but careful coding is required when dividing small numbers by similarly small numbers.

Secondly, this equation seems to shut off isotopic exchange between rain and vapor in saturated conditions. This doesn’t seem to happen in COSMOiso as described by Pfahl et al (2012, equations 4-5). Perhaps, the implementation in ICON preserves isotopic exchange in saturated conditions. If so, this should be mentioned in the text.

Thank you for the exact reading of the manuscript and for making this point! The way we had previously implemented the model equations, isotopic exchange was only happening at subsaturated conditions. Fixing this mistake in the code was one of the corrections which required us to redo all simulations.

6/eqn 7:

While this expression seems consistent with equation 7 from Blossey et al, the denominator is needlessly obscure. The quantity in parenthesis in the denominator can be written as (1 + b_l)/ (ˆlD\rho_{l,\infty}ˆ). I would advocate putting the (1+b_l) in the denominator and putting the ˆlD next to the f and the \rho_{l,\infty}ˆ* at the end.*

Also, my impression from looking at both Stewart and Blossey is that they are working from the same basic equations. I'm guessing that if the formula for ˆl S_xˆ{evap} were plugged into equation 6, something very close to equation 7 would emerge, though with the (hD/lD)ˆn in place of the combination of the diffusivity ratio and ventilation factor ratio. There is probably a way of writing these two equations so that they are easy to compare by eye and don't require a lot of algebra. Last, note that alpha>1 in equation 7 and alpha<1 in equation 6, unless my algebra was wrong.

Thank you for redoing the algebra. Following your suggestions, we have reformulated the two equations so that they can now be compared easily, which we show in the new appendix B. In addition, we have corrected alpha in the equation for Blossey et al. The reformulated equations now also show that they both turn into the same equation for standard water if the standard water variables are inserted instead of the heavy water variables. The equation resulting from this replacement and the subsequent simplifications is identical to the one used in the microphysical scheme of ICON. Note that we now present the comparison of the two equations in App. B and no longer in the main body text since we also do not discuss results of the parameterization by Blossey.

7/eqn 10:

*Shouldn't that be ˆlf/ˆhf in the denominator? Maybe eta could be defined as the product of the diffusivity and ventilation factor ratios: (ˆhD/ˆlD) * (ˆhf/ˆlf) to simplify this formula and also equation 7.*

We have also corrected this mistake. It was only a typographical error in the manuscript.

8/6-7:

Could the sentence "Evaporation of precipitation ..." be rephrased? The effects of evaporation on buoyancy and the resulting cold pools is certainly important, but it is important for other reasons as well. Thinking of isotopic applications, Risi et al (2008, JGR, doi:10.1029/2008JD009943) suggest that the recycling to vapor from downdrafts into the boundary layer could play a role in the amount effect. As this vapor is affected by rain evaporation and re-equilibration in the downdraft, evaporation could be an important process for this isotopic application as well.

As suggested, the sentence has been changed to:
"Evaporation of precipitation below cloud base is an important process for several reasons: it leads to a drop in the temperature and therefore influences dynamics, but is also important for the isotopic composition (Risi et al., 2008)."

9/sec 3:

Are these simulations free-running or are they nudged to reanalysis fields (wind, temperature, surface pressure) to preserve the "observed" meteorology? It's worth making this clear, because isotope-enabled global models are often run in nudged configurations to produce a sort of isotope reanalysis (e.g., Steen-Larsen et al, 2017, JGR, http://dx.doi.org/10.1002/2016JD025443).

We now clearly state this at the end of the first paragraph: "All simulations discussed here are free-running."

13/fig 2:

I realize that Vienna is the home of the IAEA, but does it really provide much information that isn't in the Karlsruhe plot? Is it worth having both here when they're so similar? Removing one location might enable the panels to be larger and more readable, which seems desirable.

To account for a comment by Referee 3, we have decided to stick with 5 stations, but now include Bangkok as a tropical station instead of Karlsruhe.

14/25:

I think that the threshold for cloud-affected grid points should perhaps be set much lower. I would advocate for 50% at most and think of 10% as a better characterization of the almost-cloud-free conditions that would be ideal for a IASI retrieval.

The variable used for cloud cover in ICON is very strict in the sense that 100% are reached quickly. This is why 90% percent is a reasonable threshold.

16/19:

Suggested re-wording "This _may be_ partly due to evaporation of rain drops ...". There could be other things contributing to these changes in the 4-6km layer where IASI is most sensitive, so that I would suggest less certainty here. I think of rain evaporation as being most prominent below cloud base, less so in the mid-troposphere, though I am happy to be corrected on this.

As suggested, we have included the "may".

Typographic suggestions:

1/6: *"... measurements _of_ precipitation …"*

As suggested, we have changed “...measurements in precipitation…” to “...measurements of precipitation…”

1/12: *"... as well as _that of all_ tropical data …"*

Included “that of” as suggested.

2/1: *"It is the strongest green house gas (...) _and_ distributes energy through the release of latent (...), while liquid and frozen particles influence the radiative balance (...)." I don’t think "to name only three ..." is needed.*

As suggested, the sentence now reads:
“It is the strongest green house gas (Schmidt et al., 2010) and distributes energy through the release of latent heat (Holton and Hakim, 2013), while liquid and frozen particles influence the radiative balance (Shine and Sinha, 1991).”

2/13-15: *Possible rephrasing: "Measurements of the isotopic content of vapor first required cryogenic samplers (Dansgaard, ...), but in the last 15 years laser absorption spectroscopy has made in situ measurements possible (citations)."*

We have changed the sentence according to your suggestion.

6/6: *"ilead" —> "lead"*

corrected as suggested

9/2: *"presents"*

The paragraph now starts with “In the following sections, we present first results and comparisons of model simulations...”

9/19: *comma before "respectively".*

Corrected as suggested

10/2: *Remove "timestep" after "convection". It’s unnecessary.*

The paragraph has been removed due to restructuring the manuscript.

10/15: *Try to avoid starting a sentence with a symbol when possible. Suggested rephrasing: "Two months after initialization, q_{init} …"*

The sentence has been removed due to restructuring the manuscript.

10/24: *"... importance of this parameterization in the _simulations at this resolution._" In other simulations with the same model or at other resolutions, this parameterization might not have the same role.*

Similar to your suggestion, the paragraph now ends with:
“Still, it should be considered that the amount of precipitation from convection only shows the importance of this parameterization in the simulations at this resolution. At other resolutions, the parameterization might not have the same role.”

10/25: *To make this flow better, suggested rephrasing: "The situation is different in northern hemisphere summer (...). Land areas in the northern hemisphere (bottom right) themselves supply a substantial fraction …"*

The paragraph has been restructured and now starts with:
“During northern hemisphere winter over the ocean (top left panel of Fig. 1), the precipitation is strongly dominated by water that has evaporated from the ocean. Water from the land surface hardly reaches the ocean.”

12/11: *Move d-excess definition here: "... and d-excess (= deltaD - 8 delta18O) in precipitation." and remove the sentence on lines 13-14.*

changed as suggested

14/2: *"in approximately" –> "at a height of approximately"*

corrected as suggested

20/20: *"Thirty output files ..." At the start of a sentence, spell out the number (or rephrase to avoid having it at the start).*

This sentence has been removed as we now use the decadal simulation to generate the dataset.

21/1: *"... from each file, and 200 ..." This is a compound sentence, so that there should be a comma before the "and".*

This sentence has been removed as we now use the decadal simulation to generate this dataset

21/2: *"to consider" –> "corresponding to"*

The paragraph has been removed as we now use the decadal simulation.

21/2-3: *"The resulting probability distributions are shown in the right panels of Fig. 7 (...) together with the samples along the paths of flights 309-310." I think this is more clear for the reader.*

This paragraph has been removed as we now use the decadal simulation.

24/24: *"proofs" –> "proves"*

corrected as suggested

Reply to Referee 2

Comments on

> From climatological to small scale applications: Simulating water isotopologues with ICON-ART-Iso (version 2.1)

Under revision at Geosci. Model Dev. Discuss., https://doi.org/10.5194/gmd-2017-280

Dear referee,

thank you for taking the time to review the manuscript. Your exact reading and especially the literature you have suggested have greatly improved the manuscript.

Below, you will find a point by point reply to all your comments. We have attached a manuscript highlighting all the differences between the original and the current version of the manuscript. This includes the changes from all three referees. For completeness, we have also attached the updated version of the manuscript.

On behalf of all coauthors,

Johannes Eckstein

Minor comments:

p2 l 1:

> *isotope-enabled*
>
> Following your suggestion, all occurrences of “isotope enabled” have been replaced by “isotope-enabled”.

p2 l 19:

> *It’s awkward here to contrast “climatological questions“ and “process understanding”. Climatological questions can be answered through process understanding. In addition, limited area models are not the only tool to understand processes, global models can also be used for this purpose. Reformulate, by highlighting rather the differences in spatial scales or in convective representation.*
>
> Following your suggestion, we have reformulated the sentence. It now reads:
> “Many global and regional circulation models have been equipped to simulate the atmospheric isotopologue distribution, focusing on the global scale (Risi et al., 2010; Werner et al., 2011) or regional phenomena (Blossey et al., 2010; Pfahl et al., 2012, both limited area models).”

p 3 l1:

> *“precipitation diagnostics” is mysterious here -> precipitation source regions?*
>
> As suggested, the sentence now reads “Section 3.1 looks at precipitation source regions.”.

p 3 l 19:

“climate prediction” -> “climate projections? It’s impossible to predict climate for the end of the century. In case you refer to studies at the decadal scale, climate predictability is more appropriate.

As suggested, we have changed “climate prediction studies” to “climate projections”.

p 4 l 15:

guarantee

corrected

p4 l 17:

syntax problem

Corrected: “The parameterizations which influence the water cycle also include processes that do not fractionate.”

p 5 l 21:

No, Risi et al 2010 and Werner et al 2011 did not use such a simple assumption. In stand-alone mode, both LMDZ and ECHAM models use a bucket model that collects the precipitation to represent the soil reservoir. To my knowledge, you are the first to make such a simple assumption. It’s not a problem but it should be mentionned.

Thank you for pointing this out. We have removed the sentence and restructured the paragraph, as we now use the dataset by LeGrande and Schmidt (2006) over the ocean surface.

p 8 l 5:

For the liquid fraction, does it mean that you assume that all drops are sufficiently small to equilibrate totally? If so, it’s not a problem but it should be mentionned that this is a simplifying assumption compared to offline models of rain-vapor exchanges in saturated environment (e.g. Stewart (1975); Lee and Fung (2008) calculate the equilibration as a function of the drop size) or to GCM parameterizations (e.g. Hoffmann et al. (1998) assume that only a proportion of the drops equilibrate in a saturated environment depending on the precipitation type).

Thank you for asking to clarify this point. All drops equilibrate equally. In the case of saturated downdrafts, total equilibration is assumed, but below the cloud base the parameterization follows Stewart (1975), similar to other models mentioned by your comment.

p 8 l 30:

How do you initialize water vapor composition at the model bottom and top? Interpolation needs these end members in addition to the tropopause values.

These values are given in Table 1 and a reference to these values is included in the text.

p 9 l 9-14:

Why is this paragraph here and not in the Methods section?

It is not in the methods section because these are choices made at runtime and explicitly for these simulations. We have changed the introduction to the paragraph to make this more clear. We also spend more text explaining this in the introduction to the model (Sec. 2.1)

p 10 l 12:

remove one "almost completely"

Since we now use the decadal simulation and one year spin-up time, we have removed both "almost completely".

p 10, section 3.1:

Previous studies using water tagging in models or water tracking tools should be cited and their results could be briefly compared to yours: e.g. Joussaume et al. (1984); Koster et al. (1986); Numaguti (1999); Yoshimura et al. (2004); van der Ent et al. (2010); Gimeno et al. (2012); Risi et al. (2013)

Thank you for pointing out this literature. As suggested, we now cite four of these studies and compare the results to those of our paragraph.

p 18 l 13-18:

but this does not improve the model-observations agreement…

As measurements do not differentiate between vapor originating from land and ocean surfaces, our goal is not to improve the agreement between model results and measurements. The aim is to point out how the different tracers which are made available by ICON-ART-Iso can be combined for in-depth analysis of the results.

p 18:

Can the lack of daily cycle be related to the wrong precipitation daily cycle, a known problem in many models (Betts and Jakob (2002); Guichard et al. (2004))?

Thank you for pointing us at this idea. We have not followed up on it for the current manuscript, but may look at the daily cycle in precipitation in a future study.

p 20 l 9:

How is this "sample" chosen?

We now use the decadal simulation, which we sample along the paths of all those IAGOS-CARIBIC flights which took measurements of δD.

p 21 l 22:

What explains the δD difference between these 2 parameterizations? Explain with simple physics what process is the main driver of this change. In addition, I understand that these 2 parameterizations differ for the representation of isotopic processes during rain evaporation, which occurs in the lower troposphere. Why does it have such a big impact in the upper troposphere?

The difference between the two parameterizations is now discussed in App. B. Following comments by Referee 1, we revised part of the microphysics code in the model and redid all simulations. After reexamining the results with the revised model version, we decided to postpone the comparison of the two parameterizations to a later study in order to keep the paper concise.

p 22 fig 7.

A few explanations on these distributions could be useful. For example, do you see the signature of condensate lofting/detrainement? In the upper tropospere, these processes are known to have a big impact on the isotopic composition (Moyer et al. (1996); Kuang et al. (2003); Bony et al. (2008); Sayres et al. (2010)). This could be discussed.

A focused study is required to look into the details of these distributions. The investigation of ice lofting is one subject which could surely be addressed by use of these in situ data. It will be an interesting future study to investigate this with ICON-ART-Iso.

p 23 l 9:

This is very vague: how can different processes be identified from a scatter? Be more precise.

Agreed, it is probably impossible to read processes from one scatter plot alone. We have therefore removed the sentence and recombined the last two paragraphs of the section.

p 23 l 10:

remove "of"

corrected

Overall section 3.4.2 and previous sections:

Be more quantitative when describing the model-observations agreement. Use quantitative metrics such as RMS error. This would allow to compare quantatively the model-observations agreement between different model version, different regions and seasons, different sampling criteria... It's difficult to assess the model-observations agreement by comparing by eye 2 different plots.

Thank you for pointing this out clearly. We have included some numbers of mean values and offsets. In some cases, we also give relative differences.

p 23 l 5-8:

Is the model-observations agreement better when removing these parcels with high proportion of initialization tracer?

The main source for differences between model and measurements is the fact that the model is free-running. Removing the values with high proportion of initialization water therefore does not improve the agreement between model and measurements.

p 24 22:

“discuss” -> show: you don’t discuss the reasons for these differences.

This paragraph has been changed, since we now also show these differences in the comparison of model results with the GNIP database.

p 24 l 32:

“instances” -> use a more appropriate word?

The word “instances” has been replaced by “tracers corresponding to”.

Reply to Referee 3

Comments on

> From climatological to small scale applications: Simulating water isotopologues with ICON-ART-Iso (version 2.1)

Under revision at Geosci. Model Dev. Discuss., https://doi.org/10.5194/gmd-2017-280

Dear referee,

thank you for taking the time to review the manuscript. Your critical reading and the comments have made the text much more precise in many aspects. As proposed, we now include the dataset by LeGrande and Schmitt (2006) to prescribe the surface isotope ratio of the ocean.

Below, you will find a point by point reply to all your comments. We have attached a manuscript highlighting all the differences between the original and the updated version of the manuscript. This includes the changes from all three referees. For completeness, we have also attached the updated version of the manuscript.

On behalf of all coauthors,

Johannes Eckstein

Major comments:

Section 2.3:

> *There are two serious flaws in Section 2.3 that have to be corrected for to achieve a state-of-the-art water isotope enabled GCM:*
>
> *The authors are mistaken when they think that R_{surf} is approximated by R_{VSMOW} in Werner et al., 2011. In ECHAM5-wiso, the surface reservoirs soil, skin, snow and plant layer are filled by precipitation and form R_{surf}, which is then used for evaporation processes from the surface. Only fine processes like isotope fractionation during evapotranspiration are neglected. Using R_{VSMOW} for the entire surface is a step backwards in global water isotope modelling.*
>
> Thank you for clarifying this point about ECHAM5-wiso. The fact that we use this approximation of R_{surf} is surely a big deficiency of the model. There are plans to implement water isotopologues into the surface module of ICON, but this is out of scope for this paper. In our analysis, we focus on comparisons using measurements taken over the ocean, which are less influenced by land surface evaporation. In addition, we often consider the evaporation tracers, which allow us to investigate the influence of land surface evaporation.

> *Also as a lower boundary condition for the ocean, this is not a state-of-the-art approximation and it is not done this way in recent models. Instead, a global gridded data set based on the 18O isotopic composition in sea water by LeGrande and Schmidt, 2006 (see attached figure) is taken e.g. in Werner et al., 2011. HDO in the ocean surface layer can be approximated from this.*
>
> We have implemented the possibility to use this dataset for the isotope ratio of the ocean surface. Comments by referee 1 required us to change other parts of the code and to redo all simulations. For these simulations, we now use the proposed dataset to prescribe the ocean surface isotope ratios.

P6L5-6:

Wrong. In fact, during freezing of water isotopic effects occur in a closed systems (Souchez and Jouzel, 1984) and there is even evidence of a kinetic effect (Souchez et al. 2000), but due to the comparably low diffusivities in liquid water these effects can be neglected in cloud processes in GCMs. This has to be mentioned somewhere, such inaccuracies should not make their way into scientific literature.

Thank you for clarifying this point. We have included it in the manuscript and cite the corresponding literature.

Fig. 2 and Sect.3.2:

You forgot to include a station in the tropics. Other processes (amount effect,...) become important here that have to be evaluated.

Thank you for emphasizing this point. We have replaced Karlsruhe with Bangkok (13°N) to include a tropical station.

The simulation setup and the initialization procedure is not suitable for the given goal of the study. To have a one-to-one comparison of water isotopologues in model results and observations a free running simulation with such short spin-up from such a crude initialisation is not applicable, but let me make these points one by one:

Since your aim is to evaluate your representation of water isotopologues (including the water cycle processes as well as fractionation effects) in the model and not the model meteorology, you first have to compare a nudged (specified dynamics) simulation. Otherwise you will never be able to separate the effects of an unequal meteorological situation with the water and isotope effects. And that is what you need to do in the first step, because only then you can really assess your water isotope implementation. Or the other way around, your evaluation is pointless with the used simulation.

We are evaluating the water cycle of the non-hydrostatic model ICON. For this purpose, a free-running simulation is just as valuable as a nudged model run, while the focus may be slightly different in each case. In several previous studies, the validation of isotope implenetations has been done with a free-running simulation (e.g. Noone and Simmonds, 2002; Schmidt et al., 2005; Werner et al., 2011). In our free-running simulation, it is of value to see that the different seasonalities of the istopic composition of precipitation are well reproduced, just like they are in temperature.

On top of this, we investigate the statistical distributions of the isotopes. By showing how the model reproduces also these values, we are able to validate general aspects of the isotope implementation. Of course there are discrepancies that remain, but it will be the subject of future studies to investigate these and to improve the model.

Because of the explicit convection, non-hydrostatic models are generally more difficult to nudge than their hydrostatic predecessors. This is due to convective fluxes on the model grid, which are difficult to consider in the nudging process.

Taking these points into account, we are sure that the investigation with a free-running simulation is worth to be considered. In addition, we consider these results to be an important prerequisite for future studies with the model, the main reason for presenting the investigation in the manuscript.

In particular with such a crude initialization of HDO, you need longer spin-up time, maybe a month or more. Then you will not face problems like in P21L31, so why not just do it? However, probably already the HDO field of your first simulation could serve as a (somewhat better) initialisation field for your second simulation.

We now use a full year as spin-up time for the decadal simulation. The simulation ran from January 2007 to the end of 2017. By using the first of these eleven years as spin-up time, we still have a full decade to create the climatologies.

The section comparing CARIBIC measurements to the ICON-ART-Iso results uses a free running forecast of the model while attempting to reproduce the approximate meteorological situation at the time of two flights. Therefore, the simulation cannot be initialized with the meteorology of the decadal simulation. The influence of the initialization is discussed in this chapter by making use of the initialization water tracer.

Section 3.4:

As mentioned above, the section on the comparison with CARIBIC data should be comprehensively restructured. Comparisons should be made point by point and clear conclusions should be drawn and presented out of that.

In the updated manuscript, we have enriched this section by including several mean values and offsets of the different distributions to one another. We hope this makes the chapter more valuable.

This brings me to my next point. The authors correctly write, that water isotope modelling is applied to answer climatological questions and (this should be ”and“ not ”or“ on page 2, see other REF) process understanding. This usually means the simulation of a particular phenomenon for in-depth analysis with the additional information from the water isotopes. Here, the authors are using the tool in a weather prediction setup, but they never clarify why they chose this configuration, i.e. how one could profit from this sort of ”weather model setup“. Or in other words, what advantages does this setup have over the application of the isotopes in a regular climate model configuration.

ICON can be used for climate simulations as well as for weather prediction, the difference being only a matter of simulation time and output processing. For users of the model, there is no fundamental difference and the advantages you mention for the use of the isotopes in a climate model also apply for the weather model setup. Only that the capabilities of ICON are not limited to these application, but may well be applied to questions regarding shorter times scales and local phenomena, as we demonstrate in the later chapters of the manuscript. In addition, using the numerical weather prediction physics package provides us with the microphysical scheme by Seifert and Beheng (2006), which is well suited for case studies like the one we present in Sec. 3.4.

Section 3.2:

The concept of the tagged water tool is simple and it has been developed many times before (which the authors do not even mention), see REF#2.

We now cite several of the studies suggested by referee 2 and compare the results to ours.

Thus, the concept itself does not require another reference in GMD. The process studies that are conducted with it in this paper do not provide any new insights into the hydrological cycle. Plus, there is only little connection of it to the actual topic of the paper, the only real connection is that one can approximate the spin-up time with the approach. This, however, the authors will not need anymore if they consider my point on the simulation setup (which is crucial for the evaluation and thus for the entire paper). Hence, this part of the study dangles somewhere in the nowhere here and should thus be removed completely from the paper.

We now use the decadal R2B04 simulation for this investigation. We consider climatological summer (June, July, August) and winter months (December, January, February). The results therefore well complement the influence of ocean and land surface evaporation presented in the section comparing GNIP measurements to the model results. Thank you for motivating us on this point to more closely reconnect the section to the paper!

Even in a nudged simulation, a spin-up time is needed by the model to generate consistent isotope ratios. As described above, we believe this study to be an important prerequisite for future investigations, although the conclusions may be different than those drawn from a nudged simulation.

Minor comments:

P1L6:

This sentence needs to be rephrased, it is incorrect english and it is not clear how this shall represent a range of temporal scales.

The sentence now reads: “The model is then evaluated on a range of temporal scales by comparing with measurements of precipitation and vapor.”.

P2L7-9:

This sentence is grammatically wrong (dangling participle).

The sentence now reads: “Considering the isotopologue ratio of the heavy isotopologues in vapor and precipitation (liquid or ice) provides an opportunity to develop an advanced understanding of the processes that shape the water cycle.”

P2L26 and elsewhere:

Cauquoin and Risi, 2017 has been rejected by GMD. You may want to find another citation for this.

Thank you for pointing this out. We have removed the citation.

P2L31:

Most (if not all) models can be run with a fine horizontal resolution. How does the ICON model "stand out" from other models with respect to this?

It is not the fact that the resolution can be increased which makes ICON and ICON-ART-Iso stand out, but the fact that it is a global, isotope-enabled model with a non-hydrostatic core. In addition, the numerical implementation makes it very efficient on modern computing systems. The ART modules – a fully integrated part of the ICON model – provide a flexible tracer infrastructure, which is used in ICON-ART-Iso to build a flexible isotope model. These are the characteristics that make ICON-ART-Iso stand out from other isotope-enabled circulation models and assure its long time use in the scientific community. We hope to have made this more clear in the updated version of the manuscript.

P2L32:

You use the word "flexible" here and also later on in the paper, and I think the word is being misused here. A model is not flexible when you can implement a lot of diagnostics, or run several water tracers at once. Basically you can do that with every model. Flexibility would be for example when you can easily switch these diagnostics and tracers on and off or change their attributes without having to recompile. Or being able to expand the model system such that you have several co-existing processes (e.g. convection schemes) that can be run with the same executable. I am not aware if this is possible in ICON-ART-Iso, if so you could describe it and use the word flexible, if not, you should rather use the word comprehensive or extensive.

Thank you for pointing out that this is not stated clearly enough in the manuscript. Since the isotopes are a diagnostic of the water cycle in the model, it is not possible to run several convection schemes in the same simulation. But your first point is exactly what we mean by flexible: Without recompiling, we can switch between different parameterizations, run several parameterizations for fractionation at the same time for different isotopes and even use different parameters for different isotopes that use the same parameterization. This concept is similar to what has been implemented for ICON-ART for chemical tracers and is explained by Schröter et al., 2018. We hope to have made this more clear in Sec. 2.1.

P2L32:

You mention "diagnostic moisture tracers" and "tagged water" here, but at this stage the reader has no idea what you actually mean with that. Either explain it shortly, or wait until it comes to the point.

The sentence now reads: "It is flexible in design to simulate diagnostic evaporation tracers as well as the isotopologues HDO and H218O during a single simulation."

P3L2 and L6 and throughout the manuscript:

A section does not compare or discuss anything. These formulations make no sense, instead you compare it in the section. So use e.g.: In this section, we discuss.…

Thank you for making this point, we have changed the text accordingly.

P3L26:

And why is this a very good assumption? Because the abundance of standard water is at least three orders of magnitude higher than the abundance of any rare isotopologue. Why not include this in the text?

We now give the values.

P3L27-29:

Rephrase: ...seven different forms (vapor, cloud water, ...), each of which is represented by one tracer for standard water and one tracer for the isotopologues HDO and H182O, respectively.

We have taken up your suggestion and moved the list into brackets.

P4L1:

What settings?

We have expanded the paragraph to make more clear what we mean by settings, also see our answer to comment on P2L32.

P4L21-22:

Sentence is unclear, rephrase.

We have rephrased the sentence. It now states: “In order to turn one of the fractionating processes explained below into a non-fractionating process, its respective equation for the transfer rate of the heavy isotopologues can be replaced with Eq. 1. This has been implemented as an option in all processes that describe fractionation.”

P8L23-24:

At this stage, it is totally unclear where the simulation of ”tagged water“ is supposed to aim at, so this sentence is rather confusing.

We have removed this part of the sentence.

P8L30 and throughout the manuscript:

To avoid ambiguity, the δ should be complemented by the isotope, the molecule and if relevant also by the phase, such as: δD(H 2 O ice).

As is common when dealing with the heavy isotopes of water, all delta values are taken relative to H2O. We state this in Sec. 2.1 and now also specify that we always calculate it in the vapor phase (except in Sec. 3.2, where we make a statement about this).

Sect. 2.7:

The text never says that you are using HDO measurments here (only in the table caption), that makes the read unnecessarily confusing

The sentence now reads “Values for the tropopause level and the model top are taken from MIPAS measurements (Steinwagner et al., 2007), the value at the lowest level is a standard value taken from Gat (2010).”, making clear that we use measurements.

P9L15-20:

This paragraph leaves unclear what this is supposed to be good for, why do you do that?

The initialization water allows us to see the influence of the initialization on the distribution of water vapor. Similarly, the ocean and land evaporation water tracers allow to investigate the influence the ocean and land surface each have on the distribution of vapor at a certain point of the simulation. We now state in the paragraph:
“Next to case studies, this is interesting because of the undercomplexity of the evaporation from land surfaces, see Sec. 2.3. The tracers of q^{init} hold information of the importance of the initialization at a certain time in the simulation.”

P9L22:

Please rephrase, the sentence is unclear. Also, why are you doing that?

As explained above, we now use the decadal R2B04 simulation also used to compare to GNIP measurements for this investigation. In addition, we do not use single months but we compare mean winter (December, January, February) and mean summer (June, July, August) values of ten years simulation.

Fig. 1:

Give panels a,b,c,d,e,f and change text accordingly

We have refrained from using panel numbers here as the panel title is clear enough.

P12L4:

73h is a very coarse output time step. Why so coarse? That makes only 10 steps a month, I think that is too weak if you want a robust climatology.

In the simulation now used for the investigation, we have reduced the output time step to 10 hours.

P12L5:

Why 91.25? Magic number?

This number came from not considering the first 30 output fields, which were 73 hours apart. This makes a total of 2190 hours or 91.25 days of spin-up time. In the evaluation of the new simulation, we use a full year as spin-up.

P12L12-13:

Shortly explain why you do that.

The additional evaporation tracers allow a deeper insight into the water cycle by showing the importance of land and ocean surface evaporation for each station in each month.

P12L27-32:

The temperature bias should have a large impact on the isotope ratios. That does not always seem to be the case, see .e.g. Ankara. How come?

There is surely a relationship between the surface (2m) temperature and the isotope ratios in precipitation. But there are also many other factors that strongly influence this ratio. The isotope ratio in precipitation is the result of all processes that lead to the formation of this precipitating water. To disentangle what influence the surface temperature has on these ratios is beyond the scope of this paper, but it will surely be considered in future studies.

In the depiction it is hardly possible to see how far the values are off, the vertical axes are too coarse.

Thank you for pointing this out. We have changed the vertical axes, synchronizing now for all stations but Halley Bay. This makes it easier to see differences between the stations and between the model and measurements.

P14L25:

Why 90%? Another magic number?

The cloud variable used for the threshold quickly reaches 100%. It therefore is reasonable to use a threshold of 90% to exclude all cloudy points. We have also changed the text, explaining this matter.

Sect. 3.3.1:

Do you take the model output at the same times and the same locations as the satellite makes observations (overpasses)? For this comparison you should.

We do not compare model data collocated to the measurements, but this is also not necessary. In a free-running simulation, we do not expect to get the same meteorological situation that the satellite has seen. Taking only collocated points is therefore unnecessary. We do, however, use the same regions that are used for the evaluation of the satellite data.

Fig. 3 and 4:

Give panels a,b,c,d and change text accordingly

Again, we have refrained from numbering panels when the title of each panel is very clear.

P18L4:

Two more magic numbers, please explain.

These numbers were chosen to extract datapoints that have a strong characteristic of ocean or land surface evaporation. Therefore, it is difficult to give globally valid numbers here or even numbers that are reasonable for the ocean or land in general. If ocean evaporation water reaches 90% over the ocean, the sample can be considered characteristic. (99% would be even more characteristic, of course) But over the dry Saharan desert, it is close to impossible to find water vapor made up of 90% land evaporation water. Therefore 50% is a good number here. We then use the same numbers to find characteristics in the tropical samples.

Of course these numbers are arbitrary to a certain degree. But here, they serve to illustrate a method rather than being the basis for a scientific conclusion. The combination of water evaporation tracers with isotope values shows how the two can go hand in hand to investigate moisture pathways. In the previous section, all water vapor is considered, while we here consider only datapoints characteristic of a certain source region. As is shown in the figures, the distributions differ strongly. We believe this can be developed into a powerful tool in future studies, which is the reason for presenting the method in the manuscript.

P19L16-17:

That would mean the flights take place in the extratropics only, because in the tropics these altitudes are still the troposphere. The flights do however seem to cross the equator, something is wrong here!

The flights do not cross the equator, see Fig. 6 of the GMDD manuscript. The method for deriving δD described in the manuscript is also used for the tropics.

P19L26:

What conditions? Weather in general, or humidity, or what?

The two flights – only hours apart – sampled air of a similar meteorology: the outflow region of tropical storm. The same is true for the model sample along the flight tracks. The model does not reproduce the storm exactly – as we use a forecast run – but the general situation is similar.

As in the previous sections, we do not attempt to disentangle all processes happening here, but rather show the general performance of the model in reproducing the upper tropospheric distribution of δD in vapor. In addition, we discuss how small scale processes in the model are imprinted on the isotope signal. But here, we do not compare measurements directly, well aware that this is not possible with a single, free-running forecast simulation.

P20L4-5:

The flights do not sample the model atmosphere, the flights take measurements of the real atmosphere. Your off-line interpolation of the model data samples the model atmosphere. Be more precise.

As suggested, we have reformulated the paragraph, also removing this inaccuracy.

Moreover, taking only 1h output for this comparison you should make clear that, with an approximate flight velocity of the aircraft of around 900km/h, you will only get less than 10 model points per flight you are interpolating your data to. That is very coarse given that you are aiming on comparing local phenomena. In fact, it would be better to use an on-line flight tracking tool with high temporal resolution for this.

An on-line interpolation tool is currently not available for ICON. For the simulation we use now, we have reduced the output frequency to 1 per 15 minutes and use an output resolution of 0.5° or roughly 55km on the equator and less further north. This is close to the numeric grid resolution used here (R2B06), which corresponds to about 40km resolution globally. In 15 minutes, there are about 15 measurements along roughly 225km (distance of

4 grid points). In a linear interpolation, at least 8 spatial grid points provide information. Since we also do a linear interpolation in time, there are at least 16 model values which provide information for the 15 measurements. We believe this captures the relevant features of the model, especially considering that in the end, we compare an aggregated distribution to the CARIBIC measurements.

Sect 3.4.1:

Please state when exactly was which flight.

CARIBIC flight 309 from Frankfurt to Caracas took place from September 22, 2010 10:16 UTC to September 22, 2010, 19:32 UTC. Flight 310 back from Caracas to Frankfurt started on September 22, 2010, 22:12 UTC and landed on September 23, 2010 07:31 UTC. We now give the exact departure times in the text.

P20L7:

The hurricane processed your data? Please rephrase.

We now state “In order to compare values influenced by hurricane Igor...”

P20L8:

What model simulation?

As explained in the updated manuscript, we now use the decadal R2B04 simulation for the tropical sample. We interpolate the output of this simulation to all CARIBIC flight paths and then reproduce the distribution of tropical data from these values.

P20L9:

What exactly do you mean by ”the IAGOS-CARABIC database is examined“?

We have changed the wording of the sentence: “For reference, all tropical δD values from the IAGOS-CARIBIC database are also examined.”

P21L1:

I do not understand what you mean by ”randomly drawn“ and ”randomly chosen”, please explain. If you want to make a climatological comparison here, why not make a long simulation to have a fair comparison?

As explained above, we now use the decadal R2B04 simulation. We interpolate the output of this simulation to all CARIBIC flight paths and then reproduce the distribution of tropical data from these values.

P21L23-24:

From this depiction I cannot even see this. You should make the evaluation much more quantitative.

As also suggested by referee 2, we have included mean values, absolute and relative offsets where necessary in the revised version of this chapter.

P21L31:

This is one part of what I mean with my major point on the simulation setup. If you had a longer (some months) spin-up time, you would not have to face these problems.

A longer spin-up time would make it impossible to compare to the measurements taken during the event of Hurricane Igor since the model is free-running. We consider the influence of the initialization by means of the initialization water tracer. By the time of the flights, about 50% of the water sampled in the model is influenced by the initialization.

Fig. 7:

What does the N stand for?

The N indicates the number of data points used for the creation of the distributions. We now indicate this in the figure caption.

P23L5-8:

So if you want to discuss stratospheric intrusions you can not get around methane oxidation and its influence on δD(H2O) in the stratosphere. Depending on from which altitude the air is transported downwards, this could mean strongly depleted or enriched water vapour. Also, work has already been done to parameterize this effect on HDO in GCMs (Schmidt et al. 2005, Eichinger et al. 2015), it is a shame that this is not even discussed here given that you are evaluating results in the UTLS.

Thank you for pointing this out. Since the flights no longer see a stratospheric intrusion in the new simulation (there have also been updates to other parts of the model, which change the dynamics), it has become unnecessary to discuss these here.

P23L8:

“air has been processed by the model“ What does that mean? Please rephrase.

We now state: “...indicating that the model atmosphere has seen many fractionating and transport processes. This includes air mass mixing, but also the microphysical and convective processes that are imprinted on the isotopologue ratio. The exact nature of these processes remain to be investigated by future studies.”

P23L9:

”different processes“ What processes? At least shortly list some.

See reply to the previous comment on P23L8.

Sect. 4:

Change title from ”Conclusions” to “Summary (and outlook)”, there are no conclusions that go further than what had already been written before.

As this is a technical article, it is the nature of conclusions to summarize more than to interpret results. We have therefore decided to leave the section title to read “Conclusions”.

P24L10:

What do you mean by “long term stability”?

In order to make the sentence more concise, we have removed this part of it and it now reads: “This investigation presents a first climatological application.”

Technical issues:

P1L18: *...oceans are an unmatched …*

Corrected to “...the oceans are unmatched water reservoirs, which dissolve trace substances (Jacob, 1999) and redistribute heat (Pinet, 1993)...”

P1L18: *”a reservoir to dissolve“ - refine wording*

see above reply to comment on P1L18

P1L12-13: *It is not clear what is meant by ”all of tropical data“ here.*

Corrected to: “The general features of this sample as well as those of all tropical data available from IAGOS-CARIBIC are captured by the model.”

P2L8: *... isotopologues in water vapor ... - this inaccuracy appears several times*

We believe that the context makes clear enough that *vapor* is is *water vapor* here.

P2L14-15: *Refine the english. Suggestion: The isotopologue content of water vapor has first been measured by means of cryogenic samplers (Dansgaard, 1964). In the last 15 years, also laser absoption spectroscopy methods have been developed for that use.*

We have followed the suggestion of referee 1. The sentence now reads: “Measurements of the isotopic content of vapor first required cryogenic samplers (Dansgaard, 1954), but in the last 15 years laser absorption spectroscopy has made in situ observations possible (Lee et al., 2005; Dyroff et al., 2010).”

P3L7: *... with the results of ICON-ART-Iso simulations. (You compare the results, not the simulations)*

corrected

P3L14: *... is the water isotopologue enabled …*

We have decided to write about *isotopologues* and not *isotopes*. Still, we keep with the generally accepted and shorter term of an *isotope-enabled model*.

P3L25: *To discriminate .... , unclear, rephrase.*

The index *h* is used to make variables of the heavy isotopologues different to those of standard water.

P3L26: *For clarity, you should write 1H162O here.*

Following your suggestion, we spell out the exact isotopic composition here once.

P4L1: *Remove ”As“.*

We have replace “As in...” with “Similar to...”

P4L17 *The parameterization that influence …*

We have corrected this by including “which”.

P4L29-30: *The ratio of ratios?*

Yes, α can be seen as a ratio of ratios.

P4L31 (and throughout the section): *Put equation 2 here, not at the end of the paragraph. Generally restructure the presentation of equations.*

Following your comment and several comments by referee 1, we have restructured all sections explaining the physics of fractionation.

P6L6: *ilead*

corrected

P8L20: *... in the standard setup*

corrected

P8L23: *initialization of the water isotopologues!*

The first sentence of Sec. 2.7 now reads: “A meaningful initialization is an important prerequisite for any simulation, also of the isotopologues.”

P9L9-14: *repetition*

This paragraph is not a repetition but gives the settings for the simulations which are presented in the following sections. We hope this is more clear with the restructured Sec. 2.1.

P9L15: *what are water species?*

We have changed “diagnostic water species” to “diagnostic sets of water tracers”.

P9L21: *diagnostic*

corrected

P13L3: *remove ”In doing so“*

removed as suggested

P18L15: *criterion*

corrected

P19L8: *... in the tropics serves as reference.*

Corrected and now reads: “...taken by IAGOS-CARIBIC in the tropics is also used as reference.”

P19L23: *...resolution is finer than the …*

Following your suggestion, we have replaced “exceeds” with “is finer than”.

P19L24: *remove ”very“*

corrected

P19L28: *... Hurricane Igor had passed …*

As suggested, we have included “had”.

P21L5: *laong*

corrected

P21L6: *deld*

corrected

P23L5: *show show*

The sentence has been removed.

P23L10: *...along the …*

The sentence has been removed.

P23L16: *remove ”of”*

corrected

From climatological to small scale applications: Simulating water isotopologues with ICON-ART-Iso (version 2.1)

Johannes Eckstein[1], Roland Ruhnke[1], Stephan Pfahl[2,3], Emanuel Christner[1], Christopher Diekmann[1], Christoph Dyroff[1,a], Daniel Reinert[4], Daniel Rieger[4], Matthias Schneider[1], Jennifer Schröter[1], Andreas Zahn[1], and Peter Braesicke[1]

[1]Karlsruhe Institute of Technology (KIT), Institute of Meteorology and Climate Research (IMK), Herrmann-von-Helmholtz-Platz 1, 76344 Eggenstein-Leopoldshafen, Germany
[2]ETH Zürich, Institute for Atmospheric and Climate Science, Universitätstrasse 16, 8092 Zürich, Switzerland
[3]Freie Universität Berlin, Institute of Meteorology, Carl-Heinrich-Becker-Weg 6-10, 12165 Berlin, Germany
[4]Deutscher Wetterdienst, Frankfurter Str. 135, 63067 Offenbach, Germany
[a]now at: Aerodyne Research Inc., 45 Manning Road, Billerica, MA 01821, USA

Correspondence to: Johannes Eckstein (johannes.eckstein@kit.edu)

Abstract. We present the new ~~isotope enabled~~ isotope-enabled model ICON-ART-Iso. The physics package of the global ICOsahedral Nonhydrostatic (ICON) modelling framework ~~have~~ has been extended to simulate passive moisture tracers and the stable isotopologues HDO and $H_2{}^{18}O$. The extension builds on the infrastructure provided by ICON-ART, which allows a high flexibility with respect to the number of related water tracers that are simulated. The physics of isotopologue fractionation follow the model COSMOiso. ~~First, we~~ We first present a detailed description of the physics of fractionation that have been implemented in the model. The model is then evaluated on a range of temporal scales by comparing with measurements ~~in~~ of precipitation and vapor~~representing a range of temporal scales~~.

A multi annual simulation is compared to observations of the isotopologues in precipitation taken from the station network GNIP (Global Network for Isotopes in Precipitation). ICON-ART-Iso is able to ~~reasonably simulate the~~ simulate the main features of the seasonal cycles in δD and δ^{18}O as observed at the GNIP stations. In a comparison with IASI satellite retrievals, the seasonal and daily cycles in the isotopologue content of vapor are examined for different regions in the free troposphere. On a small spatial and temporal scale, ICON-ART-Iso is used to simulate the period of two flights of the IAGOS-CARIBIC aircraft in September 2010, which sampled air in the tropopause ~~level~~ region influenced by Hurricane Igor. The general features of this sample as well as ~~all of~~ those of all tropical data available from IAGOS-CARIBIC are captured by the model.

The study demonstrates that ICON-ART-Iso is a flexible tool to analyze the water cycle of ICON. It is capable of simulating tagged water as well as the isotopologues HDO and $H_2{}^{18}O$.

1 Introduction

Water in gas, liquid and frozen form is an important component of the climate system. The ice caps and snow covered surfaces strongly influence the albedo of the surface (Kraus, 2004), the oceans are unmatched ~~reservoir to~~ water reservoirs, which dissolve trace substances (Jacob, 1999) and redistribute heat (Pinet, 1993) and all animal and plant life depends on liquid

water. The atmosphere is by mass the smallest compartment of the hydrological cycle, but it is this compartment that serves to transfer water between the spheres of liquid, frozen and biologically bound water on the earth's surface (Gat, 1996). For atmospheric processes themselves, water is also of great importance. It is the strongest green house gas (Schmidt et al., 2010) ~~,~~ and distributes energy through the release of latent heat (Holton and Hakim, 2013)~~and ~~, while liquid and frozen particles influence the radiative balance (Shine and Sinha, 1991)~~, to name only three prominent mechanisms~~.

A correct description of the atmospheric water cycle is therefore necessary for the understanding and simulation of the atmosphere and the climate system (Riese et al., 2012; Sherwood et al., 2014). The stable isotopologues of water are unique diagnostic tracers that provide a deeper insight into the water cycle (Galewsky et al., 2016). Because of the larger molar mass of the heavy isotopologues, their ratio to (standard) water is changed by phase transitions~~, a process~~. This change in the ratio is termed fractionation. ~~By considering~~ Considering the isotopologue ratio of the heavy isotopologues in vapor and precipitation (liquid or ice) ~~, the isotopologue ratio therefore~~ provides an opportunity to develop an advanced understanding of the processes that shape the water cycle.

Pioneering research on measuring the heavy isotopologues of water starting in the 1950's first examined the isotopologues in precipitation (Dansgaard, 1954, 1964). First theoretical advances on the microphysics (Jouzel et al., 1975; Jouzel and Merlivat, 1984) and surface evaporation (Craig and Gordon, 1965) enabled the implementation of heavy isotopologues in global climate models (Joussaume et al., 1984; Joussaume and Jouzel, 1993). Since then, measurement techniques and modeling of the isotopologues have advanced. ~~Cryogenic samplers first measured the isotopologue content in vapor (Dansgaard, 1954) , which has become possible by laser absorption spectroscopy~~ Measurements of the isotopic content of vapor first required cryogenic samplers (Dansgaard, 1954) , but in the last 15 years laser absorption spectroscopy has made in situ observations possible (Lee et al., 2005; Dyroff et al., 2010). Today, the isotopologue content in atmospheric vapor can also be derived from satellite measurements (Gunson et al., 1996; Worden et al., 2006; Steinwagner et al., 2007; Schneider and Hase, 2011). Many global and regional circulation models have been equipped to simulate the atmospheric isotopologue distribution, ~~either focusing on climatological questions (Risi et al., 2010; Werner et al., 2011) or process understanding~~ focusing on the global scale (Risi et al., 2010; Werner et al., 2011) or regional phenomena (Blossey et al., 2010; Pfahl et al., 2012, both limited area models). Despite this progress, the potential of isotopologues in improving the understanding and physical description of the single processes "remains largely unexplored" (Galewsky et al., 2016). A more extensive literature overview on the subject is given by Galewsky et al. (2016).

We present ICON-ART-Iso, the newly developed, isotopologue enabled version of the global ICOsahedral Nonhydrostatic (ICON) modelling framework (Zängl et al., 2015). By design, ICON is a flexible model, capable of simulations from climatological down to turbulent scales (Heinze et al., 2017). ~~Klocke et al. (2017) show the potential of using ICON for convection permitting simulations.~~ The advection scheme of ICON has been designed to be mass conserving (Zängl et al., 2015), which is essential for the simulation of water isotopologues ~~(Risi et al., 2010; Cauquoin and Risi, 2017)~~ (Risi et al., 2010) . ICON-ART-Iso builds on the flexible infrastructure provided by the extension ICON-ART ~~(Rieger et al., 2015; ?)~~ (Rieger et al., 2015; Schröter et al., 20 which has been developed to simulate aerosols and trace gases.

By equipping ICON with the capabilities to simulate the water isotopologues, a first step is made to a deeper understanding of the water cycle. From the multitude of isotopologue enabled global models (see Galewsky et al. (2016) for an overview), ICON-ART-Iso stands out by its non-hydrostatic base model core, enabling simulations with fine horizontal resolution on a global grid. It is flexible in design to simulate diagnostic ~~moisture tracers (also termed tagged water)~~ evaporation tracers as well as the isotopologues HDO and $H_2{}^{18}O$ during a single simulation.

This article first gives some technical details on ICON and ICON-ART. This is followed by a detailed description of the physics special to ICON-ART-Iso, which have been implemented in ICON to simulate the isotopologues (Sec. 2).

The remaining sections describe model results and first validation studies: Section 3.1 looks at ~~precipitation diagnostics~~passive moisture tracers. Focus is laid on the source regions - ocean or land - of the ~~precipitating water~~ water that forms precipitation. The next section (Sec. 3.2) compares data from a simulation spanning more than ~~seven~~ ten years on a coarse grid to measurements from different stations of the GNIP network. A further validation with measurements is performed in Sec. 3.3. Retrievals from IASI satellite measurements are compared with ICON-ART-Iso results for two weeks in winter and summer 2014, considering the seasonal and daily cycle in different regions. Section 3.4 then discusses the comparison with IAGOS-CARIBIC measurements. In situ data from two flights are compared with ~~simulations of ICON-ART-Iso~~results of ICON-ART-Iso simulations. Section 4 summarizes and concludes the study.

2 The model ICON-ART-Iso

This section presents the technical and physical background of the model ICON-ART-Iso. First, ICON and the extension ICON-ART are introduced. Next, general thoughts on simulating a diagnostic water cycle are presented. Starting in Sec. 2.3, the main processes that influence the distribution of the isotopologues are discussed in separate sections: surface evaporation, saturation adjustment, cloud microphysics and convection. ~~Finally~~To close this technical part, Sec. 2.7 discusses the initialization of the model.

2.1 Introduction to the modeling framework ICON-ART

ICON-ART-Iso is the ~~isotope enabled~~ isotope-enabled version of the model ICON. ICON is a new non-hydrostatic general circulation model which is developed and maintained in a joint effort by Deutscher Wetterdienst (DWD) and Max-Planck-Institute for Meteorology (MPI-M). Its horizontally unstructured grid can be refined locally by one-way or two-way nested domains with a higher resolution. The model is applicable from global to turbulent scales~~.~~: At DWD, ICON is used operationally for global numerical weather prediction ~~,~~ (currently 13 km horizontal resolution, with a nest of 6.5 km resolution over Europe). Klocke et al. (2017) show the potential of using ICON for convection permitting simulations and it already proved successful as a Large Eddy Simulation (LES) model (Heinze et al., 2017)~~, and is currently~~. It is currently also being prepared for climate ~~prediction studies~~ projections at MPI-M. More details on ICON are given by Zängl et al. (2015).

ICON-ART-Iso builds on the numerical weather prediction physics parameterization package of ICON. The physical parameterizations that have been implemented for the simulation of the isotopologues mainly correspond to those of the model

COSMOiso as presented by Pfahl et al. (2012). As the same parameterizations have been described before, the following subsections give only a short summary of each of the different fractionation processes.

In ICON, all tracer constituents are given as mass fractions $q_x = \frac{\rho_x}{\rho}$, where $\rho = \sum_x \rho_x$ is the total density, including all water constituents x. To discriminate values of the heavy isotopologues, these will be denoted by the index h while standard (light) water will be indexed by l. ICON standard water is identified with the light isotopologue $^1H_2{}^{16}O$, which is a very good assumption also made by ~~Pfahl et al. (2012) and Blossey et al. (2010)~~ Blossey et al. (2010) and Pfahl et al. (2012) : Standard water is much more abundant than the lighter isotopologues, with a ratio of one to $3.1 \cdot 10^{-4}$ for HDO and $2.0 \cdot 10^{-3}$ for $H_2{}^{18}O$ (Gonfiantini et al., 1993) . Water in ICON-ART-Iso exists in seven different forms (vapor, cloud water, ice, rain, snow, graupel and hail), each of which is represented by one tracer for standard water and each of the isotopologues~~: vapor, cloud water, ice, rain, snow, graupel and hail~~. The amount of the isotopologues is expressed relative to standard water by the isotopologue ratio $R = {}^hq_x / {}^lq_x$. This is referenced to standard ratios of the Vienna Mean Ocean Standard Water (R_{VSMOW}) in the δ notation: $\delta = R_{\mathrm{sample}}/R_{\mathrm{VSMOW}} - 1$, with δ values then given in ~~permil~~per mil. If not noted otherwise, δ values are always evaluated for the vapor phase in this paper, which is why this specification is omitted throughout the text.

As in the current version of ICON-ART ~~(?)~~ (Schröter et al., 2018) , an XML table is used to define the settings for each of the isotopologues. While this paper mostly discusses realizations of HDO and $H_2{}^{18}O$, this choice is technically arbitrary. The XML table is used to define the tracers at runtime, making a recompilation of the model unnecessary. All tuning parameters can be specified separately for each isotopologue in the XML table and the number of realizations is limited only by the computational resources. Each parameterization describing fractionation can also be turned off separately for each isotopologue, making very different experiments possible during one simulation. This makes the model very flexible and allows using several different water tracers during one model run~~, where each of them makes use of different fractionation parameterizations~~.

2.2 Simulating a diagnostic water cycle

~~In general, the~~ The isotopologues are affected by all ~~those~~ the processes that also influence standard water in ICON: Surface evaporation, saturation adjustment to form clouds, cloud microphysics and convection. Each of these main processes is ~~described~~ represented by several parameterizations. Some of these parameterizations include phase changes of or to vapor ~~,~~ ~~which~~ and in turn lead to a change in the isotopologue ratio - which is termed isotopic fractionation. In addition, advection and turbulent diffusion are non-fractionating processes that change the spatial distribution of all trace substances.

An important prerequisite to a simulation of water isotopologues is a good implementation of advection~~(Cauquoin and Risi, 2017)~~. ICON-ART makes use of the same numerical methods that are used for advecting the hydrometeors in ICON itself. These assure local mass conservation (Zängl et al., 2015) and mass-consistent transport. The latter is achieved by making use of the same mass flux in the discretized continuity equations for total density and partial densities, respectively (Lauritzen et al., 2014). The advection schemes implemented in ICON conserve linear correlations between tracers and assure the monotonicity of each advected tracer. Note, however, that this does not ~~gaurantee~~ guarantee monotonicity of the isotopologue ratios (see Morrison et al., 2016).

The parameterizations that influence the water cycle also include processes that do not fractionate. For all non-fractionating processes, the transfer rate ${}^{h}S$ of the heavier isotopologues are defined by Eq. 1.

$$ {}^{h}S = {}^{l}S \cdot \frac{{}^{h}q_x^{\text{source}}}{{}^{l}q_x^{\text{source}}} R_{\text{source}} \tag{1} $$

Here, ~~q_x denotes the mass ratio of the hydrometeor x, which is taken from the source of the process.~~ ${}^{l}S$ is the transfer rate of ICON standard water~~in q_x. This equation can also be applied to processes that would normally change~~ , while R_{source} is the isotopologue ratio in the source reservoir of the transfer.

In order to turn ~~off fractionation~~any fractionating processes into a non-fractionating one, its respective equation for the transfer rate of the heavy isotopologues can be replaced with Eq. 1. This has been implemented as an option in all processes that describe fractionation, that are explained below. If all processes are set to be non-fractionating in this way, the isotopologue ratio does not change and the species will resemble the standard water ~~in~~ of ICON. This is an important feature which can be used to test the model for self-consistency or to investigate source regions with diagnostic moisture tracers, so called tagged water (e.g. Bosilovich and Schubert, 2002). An application of this will be shown in Sec. 3.1.

Whenever phase changes ~~including~~ occur that include the vapor phase~~occur~~, the isotopologue ratio changes because ~~of the~~ the heavier isotopologues have different diffusion constants and ~~the~~ a different saturation vapor pressure ~~of the heavier isotopologues~~compared to standard water. For the diffusion constant ratio, two choices have been implemented for HDO and $H_2{}^{18}O$, ~~using~~ making available the values of Merlivat and Jouzel (1979) or Cappa et al. (2003). The differences in saturation pressure are expressed ~~with~~ by the equilibrium fractionation factor α, which is the ratio of ~~isotopologues~~ isotopologue ratios in thermodynamic equilibrium ~~. This ratio α depends on temperature and is different over water and over ice (termed α_{liq} and α_{ice}). For all parameterizations,~~ (Mook, 2001) , see Eq. 2~~holds, where~~ .

$$ \alpha = \frac{R_v}{R_{\text{cond}}} < 1 \tag{2} $$

Here, R_v stands for the isotopologue ratio in the vapor phase, while R_{cond} stands for that in the condensed phase. The ratio α depends on temperature and is different over water and over ice (termed α_{liq} and α_{ice}). The parameterizations by Majoube (1971) and by Horita and Wesolowski (1994) have been implemented for α_{liq} and those by Merlivat and Nief (1967) for α_{ice}. ~~The~~ Note the definition for α given in Eq. 2 is also used in COSMOiso (Pfahl et al., 2012), ~~but~~ and is the inverse of the definition used by others, e.g. by Blossey et al. (2010).

~~$$ \alpha = \frac{R_v}{R_{\text{cond}}} < 1 $$~~

2.3 Surface evaporation

Surface evaporation is the source for the atmospheric water cycle. In ICON-ART-Iso, the evaporative surface flux is split into evaporation from land and water surfaces, transpiration from plants and dew and rime formation. Transpiration is considered a non-fractionating process (Eq. 1), which is an assumption also made by Werner et al. (2011) or Pfahl et al. (2012). Dew and

rime formation (and condensation on the ocean surface) are considered to fractionate according to equilibrium fractionation (Eq. 2). For the evaporation part of the full surface flux, two parameterizations have been implemented (Pfahl and Wernli, 2009; Merlivat and Jouzel, 1979). Both build on the Craig-Gordon model (Craig and Gordon, 1965; Gat, 2010). Equation 3 gives the general expression for R_{evap}.

$$R_{\text{evap}} = k \cdot \frac{\alpha_{\text{liq}} R_{\text{surf}} - h R_v}{1 - h} \tag{3}$$

Here, h is the specific humidity of the lowest model layer relative to the specific humidity at the surface and k is the non-equilibrium fractionation factor. The two parameterization differ in their description of k. While Merlivat and Jouzel (1979) give a parameterization that depends on the surface wind, Pfahl and Wernli (2009) have simplified this to be wind speed independent. In summary, Eq. 4 is used to calculate the surface flux of the isotopologues, ${}^{h}F^{tot}$.

$${}^{h}F^{tot} = {}^{l}F^{\text{evap}} \cdot R_{\text{evap}} + {}^{l}F^{\text{transp}} \cdot R_{\text{surf}} + {}^{l}F^{\text{dew}} \cdot \frac{R_v}{\alpha_{\text{liq}}} + {}^{l}F^{\text{rime}} \cdot \frac{R_v}{\alpha_{\text{ice}}} \tag{4}$$

For transpiration and evaporation, the isotopologue ratio of the surface and ground water (R_{surf}) is necessary. The surface model TERRA ~~of ICONwas not equipped with isotopologuesfor ICON-ART-Iso~~(included in ICON) was not extended with isotopologues, so R_{surf} is not available as a prognostic variable. ~~It~~ Over land, it is therefore approximated by R_{VSMOW} in Eq. 3 and 4. ~~While this may be regarded as a valid approximation over the ocean (there are only small variations, see LeGrande and Schmidt, 200~~ ~~it can only be regarded as a first order step over land. Nevertheless, it is common procedure in most isotopologue enabled atmospheric models (e.g. Risi et al., 2010; Werner et al., 2011)~~ Of course, this is a simplification that allows testing the atmospheric physics package and will be developed further. Over the ocean, the dataset provided by LeGrande and Schmidt (2006) has been implemented. Values for HDO are given in this dataset, while those for $H_2{}^{18}O$ are determined from the relationship given by the global meteoritic water line (GMWL), $\delta D = 8 \cdot \delta^{18}O + 10‰$ (Craig, 1961) .

2.4 Saturation adjustment

Cloud water is formed by saturation adjustment in ICON. Vapor in excess of saturation vapor pressure is transferred to cloud water and temperature is adjusted accordingly. This is repeated in an iterative procedure. For the isotopologues, the iteration does not have to be repeated. Instead, Eq. 5 is applied directly, using the adjusted values of ICON water. This is the same equation used in COSMOiso (Pfahl et al., 2012) and by Blossey et al. (2010).

$${}^{h}q_c = \frac{{}^{h}q_v + {}^{h}q_c}{1 + \alpha_{\text{liq}} \frac{{}^{l}q_v}{{}^{l}q_c}} \tag{5}$$

2.5 Microphysics

Several grid-scale microphysical schemes are available in ICON. ICON-ART-Iso makes use of the two moment scheme by Seifert and Beheng (2006). ~~It~~ This scheme computes mass and number densities of vapor, cloud water, rain and four ice classes (ice, snow, graupel and hail) and can be used to simulate aerosol-cloud interaction, see Rieger et al. (2017). As the isotopologues are diagnostic values, the number densities do not have to be simulated separately. The two moment

scheme describes more than 60 different processes, but only those processes that include the vapor phase ~~ilead~~ lead to fractionation. All others are described by Eq. 1 in the model. Isotopic effects also occur during freezing of the liquid phase (Souchez and Jouzel, 1984; Souchez et al., 2000) , but this is neglected due to the low diffusivities, as in COSMOiso. In accordance with Blossey et al. (2010) and Pfahl et al. (2012), sublimation is also assumed not to fractionate. Condensation to form liquid water happens only during the formation of cloud water and is accounted for by the saturation adjustment. The fractionating processes that remain are ice formation by nucleation~~(of ice),~~ , vapor deposition (on all four ice classes) and evaporation of liquid hydrometeors. Besides rain, a fraction of the three larger ice classes (snow, graupel, hail) can evaporate after melting. This liquid water fraction is currently not a prognostic variable.

The two moment scheme by Seifert and Beheng (2006) uses mass densities instead of mass ratios, so we adopt the change in notation here, denoting mass densities by ρ. Vapor pressures are denoted by e. The star (*) indicates values at saturation with respect to liquid (index l) or ice (index i).

For evaporation ~~, two parameterizations have been implemented to describe fractionation. One choice is~~ of rain and melting hydrometeors, the semi-empirical parameterization ~~by Stewart (1975) also implemented in COSMOiso (Pfahl et al., 2012) . The change in mass, ${}^h S_x^{\mathrm{evap}}$, is calculated from ${}^l S_x^{\mathrm{evap}}$ as~~ of Stewart (1975) has been implemented and is discussed in this paper. It allows the exchange of heavy isotopologues with the surroundings in supersaturated as well as subsaturated conditions. The corresponding transfer rate is given in Eq. 6.

$$ {}^h S_x^{\mathrm{evap}} = {}^l S_x^{\mathrm{evap}} \left(\frac{{}^h D}{{}^l D} \right)^n \frac{\alpha_{\mathrm{liq}}\, {}^l\rho_{l,v}^* \frac{{}^h\rho_x}{{}^l\rho_x} - {}^h\rho_v}{{}^l\rho_{l,v}^* - {}^l\rho_v} $$

The equation is given in the formulation for the evaporation of rain, with details on the evaporation of melting ice hydrometeors explained below. In this process, it is assumed that the whole drop has time to equilibrate, which is a simplification when compared to e.g. Lee and Fung (2008) .

$$ {}^h S_r^{\mathrm{evap}} = A \left(\frac{{}^h D}{{}^l D} \right)^n \left[R_r \alpha_{\mathrm{liq}}\, {}^l\rho_{l,\infty}^* - {}^h\rho_v \right] \tag{6} $$

$$ A = \frac{4\pi a\, {}^l f\, {}^l D}{1 + B_l} \tag{7} $$

$$ B_l = \frac{{}^l D\, L_e^2\, {}^l e_{l,\infty}^*}{k_a \mathcal{R}_v^2 T_\infty^3} \tag{8} $$

Here, ~~ρ_x stands for the mass density of either rainor melting snow, graupel or hail while ρ_v indicates the mass density of the vapor phase~~a is the radius of the hydrometeor, ${}^l f$ is the ventilation factor, R_v and R_r are the isotopologue ratios in the vapor and the hydrometeor, $\mathcal{R}_v$ the gas constant of water vapor and L_e and k_a the latent heat of evaporation and the heat conductivity in air. The index ∞ indicates that values are evaluated for the surroundings. The ratio of the diffusion constants D is given by the literature values cited above and can be chosen at the time of simulation for each isotopologue. The tuning parameter n is set to 0.58 by default ~~(see again Stewart, 1975)~~ (Stewart, 1975) , but can be changed at runtime.

~~Another option to describe fractionation during evaporation of hydrometeors is the parameterization following the theoretical approach by Blossey et al. (2010) , given in Eq. 9.~~

$$ {}^{h}S_x^{\text{evap}} = 4\pi a \, {}^{h}f \frac{\left((1+b_l)\frac{R_v}{R_{\text{hyd}}}\alpha_{\text{liq}} - b_l\right){}^{l}\mathcal{S}_l - 1}{\frac{\alpha_{\text{liq}}}{\zeta R_{\text{hyd}}}\left(\frac{\mathcal{R}_v T_\infty}{{}^{l}D\, e^*_{l,\infty}} + \frac{L_e^2}{k_a \mathcal{R}_v T_\infty^2}\right)} $$

$$ b_l = \frac{{}^{l}D\, L_e^2\, \rho^*_{l,\infty}}{k_a \mathcal{R}_v T_\infty^2} $$

~~The equation~~ Note that an alternative parameterization to describe the fractionation of evaporating or equilibrating hydrometeors (that of Blossey et al. (2010)) has also been implemented in the model. For completeness, the physics of this parameterization is briefly explained in App. B in comparison to Stewart (1975) . An investigation of this parameterization and the difference to Stewart (1975) will be provided in a later study.

The underlying equation for both parameterizations is derived from fundamentals of cloud microphysics (see Pruppacher and Klett, 2012)~~, with the adaptation for the isotopologues explained in detail by Blossey et al. (2010) . The same equations are used to derive ${}^{l}S_x^{\text{evap}}$~~. It is also used in the microphysical scheme ~~in ICON(Seifert and Beheng, 2006) . Here, a is the radius of the hydrometeor, ${}^{h}f$ is the ventilation factor (set equal to ${}^{l}f$ in default setup)~~ of ICON, ~~R_v~~ where ${}^{l}S_x^{\text{evap}} = A({}^{l}e^*_{l,\infty} - {}^{l}e_v)$. The definitions of a and ~~R_{hyd} are the isotopologue ratios in the vapor and the hydrometeor, $\mathcal{S}_l$ the subsaturation ratio, $\zeta = {}^{h}D/{}^{l}D$ the ratio of diffusion constants, $\mathcal{R}_v$ the gas constant of water vapor,~~ ${}^{l}f_v$ depend on whether S_x is calculated for rain (Seifert, 2008) or melting ice class hydrometeors (Seifert and Beheng, 2006) . For melting ice class hydrometeors, the melting temperature of ice ($T_0 = 273.15\,\text{K}$) is used for the calculation of α_{liq} and in place of T_∞ ~~and $e^*_{l,\infty}$ the temperature and saturation vapor pressure in the surroundings and L_e and k_a are the latent heat of evaporation and the heat conductivity~~. This implies an additional factor of T_∞/T_0 for melting ice hydrometeors, as ${}^{l}e^*_{l,\infty}$ is always evaluated at T_∞. Equation 6 otherwise also holds true for the evaporation of melting ice hydrometeors.

Fractionation during nucleation of ice particles or deposition on one of the four ice ~~classes~~ class hydrometeors is parameterized following Blossey et al. (2010), as in COSMOiso (Pfahl et al., 2012). The flux is assumed to interact only with the outermost layer of the hydrometeor, the isotopologue ratio of which is set to be identical to that of the depositional flux. The transfer rate ${}^{h}S_x^{\text{ice}}$ is then given by Eq. 9 with the fractionation factor α_k as given in Eq. 10. All symbols are used as ~~in Eq. 9~~above, with L_s being the latent heat of sublimation.

$$ {}^{h}S_x^{\text{ice}} = \alpha_k R_v \, {}^{l}S_x^{\text{ice}} \tag{9} $$

$$ \alpha_k = \frac{(1+b_i)\,{}^{l}\mathcal{S}_i}{{}^{h}f\frac{1}{\zeta}\left({}^{l}\mathcal{S}_i - 1\right) + \alpha_{\text{ice}}\left(1 + b_i\,{}^{l}\mathcal{S}_i\right)} \frac{(1+B_i)\,{}^{l}\mathcal{S}_i}{\frac{{}^{l}f\,{}^{l}D}{{}^{h}f\,{}^{h}D}\left({}^{l}\mathcal{S}_i - 1\right) + \alpha_{\text{ice}}\left(1 + B_i\,{}^{l}\mathcal{S}_i\right)} \tag{10} $$

$$ bB_i = \frac{{}^{l}D_v\, L_s\, \rho^*_{i,\infty}}{k_a \mathcal{R}_v T_\infty^2} \frac{{}^{l}D_v\, L_s^2\, {}^{l}e^*_{i,\infty}}{k_a \mathcal{R}_v^2 T_\infty^3} \tag{11} $$

2.6 Convection

ICON uses the Tiedtke-Bechtold scheme for simulating convective processes (Tiedtke, 1989; Bechtold et al., 2014). The scheme uses a simple cloud model considering a liquid fraction in cloud water (denoted here by ω) and the remaining solid fraction $(1-\omega)$. Fractionation happens during convective saturation adjustment (during initialization of convection and in updrafts), in saturated downdrafts and in evaporation below cloud base. The parameterizations are the same that have been implemented by Pfahl et al. (2012) in COSMOiso.

Convective saturation adjustment calculates equilibration between vapor and the total condensed water (liquid and ice). The parameterization used for grid scale adjustment therefore has to be expanded in order to be used in convection if the liquid water fraction is smaller than one. The isotopologue ratio is determined over liquid and ice particles separately. A closed system approach (Gat, 1996) is used for the liquid fraction ($R_v^{\text{by liq}}$ of Eq. 12). The underlying assumption for Eq. 13 used for the ice fraction is a Rayleigh process with the kinetic fractionation factor α_{eff} following Jouzel and Merlivat (1984). The two are then recombined according to the fraction of liquid water, following Eq. 14. This procedure has been adopted from COSMOiso (Pfahl et al., 2012).

$$R_v^{\text{by liq}} = R_v^{\text{old}} \frac{\alpha_{\text{liq}}}{1 + \frac{{}^{l}q_v^{\text{new}}}{{}^{l}q_v^{\text{old}}}(\alpha_{\text{liq}} - 1)} \tag{12}$$

$$R_v^{\text{by ice}} = R_v^{\text{old}} \left(\frac{{}^{l}q_v^{\text{new}}}{{}^{l}q_v^{\text{old}}} \right)^{\alpha_{\text{eff}}-1} \tag{13}$$

$$R_v = (1-\omega) \cdot R_v^{\text{by ice}} + \omega \cdot R_v^{\text{by liq}} \tag{14}$$

Here, the indices `old` and `new` denote the values of the respective variables before and after the convective saturation adjustment. The factor α_{eff} which appears in Eq. 13 is determined by Eq. 15. The supersaturation with respect to ice, ξ_{ice}, is calculated from Eq. 16, where $T_0 = 273.15\,\text{K}$ is used. The tuning parameter λ is set to 0.004 in the standard setup, following Pfahl et al. (2012) and Risi et al. (2010).

$$\alpha_{\text{eff}} = \frac{\xi_{\text{ice}}\zeta}{\xi_{\text{ice}} - 1 + \alpha_{\text{ice}}\zeta} \tag{15}$$

$$\xi_{\text{ice}} = 1 - \lambda(T - T_0) \tag{16}$$

Convective downdrafts are assumed to remain saturated by continuously evaporating precipitation (Tiedtke, 1989). ~~Equilibrium~~ In these saturated downdrafts, equilibrium fractionation is applied for the liquid fraction, while the ice fraction is assumed to sublimate without fractionation.

Evaporation of precipitation below cloud base is an important process for several reasons: it leads to a drop in the temperature and ~~is therefore an important process in convection~~therefore influences dynamics, but is also important for the isotopic composition (Risi et al., 2008) . To describe fractionation here, the parameterization by Stewart (1975) is again applied to the liquid fraction. Different to Eq. 6 for evaporation during microphysics, the integrated form is now applied. In following Stewart (1975), the ratio in the liquid part of the general hydrometeor after evaporation $R_{\text{adj}}^{\text{liq}}$ is given with Eq. 17. Here, f is the fraction

of remaining condensate. $R_{\text{hyd}}^{\text{old}}$ is the isotopologue ratio in the hydrometeor before adjustment and rH is the relative humidity calculated as the vapor pressure over saturation vapor pressure.

$$R_{\text{adj}}^{\text{liq}} = \gamma R_v + f^{\beta}\left(R_{\text{hyd}}^{\text{old}} - \gamma R_v\right) \tag{17}$$

$$\gamma = \frac{\text{rH}}{\alpha_{\text{liq}} - \mu} \tag{18}$$

$$\beta = \frac{\alpha_{\text{liq}} - \mu}{\mu} \tag{19}$$

$$\mu = (1 - \text{rH})\left(\frac{^{h}D}{^{l}D}\right)^{-n} \tag{20}$$

Using Eq. 17, the isotopologue ratio in the adjusted hydrometeor is given with Eq. 21. The ice fraction is assumed to sublimate without fractionation, maintaining its isotopologue ratio.

$$R_{\text{adj}} = (1-\omega)R_{\text{hyd}}^{\text{old}} + \omega R_{\text{adj}}^{\text{liq}} \tag{21}$$

Following Pfahl et al. (2012), an additional equilibration has been implemented to determine the final isotopologue ratio of the hydrometeors, which is given in Eq. 22. The parameter ξ_{add} is a tuning parameter that is set to 0.5 in the standard setup.

$$R_{\text{adj}}^{\text{final}} = R_{\text{adj}} + \xi_{\text{add}} \cdot \omega \left(\frac{R_v}{\alpha_{\text{liq}}} - R_{\text{adj}}\right) \tag{22}$$

2.7 ~~General initialization~~ Initialization of the isotopologues

~~The first step necessary for simulating the isotopologuesis a meaningful initialization~~A meaningful initialization is an important prerequisite for any simulation, also of the isotopologues. In addition to an initialization with a constant ratio to standard water, ~~which is interesting for simulating tagged water,~~ the isotopologues can be initialized with the help of mean measured δ values. Values at the lowest model level, the tropopause level (WMO definition, see Holton et al., 1995) and model top are prescribed for vapor and linear and log-linear interpolation is applied below and above the tropopause, respectively. Values for the tropopause level and the model top are taken from MIPAS measurements (Steinwagner et al., 2007)~~and~~ , the value at the lowest level is a standard value taken from Gat (2010) . All values are given in Table 1. By using the local tropopause height, an adaptation to the local meteorological situation is assured. To calculate the δ value of the hydrometeors, a constant offset is applied to the local δ value of vapor. ~~Values~~ The literature provides values for HDO, while those for $H_2{}^{18}O$ are determined from the relationship given by the global meteoritic water line ~~(GMWL), $\delta D = 8 \cdot \delta^{18}O + 10‰$ (Craig, 1961)~~ (GMWL, Craig, 1961) .

3 Model evaluation results

~~The following section~~ In the following sections, we present first results and comparisons of model simulations with measurements spanning several spatio-temporal scales: Sec. 3.1 shows how the ~~models capability to simulate~~ model simulated diagnostic H_2O can be used to investigate source regions of the ~~modeled~~ (modeled) water cycle. Sec. 3.2 ~~then~~ compares results for precipitation from ~~a~~ the same long model integration with measurements taken from the GNIP network (Terzer et al., 2013;

	literature	HDO	$H_2{}^{18}O$
δ_{bottom}	Gat (2010)	-50	-5
$\delta_{\text{tropopause}}$	Steinwagner et al. (2007)	-650	-80
δ_{top}	Steinwagner et al. (2007)	-400	-48.75
δ_{offset}	Gat (2010)	-100	-11.25

Table 1. Values for the initialization with mean measured δ values. Literature ~~sources give~~ provides the values for HDO, values for $H_2{}^{18}O$ have been determined from GMWL (Craig, 1961).

IAEA/WMO, 2017). Sec. 3.3 looks at seasonal and regional differences by comparing model output with pairs of $\{H_2O, \delta D\}$ derived from IASI satellite measurements (Schneider et al., 2016). Finally, Sec. 3.4 presents a first case study, in which simulated values of δD are compared with measurements from the ~~CARIBIC~~ IAGOS-CARIBIC project (Brenninkmeijer et al., 2007). All simulations discussed here are free-running.

~~The following sectionsuse modeled values of~~ In the following sections, we focus on H_2O (ICON standard water) and of HDO and $H_2{}^{18}O$. ~~For the simulations discussed in the following sections, the~~ The settings for each isotopologue are defined at runtime, which is why the specifications for the simulations are given here. The diffusion constant ratio is set to the values of Merlivat and Jouzel (1979) and the equilibrium fractionation is parameterized following Majoube (1971) over liquid water and following Merlivat and Nief (1967) over ice. Surface evaporation is described by the parameterization ~~by~~ of Pfahl and Wernli (2009). The parameterization by Merlivat and Jouzel (1979) has little influence on the values in the free troposphere and is not ~~further discussed~~ discussed further. The dataset by LeGrande and Schmidt (2006) for the isotopic content of the ocean surface is used for all isotopologues. Grid scale evaporation of hydrometeors is described by the parameterization by Stewart (1975) if not noted differently.

In addition to ICON standard water, three diagnostic ~~water species~~ sets of water tracers are simulated. All fractionation is turned off, so they resemble H_2O. But the evaporation and initialization is different: water indexed by `init` (~~e.g.~~ as in q^{init}) is set to ICON water at initialization, but evaporation is turned off. In the course of the simulation, the water of this type precipitates out of the model atmosphere. Water indexed by `ocn` and `lnd` ~~on the contrary~~ are initialized with zero and evaporate from the ocean (q^{ocn}) and land areas (q^{lnd}), respectively. The sum of q^{init}, $q^{\text{ocn}}$and q^{lnd}always equals the mass mixing ratio of ICON standard water, indexed as q^{ICON}. These tracers allow us to infer the relative importance of ocean and land evaporation - essentially the source of water in the model atmosphere - at all times. In addition to case studies, this is interesting because of the simplified implementation of isotopic processes during land evaporation in the current version of ICON-ART-Iso, see Sec. 2.3. The tracers of q^{init} provide information on the importance of the initialization at a certain time in the simulation.

3.1 An application of ~~dignostic~~ diagnostic water tracers: Precipitation source regions

This section examines the moisture source regions of ~~vapor that is removed again by~~ precipitation over ocean and land~~,~~ ~~respectively.The study uses two model runs that were initialized on November 5, 2013 and May 5, 2014 and both simulated~~

~~four months~~. Gimeno et al. (2012) give a review of the subject, while e.g. Numaguti (1999) , Van der Ent et al. (2010) and Risi et al. (2013) study this question by use of other models and in more detail.

Here, we use a decadal model integration. The simulation was initialized with ECMWF (European Centre for Medium-Range Weather Forecast) Integrated Forecast System (IFS) operational analysis data on January 1, 2007, 0UTC, to simulate 11 years on an R2B04 grid ($\approx 160\,\mathrm{km}$ horizontal resolution). The time step was set to 240 s (convection called every second step) and output was saved on a regular $1° \times 1°$ grid every 10 h in order to obtain values from all times of the day. Sea surface ~~temperature~~ temperatures and sea ice cover were updated daily, by linearly interpolating monthly data provided by the AMIP II project (Taylor et al., 2000). ~~A horizontal resolution of R2B06 was used, which corresponds to approximately 40(Zängl et al., 2015) and the time step was set to 180, with the convection timestep called every second time step.~~ The first year is not considered as spin-up time of the model and the simulation is evaluated up to the end of 2017.

~~This section looks~~ We look at the total precipitation P in ~~January and July for the two model runs initialized in November and May, respectively~~northern hemisphere winter (December, January and February, denoted by DJF) and summer (June, July, August, denoted by JJA). Figure 1 displays zonal sums of P^{init}, P^{ocn} and P^{lnd} relative to standard water precipitation P^{ICON} as a function of latitude. The sum of precipitation that ~~orginiates~~ originates from convection is also given for each water species. The top panels give winter values while the bottom panels display the results for summer months.

The area covered by ocean is not equally distributed over different ~~latitudes~~latitudinal bands, which is the reason why ocean and land points are considered separately. The center panels show the fraction of precipitation that has fallen over the ocean relative to the total precipitation and the area fraction of the ocean in each latitudinal band. Despite the ~~different~~ characteristics of the different seasons, which will be discussed in the following paragraphs, the latitudinal distribution of the ocean area fraction largely determines the overall fraction of rain that falls over the ocean or over land. This is why the other panels display values of P relative to the sum over each compartment, not to the total sum.

~~Figure 1 shows the precipitation two months after initialization~~To evaluate the model simulation, we use values starting in the second year. At this time, the tropospheric moisture has ~~almost completely been replaced almost completely~~ been completely replaced by water that has evaporated during the model run. This is demonstrated by the ~~very low~~ values of P^{init} close to zero in all four panels in Fig. 1. Technically, this means that the ternary solution of q^{init}, q^{ocean} and q^{land} that makes up q^{ICON} is practically reduced to a binary solution of only q^{ocean} and q^{land}. ~~q^{init} does not have to be considered in the troposphere two months after initialization~~Other experiments show that this is already true after a few weeks (not shown).

During northern hemisphere winter over the ocean (top left panel of Fig. 1), the precipitation is strongly dominated by water that has evaporated from the ocean. Water from the land surface hardly reaches the ocean. Over land areas, the ocean is also the dominant source for precipitation, reaching more than 50% at almost all latitudes. In the northern ~~and southern hemisphere mid latitudes~~hemisphere mid latitude land areas, more than 70% of the precipitated water originates from the ocean. ~~Only the tropics~~ The tropical and southern hemisphere land areas (in DJF) receive up to 40% of precipitation from land evaporation. Most precipitation at tropical and subtropical latitudes over the ocean originates from convection (indicated by dashed lines)~~, while the~~ . The role of convection is much smaller over land areas ~~. This process depends on model resolution. In~~ and again stronger in the southern hemisphere. Note that in a simulation with very high horizontal resolu-

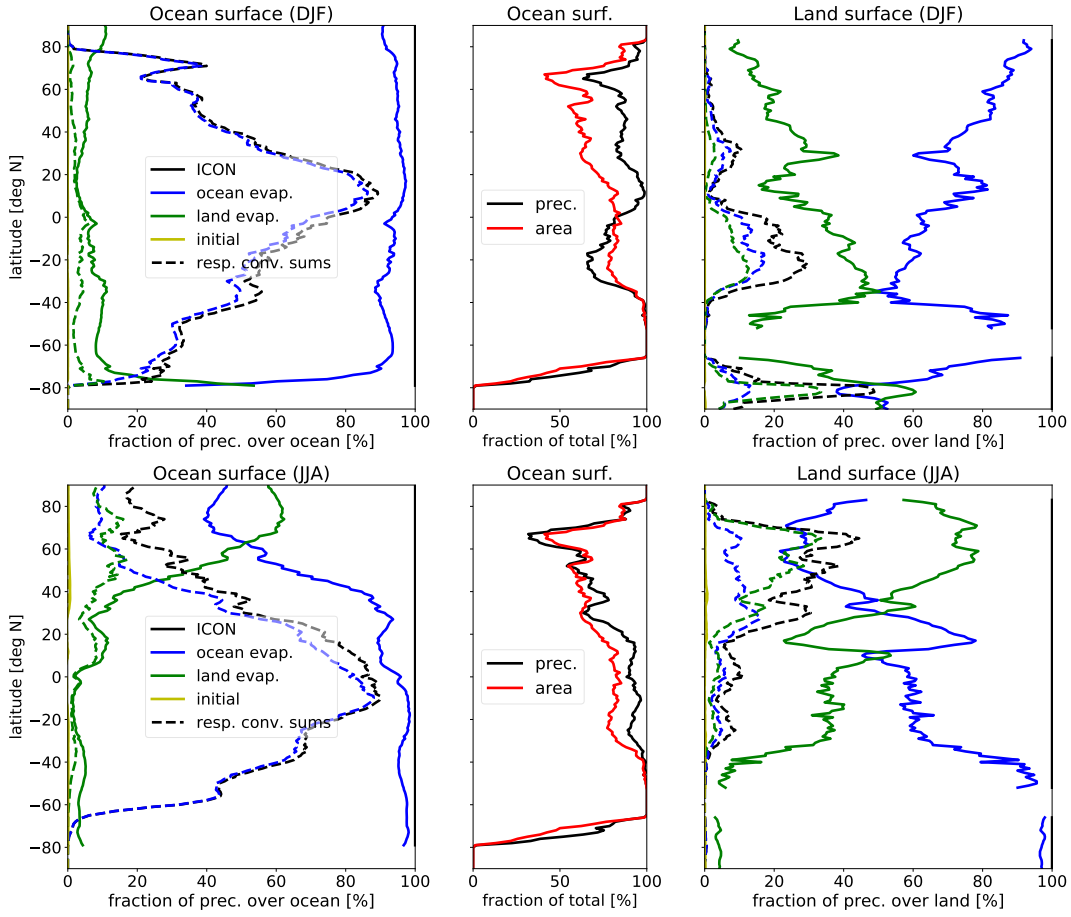

Figure 1. Fractional contributions of P^{ICON}, P^{init}, P^{ocn} and P^{lnd} to zonal sums of total precipitation for ~~January~~ northern hemisphere winter (DJF, top) and ~~July~~ summer (JJA, bottom), as a function of latitude. Left and right panels show sums over the ocean and land grid points, respectively. Dashed lines indicate the contribution of convective precipitation for each source of atmospheric water. Center panels display the fraction of precipitation over the ocean relative to total precipitation (over land plus ocean) and the fraction of the area covered by ocean.

tion (for an example using ICON, see Klocke et al., 2017) , more convective processes could have been directly resolved. ~~The~~ In this specific case of a resolution close to 160 km, practically no convection is directly resolved by the model. It should therefore be considered that the amount of precipitation from convection ~~therefore points at~~ only shows the importance of this parameterization in the ~~model~~simulations at this resolution.

The ~~situation~~ distribution of precipitation water sources is different in northern hemisphere summer (bottom row of Fig. 1)~~, especially in the northern hemisphere~~. In summer, the northern hemisphere land areas (bottom right) supply themselves a substantial fraction of the moisture that then precipitates. The importance of convection is ~~slightly~~ increased in northern hemisphere summer with its maximum influence shifted ~~northward~~into northern mid-latitudes. Despite the larger moisture availability over the ocean, the far northern hemisphere land areas also supply the larger part of moisture that precipitates over the ocean in ~~July~~summer, see the lower left hand panel.

These results are comparable to the studies by Numaguti (1999) , Van der Ent et al. (2010) and Risi et al. (2013) . While these studies look at regional differences, the latitudinal dependence is similar to the results presented here. This first application of ICON-ART-Iso - while no isotopologues are used - shows how diagnostic moisture tracers can be applied to better understand specific aspects of the atmospheric water cycle.

3.2 ~~A~~ The multi annual simulation compared to GNIP data

For a first validation of δD and δ^{18}O values, ~~this section uses a multi annual~~ we use the decadal ICON-ART-Iso model integration ~~and compares~~ of the previous section and compare results to data taken from the GNIP network (Global Network for Isotopes in Precipitation, see Terzer et al., 2013; IAEA/WMO, 2017). ~~The simulation was initialized with ECMWF (European Centre for Medium-Range Weather Forecast) Integrated Forecast System (IFS) data at January 1, 2007, 0UTC, to simulate almost 7 years on an R2B04 grid ($\approx 160\,$km horizontal resolution). The time step was set to 240(convection called every second step) and output was saved on a regular $1° \times 1°$ grid every 73in order to obtain values from all times of day. Sea surface temperatures and sea ice cover are, again, updated daily, using the data provided by Taylor et al. (2000) . The first 91.25 days are not considered as spin-up time of the model~~In this section, we analyze δ values in total precipitation.

Five GNIP stations were chosen for their good data ~~coverage~~ availability in the respective years, sampling different climate zones: ~~Karlsruhe in southwestern Germany ($49.0°N$,$8.3°E$),~~ Vienna in eastern Austria ($48.2°N$,$16.3°E$) in central Europe, Ankara in central Anatolia ($40.0°N$,$32.9°E$), Bangkok in tropical southern Asia ($13.7°N$,$100.5°E$), Puerto Montt in central Chile ($41.5°S$,$72.9°W$) and Halley station in Antarctica ($75.6°S$,$20.6°W$). The closest grid point to each of these stations was taken from the model output and the multi-year mean ~~was calculated for~~ of each calender month ~~of~~ was calculated for δD, δ^{18}O and d-excess (d-excess $= \delta\mathrm{D} - 8\,\delta^{18}\mathrm{O}$) in precipitation, total precipitation P and two meter temperature T_{2m}. The corresponding values are available from ~~the GNIPdatabase~~GNIP. Results are displayed in Fig. 2. The panels for total precipitation also include the mean values of precipitation from ocean and land evaporation (see previous section). ~~d-excess values have been calculated as d-excess $= \delta\mathrm{D} - 8\,\delta^{18}$O. All panels also show the intervals of~~ All panels (except for the precipitation amount) show the 1σ standard deviation range for model and measurement data.

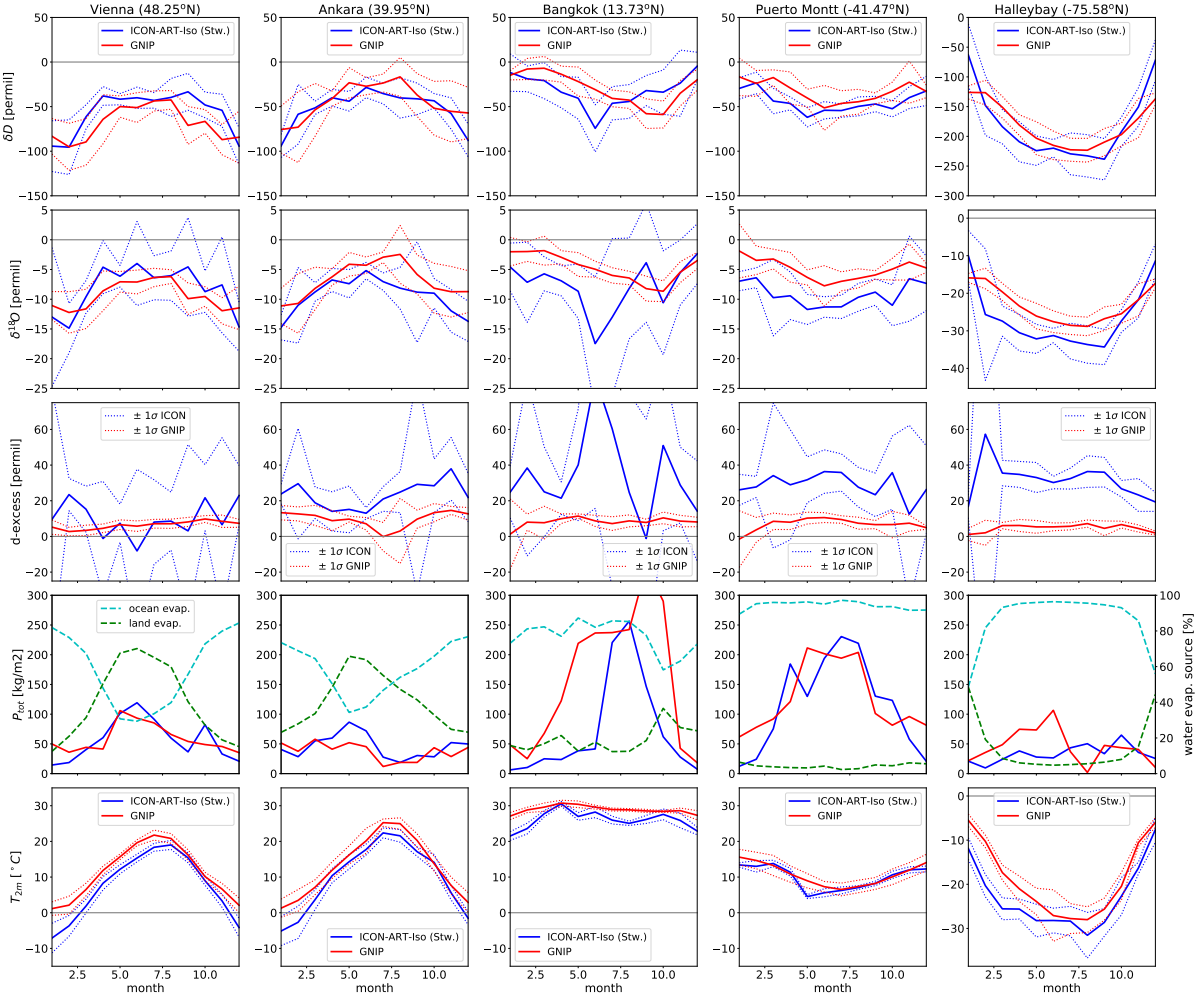

Figure 2. Monthly mean data for five GNIP stations (left to right: ~~Karlsruhe,~~ Vienna, Ankara, Bangkok, Puerto Montt and Halley station). Variables listed from top to bottom: δD, δ^{18}O, d-excess ($\delta\mathrm{D} - 8\,\delta^{18}\mathrm{O}$), total precipitation P_{tot} and two meter temperature (T_{2m}). Plots showing P_{tot} also include the percentage of land and ocean evaporation in precipitation. ~~All figures~~ The 1σ standard deviation interval is indicated by dashed lines (except P for ~~sake of~~ readability)~~also indicate the one standard deviation (σ) interval (dotted lines)~~.

For most stations, the seasonal cycle of precipitation is reproduced by the model. This includes the summer minimum for Ankara and the strong winter precipitation in Puerto Montt. Precipitation is ~~overestimated for Karlsruhe by roughly 50~~underestimated for Bangkok, especially in northern hemisphere spring. For all stations, the influence of land evaporation is strongest in their respective summer. ~~The central European stations~~ Vienna and Ankara show a decreasing influence of the ocean in winter~~with increasing distance to the ocean and~~ , typical for a more continental climate. For Puerto Montt, located between the Pacific and the Andean mountain range, and for ~~Halley station~~Bangkok, almost all precipitating water originates from the ocean.

The seasonal cycle of temperature is reproduced for all stations. Winter temperatures are too cold in ~~the model~~ this model configuration for all stations. This temperature bias can partly be explained by the fact that the altitude of all stations is higher in the model because of the coarse grid, e.g. 550 m for the grid point identified with Vienna versus 198 m for the GNIP station. Also, the measured temperatures are slightly higher than mean monthly ERA-Interim (Dee et al., 2011) two meter temperatures for the corresponding grid points (not shown).

~~Considering these meteorological biases, it can be stated that~~ Despite some biases, the mean values of δD and δ^{18}O are well reproduced by ICON-ART-Iso for all five stations. The seasonal cycle is captured correctly on the northern as well as on the southern hemisphere. Values of d-excess are also of ~~correct~~ similar magnitude. Model data is more variable than the measurements~~, but they are often in~~ . However, the model data is mostly within the standard deviation range of measurements. This demonstrates the capability of ICON-ART-Iso to simulate climatological patterns. The seasonal cycle and regional differences in δD and δ^{18}O are correctly reproduced ~~by the model in multi-year mean values of precipitation~~in this climatological integration.

3.3 Comparison with IASI satellite data for a seasonal perspective

~~This section compares~~ Here, we compare pairs of $\{H_2O, \delta D\}$ retrieved from MetOp/IASI remote sensing measurements with data from two simulations. ~~In doing so, the~~ The section closely follows the case studies presented by Schneider et al. (2017), who ~~compare IASI~~ compared IASI retrievals and data from the global, hydrostatic model ECHAM5-wiso (Werner et al., 2011).

3.3.1 IASI satellite data and model postprocessing

IASI (Infrared Atmospheric Sounding Interferometer) A and B are instruments on board the MetOp-A and MetOp-B satellites (Schneider et al., 2016). They measure thermal infrared spectra in nadir view from which free tropospheric $\{H_2O, \delta D\}$ pair data are derived. As the satellites circle the earth in polar, sunsynchronous orbit, each IASI instrument takes measurements twice a day at local morning (approximately 9:30) and evening (approximately 21:30) hours. ~~These data~~ The measurements are most sensitive ~~in~~ at a height of approximately 4.9 km. An IASI $\{H_2O, \delta D\}$ pair retrieval method has been developed and validated in the framework of the project MUSICA (MUlti-platform remote Sensing of Isotopologues for investigating the Cycle of Atmospheric water). The MUSICA retrieval method is presented by Schneider and Hase (2011) and Wiegele et al. (2014) with updates given in Schneider et al. (2016).

Schneider et al. (2017) present guidelines for comparing model data to the remote sensing data. First, a Retrieval Simulator software is used for simulating the MUSICA averaging kernel, using the atmospheric state of the model atmosphere. The simulated kernel is than applied to the original model state ($\boldsymbol{x}$) in order to calculate the state that would be reported by the satellite retrieval product ($\hat{\boldsymbol{x}}$, see Eq. 23).

$$\hat{\boldsymbol{x}} = \boldsymbol{A}(\boldsymbol{x} - \boldsymbol{x}_\mathrm{a}) + \boldsymbol{x}_\mathrm{a} \tag{23}$$

Here, $\boldsymbol{A}$ is the simulated averaging kernel and $\boldsymbol{x}_\mathrm{a}$ the a priori state. The a priori value used in the retrieval process for 4.9 km is at ~~{1780 ppm, −217.4 permil}~~{1780 ppm, −217.4‰}. This value represents the climatological state of the atmosphere. In the retrieval process, the satellite radiance measurements are used for estimating the deviation of the actual atmospheric state from the a priori assumed state, where it is important to note that the remote sensing retrieval product is not independent from the a priori assumptions (see Schneider et al. (2016) for more details). In Schneider et al. (2017), these guidelines have been followed for comparison of IASI data with ECHAM5-wiso model data. We use the same approach for comparisons to ICON-ART-Iso and our results can be directly compared to the results ~~achieved with~~ from the hydrostatic, global model ECHAM5-wiso.

In order to compare ICON-ART-Iso measurements with IASI data, ~~two simulations of four months are~~ a simulation of twelve months is used, which ~~were~~ was initialized on November 5, ~~2013, and May 5, 2014 (the same simulations have been used~~ 2013. This simulation uses a finer resolution of R2B06, corresponding to roughly 40 km. Again, we use varying ocean surface temperatures and sea ice cover, see the specifications in Sec. 3.1~~)~~. As in Schneider et al. (2017), two target time periods are investigated from February 12-18 and August 12-18, respectively. As has been ~~shown~~ pointed out in Sec. 3.1, the amount of water remaining in the troposphere from initialization is negligible by using lead times of three months~~(also for vapor, not shown)~~. For this study, model output was interpolated to a regular $0.36° \times 0.36°$ grid, which is close to the 40 km ~~(R2B06)~~ resolution of the numerical ICON grid ~~close to the equator~~in the tropics. Output was written for every hour of simulation.

IASI observations are only available at cloud free conditions. In order to exclude cloud affected grid points in the ICON data, the total cloud cover simulated by ICON was used, denoted by C_clct. All points with $C_\mathrm{clct} > 90\%$ were excluded. The parameter C_clct goes into saturation quickly and 90% is reached even for thin clouds. Surface emissivity E_srf is a necessary input parameter for the Retrieval Simulator. In this first study, E_srf was set to 0.96 over land and 0.975 over the ocean. This is in accordance with the mean values as given by Seemann et al. (2008). In addition, Schneider et al. (2017) show in a sensitivity study that errors on the order of 10% in this value have only a limited influence on the averaging kernels as simulated by the Retrieval Simulator. ~~From the output of the Retrieval Simulator, values were only used~~ We follow the method outlined by Schneider et al. (2017) and use values only where the sensitivity metric $s_\mathrm{err} < 0.05$~~, as recommended by Schneider et al. (2017) . This assures meaningful results~~.

We examine results for different areas over ocean and over land, using all data from the satellite and the model in the respective areas. The scatter of $\{\mathrm{H_2O}, \delta\mathrm{D}\}$ is not shown directly. Instead, the figures show the isolines of relative normalized frequency, which is explained in App. A. In addition, Rayleigh fractionation curves are indicated in all figures. These are the same as those given by Schneider et al. (2017).

3.3.2 Seasonal and daily cycle

Seasonal and daily cycle are investigated in $\{H_2O, \delta D\}$ space. The seasonal cycle is discussed for different regions over the central Pacific Ocean. The daily cycle is considered in the tropics and subtropics, also investigating differences between land and ocean areas.

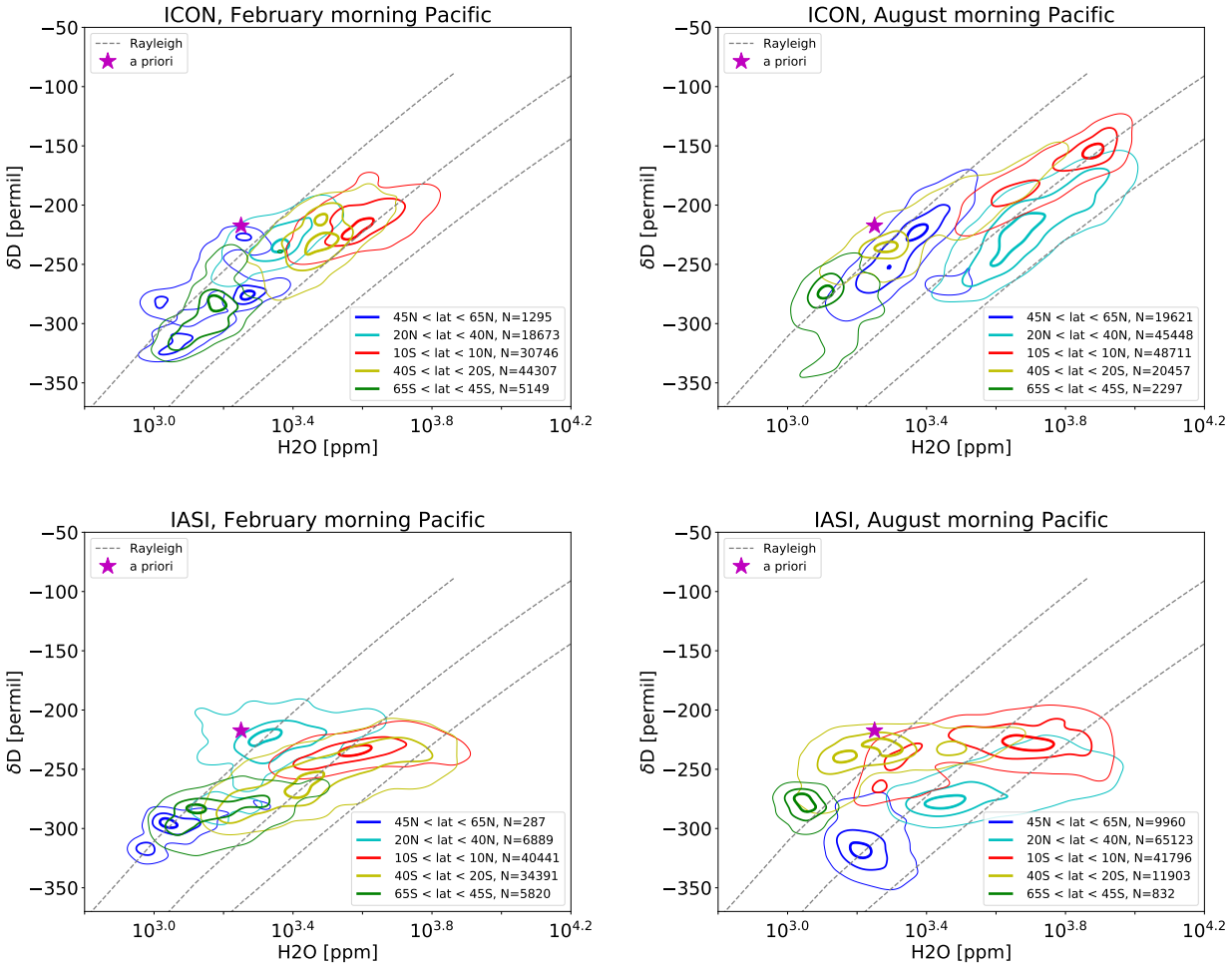

Figure 3. Isolines of the relative normalized frequency distribution for pairs of δD and H_2O (see App. A for ~~this~~ the method) after processing ICON-ART-Iso data with the IASI Retrieval Simulator of Schneider et al. (2017) (top) and IASI data for the same time (bottom). Data from morning overpasses are shown for 12 to 18 February (left) and 12 to 18 August (right), 2014, for different latitudinal bands over the Pacific Ocean (longitude $\lambda < 140°W$ or $\lambda > 140°E$). Contour lines are indicated at 0.2, 0.6 and 0.9 of the normalized distribution.

First, the seasonal cycle over the Pacific Ocean is examined by comparing the two target periods in different areas ($\lambda < 140°W$ or $\lambda > 140°E$ longitude and different latitudinal bins). Results are presented in Fig. 3, ~~which also gives~~ that incluedes

the exact latitudes. IASI data (bottom panels) show specific characteristics of the different regions. H_2O content is highest for tropical air masses and lowest for the highest latitudes in February and August. At the same time, tropical air is least depleted in HDO, while the highest latitudes show the lowest values of δD, i.e. are more depleted. When comparing February and August values at each latitude, a clear seasonal signal appears everywhere except for the tropics: During summer of the corresponding hemisphere, the air is more humid and more depleted in HDO. The distributions seem to shift from season to season along a line perpendicular to those of the Rayleigh model. The distribution in the tropics shows a broadened shape in August.

The results of ICON-ART-Iso are shown in the top panels of Fig. 3. The latitudinal dependence is similar to IASI: high H_2O and δD in the tropics and the lower values for mid-latitudes. The range of values is also very similar. The seasonal cycle in H_2O and δD is also reproduced to some degree, especially in the subtropical latitudes. The most obvious differences to IASI results occur in the northern hemisphere mid-latitudes in summer, which show less negative values of δD in the model than in the satellite data, especially for humid situations. In winter, this may also be the case, but there are only few humid values simulated at all or available in the satellite dataset. In general, the model shows a similar behavior as ECHAM5-wiso, the results of which are presented by Schneider et al. (2017).

For the daily cycle in the tropics and subtropics, land and ocean points are considered separately (Fig. 4, see caption for exact definition of the bins). IASI shows a clear signal of the daily cycle for both the tropics and subtropics over land (bottom panels of Fig. 4). There is no such signal over the ocean, where morning and evening distributions are almost identical. Over land, the water vapor in the tropics and subtropics is more depleted of HDO in the morning. There is also a daily cycle in H_2O in the tropics: During morning overpasses, H_2O values are higher than in the evening. Schneider et al. (2017) argue that this is due to the cloud filter, which removes areas of heavy convection in the evening. In the morning, the clouds have disappeared, but high humidity remains, especially in the lower troposphere. This ~~is partly~~ may partly be due to evaporation of rain drops, which explains the enhanced depletion in HDO (Worden et al., 2007). Over the Sahara (the subtropical land area considered), the daily cycle is different: While mixing ratios of H_2O rise only slightly during the day, there is a strong increase in the HDO content in the evening. This behavior can be attributed to vertical mixing (Schneider et al., 2017, and references therein).

The data retrieved from ICON-ART-Iso model simulations is shown in the top panels of Fig. 4. Tropical air (top left) over the land shows slightly lower mixing ratios for H_2O than IASI. The humidity of tropical ocean points is better reproduced. The difference in δD is stronger for both areas, with δD values being too high in the model. There is no daily cycle in the tropics for ICON-ART-Iso. The subtropical mixing ratios (top right) of H_2O over the ocean are similar to those in the tropics but cover a smaller range than those retrieved from IASI. The very humid and very dry parts of the IASI distribution are not reproduced by the model. ~~Over land, the values retrieved from ICON-ART-Isoshow a weak daily cycle, which is, however, much smaller compared to the IASI data.~~ δD values in ICON-ART-Iso are ~~substantially~~ larger than in the IASI retrievals. As pointed out by Schneider et al. (2017), the daily cycle in IASI also manifests itself in the number of samples passing the IASI cloud filter and quality control. The IASI cloud filter removes much more evening observations than morning observations, meaning more cloud coverage in the evening than in the morning. In contrast, the ICON-ART-Iso cloud filter removes a similar number of data for morning and evening~~simulations~~, i.e. in the model morning and evening cloud coverage is rather similar. This may also influence the results.

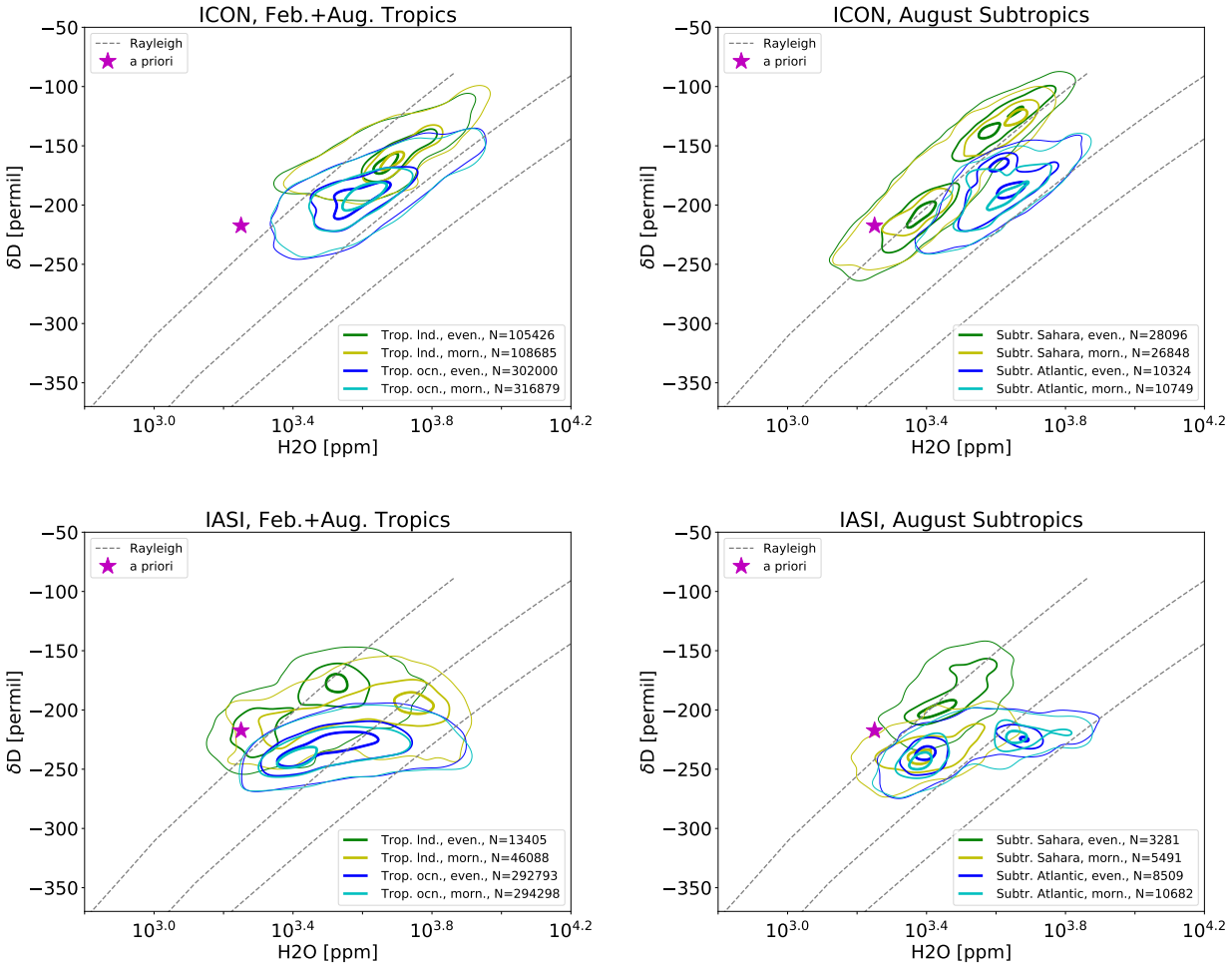

Figure 4. Isolines of the relative normalized frequency distribution for pairs of δD and H_2O (see App. A for ~~this~~ the method) after processing ICON-ART-Iso data with the IASI Retrieval Simulator of Schneider et al. (2017) (top) and IASI data for the same time (bottom). Left: Data corresponding to morning and evening overpasses for the tropics ($10^\circ S < \varphi < 10^\circ N$, all longitudes, summer and winter simulation) over land and over the ocean. Right: Morning and evening overpasses for the subtropics ($22.5^\circ S < \varphi < 35^\circ N$, summer simulation) over land (Saharan desert region, $10^\circ W < \varphi < 50^\circ E$) and Atlantic Ocean ($50^\circ W < \varphi < 30^\circ W$). Contour lines are indicated at 0.2, 0.6 and 0.9 of the normalized distribution.

To further analyze the influence of ocean and land areas, the analysis of the daily cycle is repeated, making use of the humidity tracers q^{ocn} and q^{lnd}. As has been ~~shown~~ pointed out in Sec. 3.1, q^{init} is negligible ~~already two months after initializations~~three months after initialization. To distinguish between grid points mostly influenced by ocean or land evaporation, we additionally use the following criteria to define ocean and land points: $q^{\mathrm{ocn}}/q^{\mathrm{ICON}} > 0.9$ for ~~oceanic grid points~~ grid points over the ocean, $q^{\mathrm{lnd}}/q^{\mathrm{ICON}} > 0.5$ for land grid points predominantly affected by land evaporation. ~~The contributions~~ This investigation serves to showcase how the ocean and land evaporation tracers can be used and the threshold values are therefore arbitrary to some degree. The tracer fields of water evaporating from ocean and land have not been processed with the retrieval simulator, instead values interpolated to 4.9 km are directly used.

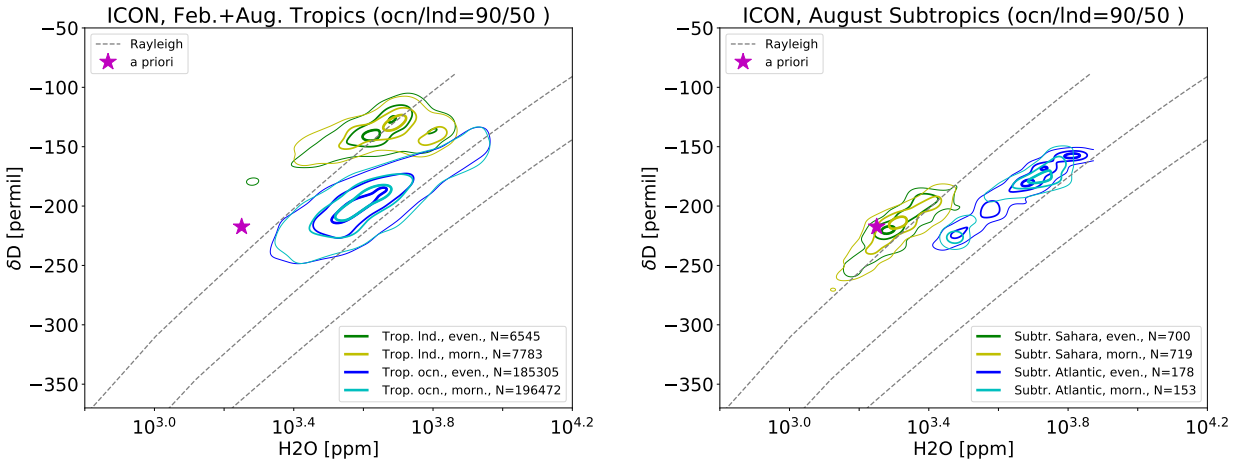

Figure 5. As Fig. 4 for ICON-ART-Iso. In addition to the land-ocean mask, land data must pass the condition $q_v^{\mathrm{lnd}}/q_v > 0.5$ and ocean data must pass $q_v^{\mathrm{ocn}}/q_v > 0.9$.

The result is shown in Fig. 5 for tropics and subtropics, using the same method as for Fig. 4. The characteristics of the different regions show up much more clearly with ~~these~~ the additional criteria. For the tropical ocean, the distribution of H_2O is similar, but the values are slightly more depleted in HDO~~, removing that end of the distribution that apparently has a strong influence by land evaporate~~. The distribution of pairs attributed to the land surface is reduced to values with relatively high humidity and enriched in HDO. The latter might be due to the signal of plant evapotranspiration, which is considered a non-fractionation process.

In the subtropics, the distributions over land change their shape completely and are ~~partly~~ separated from those over the ocean. The distribution for the subtropical ocean remains largely unchanged, becoming slightly more elongated with lower values in δD. For the land surface, the additional ~~criaterion~~ criterion strongly reduces the number of values that are considered. ~~50land evaporate~~ This implies that over the Saharan desert~~implies two different regimes: Either the air~~ , air mostly influenced by land evaporation (50% or more) is very dry and highly processed (low δD)~~, or the moisture content is large with relatively~~

~~high values in δD. This subset of the full distribution with high δDvalues also shows a strong daily cycle which is on the same order of magnitude as in the IASI data of Fig. 4~~.

This section shows that ICON-ART-Iso is able to reproduce regional differences and the seasonal cycle of $\{H_2O, \delta D\}$ of vapor in the lower troposphere. The additional water diagnostics are used to study the behavior of the model in more detail and ~~may~~ will help in investigating the measured distributions in future studies.

3.4 Comparing with in situ IAGOS-CARIBIC measurements

~~This sectionpresents~~ In this section, we present a first case study, in which results of ICON-ART-Iso are compared to in situ measurements of δD taken by the IAGOS-CARIBIC passenger aircraft at 9-12 km altitude. Two flights in September 2010 are considered, which took place a few days after the passage of the tropical cyclone Igor over the Atlantic ocean. The full dataset of all δD measurements ~~of IAGOS-CARIBIC taken~~ taken by IAGOS-CARIBIC in the tropics is also used as reference.

3.4.1 IAGOS-CARIBIC data and model postprocessing

In the European research infrastructure IAGOS-CARIBIC, a laboratory equipped with 15 instruments is deployed ~~onboard~~ on board a Lufthansa A340-600 for four intercontinental flights per month. Measurements of up to 100 trace gases and aerosol parameters are taken in situ and in air samples (Brenninkmeijer et al., 2007). δD is measured using the instrument ISOWAT (Dyroff et al., 2010). It is a tunable diode-laser absorption spectrometer that simultaneously measures HDO and H_2O at wave numbers near $3765\,cm^{-1}$ to derive δD in vapor. The instrument is calibrated based on regular calibration measurements (each 30 min) of a water vapor standard with 500 ppm H_2O and ~~δD = −109 permil~~$\delta D = -109‰$. The δD offset is derived by considering the data of the driest 5% of the air masses sampled during each flight, which is typically 4-8 ppm H_2O. At the flight altitude of 10-12 km, this is without exception lowermost stratospheric air (LMS), for which a δD of -600‰ is assumed (Pollock et al., 1980; Randel et al., 2012). An assumed uncertainty of this LMS value of 400‰ translates to a relevant uncertainty of 20‰ at 100 ppm H_2O. Due to further sources of measurement uncertainty, the data has a total flight specific systematic uncertainty up to 100‰. The total uncertainty is humidity dependent, decreasing towards higher humidity (e.g. 100‰ at 80 ppm H_2O ~~vs.~~ versus less than 20‰ at 500 ppm H_2O, see Christner (2015) for more details).

The in-situ IAGOS-CARIBIC data is suitable for the analysis of processes on small scales. δD measurements are available ~~as mean over one minute~~ one minute means, which translates to a spatial scale of approximately 15 km. This horizontal resolution ~~exceeds~~ is finer than the chosen ICON-ART-Iso configuration (R2B06 corresp. to 40 km) and is therefore ~~very suitable for validation in form of~~ suitable for a case study validation. Unfortunately, the uncertainty of δD data at humidity below approximately 40 ppm H_2O is too high to be used for analysis. Because of the systematic total uncertainty (see above), we use mean δD values from two flights through similar conditions.

In this section, measurements from a return flight from Frankfurt to Caracas on September 22, 2010 are analyzed (IAGOS-CARIBIC flight nrs. 309 and 310, taking off at 10:16 UTC in Frankfurt and 22:12 UTC in Caracas, respectively). The two flights crossed the Atlantic approximately two days after Hurricane Igor had passed the flight track. The storm caused large-

scale lofting of tropospheric air masses and a moistening at flight level. The high humidity at flight level (9-12 km) allowed many accurate δD-measurements to be taken.

An ICON-ART-Iso simulation was initialized with ECMWF IFS analysis data from September 12, 2010 and with the isotope values initialized as explained in Sec. 2.7. This corresponds to a ten day forecast for the time of the two flights. ~~Not~~ In this case, not all tropospheric water from the initialization has been replaced by water evaporated during the simulation at ~~this time . But~~ the time of analysis. However, the δD values adjust to local meteorology within a few days, developing realistic horizontal and vertical gradients. The simulation was set up on an R2B06 grid (≈ 40 km) with a time step of 240 s (convection called every second step). The ~~hourly output~~ output with a frequency of one snapshot per 15 minutes was examined on a $0.5°$ regular grid and interpolated linearly to the position of the aircraft. Fig. 6 shows δD in water vapor in the upper troposphere ~~along with the flight paths of the IAGOS-CARIBIC flights. The~~ roughly 24 hours before the flights cross the Atlantic~~shortly after the hurricane , sampling the model atmosphere where it has been influenced by the storm~~. The vortex signal of the hurricane clearly shows up in the δD field. The flight paths are also indicated in Fig. 6.

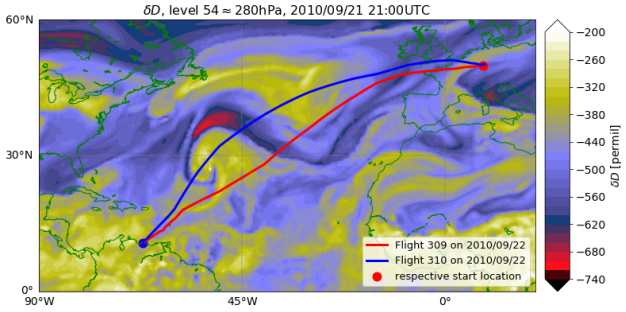

Figure 6. δD in water vapor on model level 54 (≈ 260 hPa) on September ~~22~~21, ~~10UTC~~21UTC, the date prior to that of the IAGOS-CARIBIC flights. The storm is visible in the western half of the plotted area (center approximately at ~~$20°N, 60°W$~~$30°N, 50°W$). The flight paths of IAGOS-CARIBIC flights 309 and 310 are also indicated by two lines, where the departure ~~location is~~ locations are emphasized.

3.4.2 Results for flights in tropical regions

In order to compare ~~data processed~~ values influenced by hurricane Igor, model and measurement data from flights 309 and 310 are considered in latitudes around the storm track only ($0°N < \varphi < 30°N$). ~~A sample of~~ For reference, all tropical δD values ~~taken from a model simulation and~~ from the IAGOS-CARIBIC database ~~is also examinedfor reference~~are also examined. To create a comparable dataset from model data, the results of the decadal simulation presented in Sec. 3.1 were interpolated to the location of these measurements and are treated in the same manner. As in Sec. 3.3, the distribution of pairs of $\{H_2O, \delta D\}$ are examined. The results are shown in Fig. 7.

The distribution of IAGOS-CARIBIC δD-measurements is shown in the ~~top~~ left panel of Fig. 7~~(panel A)~~. The tropical measurement sample (blue contours) consists of all ~~respective~~ relevant measurements ($23.5°S < \varphi < 23.5°N$). While most

tropical values are centered around -500‰ in δD and 100 ppm to 150 ppm H_2O, there is also a tail towards more humid pairs in the distribution. The lower limit in δD follows the curves of Rayleigh fractionation. The measurement data from flights 309 and 310 (red contours) show different characteristics. The range in H_2O is similar to the maximum density values of all tropical values, but the samples are more depleted in HDO. The humid branch is ~~missing~~not continuous and the area of high humidity is sparsely populated. In general, both distributions are limited by the detection limit of 40 ppm in H_2O, while contour lines may reach slightly lower values because of the smoothing that is applied in processing the data (see App. A).

~~To create the larger sample of pairs of δDand from model data, a longer simulation of ICON-ART-Isowas used (the same simulation that was compared with IASI data in August 2014, see Sec. 3.3). 30 output files were randomly chosen and from each file and 200 data points were randomly drawn from tropical latitudes in each file. Data was only considered within the pressure range of 180 hPa $< p <$ 280 hPa to consider the flight altitude of IAGOS-CARIBIC. Together with the samples along the paths of flights 309-310, the probability distribution~~ Model results are shown in the right ~~panels~~ panel of Fig. 7~~(panels B and D). For the top panel (B), the parameterization of Stewart (1975) for fractionation during evaporation of the hydrometeors is used (as in all other sections). For comparison, the lower right panel (D) uses the parameterization of Blossey et al. (2010) . Model data laong~~ . For this figure, model data along the flight tracks ~~are~~ is used only where accurate ~~deld-measurements~~ δD-measurements are available.

A limit of 40 ppm is also applied to the model data. The isolines ~~covering~~ stretching to lower value pairs again result from smoothing the data. ~~The bottom left panel of Fig. 7 (panel C) shows the distributions without this limit (using the parameterization of Blosse The distribution is different for dry situations, which shows that there are situations which are not captured by the IAGOS-CARIBIC measurements.~~

The distribution from the tropical model sample is in some ways similar to the one by all tropical ~~CARIBIC~~ IAGOS-CARIBIC measurements (comparing the blue contours of ~~panel A to B and D~~the two panels): There is a tail towards high humidities and the upper limit of δD is roughly at -400‰, while the lower limit is given by the second Rayleigh curve. ~~This is true for both parameterizations of fractionation during evaporation~~The model sample is 4% lower in δD on average (H_2O reduced by 18%). The mean for all values within the lowest density contour in $\{H_2O, \delta D\}$ is at $\{193.5\,\text{ppm}, -478.0‰\}$ for measurements, while it is at $\{175.4\,\text{ppm}, -482.0‰\}$ for the model sample ($\{131.7\,\text{ppm}, -481.6‰\}$ for measurements versus $\{72.7\,\text{ppm}, -543.6‰\}$ in case of the highest density contour).

The main characteristics of the distribution for the two flights ~~is slightly different between IAGOS-CARIBIC and ICON-ART-Iso~~followin Hurricane Igor is captured by the model ICON-ART-Iso (comparing the red contours of ~~panel A to B and D) . The modeled distribution includes more humid values than the measurements. It is shifted to more negative values~~ the two panels) and the center of the distribution is below the full tropical sample. The model sample is slightly reduced in δD ~~relative~~ (1.1%) when comparing to the full tropical sample, ~~as in the measurements~~but 12.3% more humid. From this simulation and these measurements alone, it is difficult to say if these discrepancies result from errors in the meteorological representation of the hurricane or in the physical parameterizations of the model. The good agreement between model and measurements in general is promising, while details will need to be examined in ~~a future study.~~

A

B

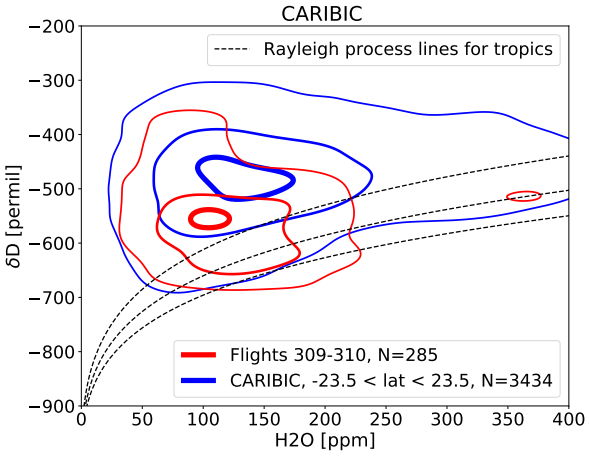

C

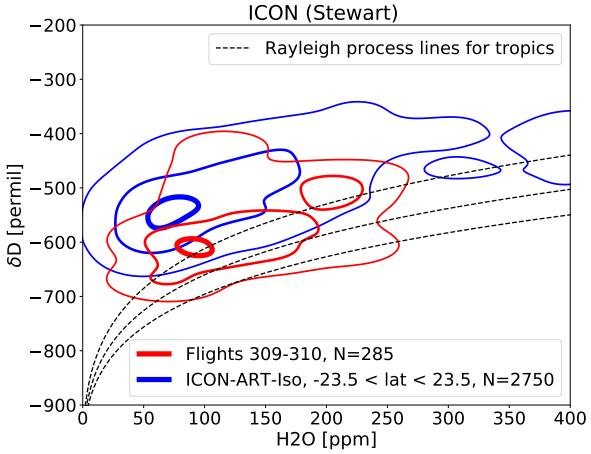

D

Figure 7. Isolines of the relative normalized frequency distribution (contours at 0.10.05, 0.4 and 0.9, see App. A for the method) of IAGOS-CARIBIC measurements (top left, A) and ICON-ART-Iso model simulations for tropical samplesand IAGOS-CARIBIC flights 309-310. Model data is , interpolated onto the paths of the two IAGOS-CARIBIC flights for two realizations of using different parameterizations of fractionation during evaporation of hydrometeors 309-310 (following Stewart (1975) , top right, panel B, and Blossey et al. (2010) , bottom right, panel D). The total number of datapoints in each distribution is given by the value N. Model data is considered only in locations where there are also with measurements and the H_2O measurement limit of 40 ppm is also considered (right panels B and D). In the bottom left panel C, this limitation is dropped, the parameterization of Blossey et al. (2010) is used here. The tropical in model samples were created by randomly drawing datafrom a four months simulation (of Sec. 3.1), considering the limits in pressure of IAGOS-CARIBIC ($180\,\mathrm{hPa} < p < 280\,\mathrm{hPa}$).

~~In this respect it is interesting to compare the two parameterizations for fractionation during evaporation (panels B and D of Fig. 7). The parameterization of Blossey et al. (2010) , panel D, produces values of δD~~that ~~are approximately 50lower than those using the parameterization by Stewart (1975) , panel B. At the first impression, the results using the parameterization by Blossey et al. (2010) seem more similar to the IAGOS-CARIBIC measurements, but it is again difficult to decide from this model run alone. The comparison demonstrates the capability of the model to simulate different realizations of during one model integration. It also shows the range of influence that a specific parameterization can have on the results~~future studies.

By using the other three diagnostic moisture tracers (initialization water q^{init} and water evaporating from the ocean and land, q^{ocn} and q^{lnd}), the model results are examined further. The two transatlantic flights spent little time over land areas. Accordingly, q_v^{lnd} only reaches an average of ~~3 5~~2.8% for both flights, ~~15~~19.9% at maximum. ~~Roughly 50~~An average of 47.2% of the sampled water originates from the initialization (59.6% maximum), while the remainder has evaporated from the ocean in the course of the simulation. Part of the discrepancies between model and measurements may thus result from the ~~rough~~ simplified representation of δD in the initial vapor field, while the influence of the approximated land surface isotope values remains limited.

This is analyzed in more detail in Fig. 8. Values of δD and H_2O along the flight paths are combined with information on the origin of the water that is sampled in the model. ~~Here,~~ W stands for the ratio of vapor that originates from land or ocean evaporation or initialization, e.g. $W^{\text{init}} = q_v^{\text{init}}/q_v$. In Fig. 8, the scatter is colorcoded by W^{ocn}. Because W^{lnd} is very low during ~~the longer~~ most parts of the flights and especially so over the ocean, $W^{\text{ocn}} = 1 - W^{\text{init}}$ is a good approximation. In Fig. 8, green colors indicate $W^{\text{lnd}} > 10\%$, where the approximation of a binary solution is not valid.

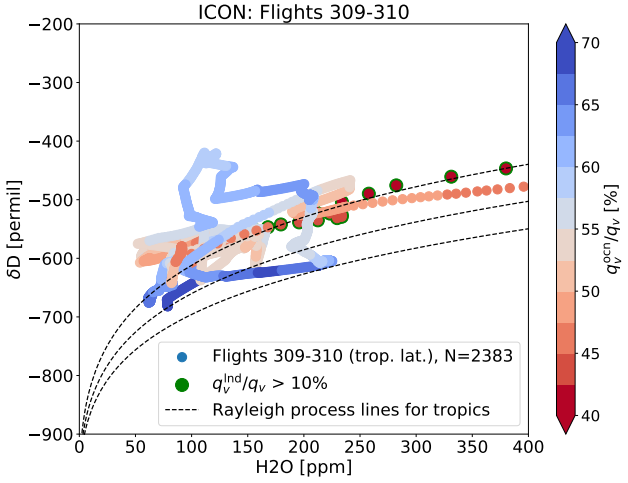

Figure 8. Scatter of δD against H_2O from ICON-ART-Iso interpolated to the flight paths of IAGOS-CARIBIC flights 309 and ~~310, using the parameterization of Stewart (1975) .~~ 310. Color coding indicates the ratio of $W^{\text{init}} \approx 1 - W^{\text{ocn}}$ in percent. Locations with $W^{\text{lnd}} > 10\%$ are marked in green. Values are considered where $p < 280\,\text{hPa}$.

Fig. 8 shows the strong influence of the ocean. More than 50% of the sampled vapor originates from ocean evaporation for long parts of the flights. ~~Water with high ratios of q_v^{Ind} is generally less depleted in .~~

Those values with the highest values of W^{init} ~~are very dry and show show high δD. Vertical cross sections along the flight tracks (not shown) indicate that these values come from the second half of flight 310, which encountered an intrusion of upper tropospheric or stratospheric air. This part of the model atmosphere is strongly influenced by the initialization profile~~(low W^{ocn}) mostly follow the course of the Rayleigh fractionation lines. The lowest and highest values in δD are reached where W^{ocn} is high (low values of W^{init})~~and the air has been heavily processed by the model.~~

~~The pairs of $\{H_2O, \delta D\}$ displayed in Fig. 8 show signals of different processes, which can be read from the scatter (see Worden et al., 2007) . Only short parts along of the flight tracks sample data indicating a Rayleigh process. A broad range of values is simulated for high W^{ocn} or high W^{init}. This demonstrates that ICON-ART-Isois capable of capturing different non-Rayleigh~~ , indicating that the isotopologues in the model have seen many fractionating and transport processes. This includes air mass mixing, but also the microphysical and convective processes that are imprinted on the isotopologue ratio. The exact nature of these processes remain to be investigated in future studies.

4 Conclusions

We present ICON-ART-Iso, the ~~isotope enabled~~ isotope-enabled version of the global atmospheric model ICON ~~. The article describes~~ (Zängl et al., 2015) . We describe the model formulation ~~of~~ as well as a set of evaluation studies. By using parts of the ICON-ART infrastructure (Schröter et al., 2018) , the model is very flexible in terms of the simulated moisture tracers. These can be set to resemble either H_2O (tagged water) or the stable isotopologues HDO or $H_2{}^{18}O$ if fractionation is turned on. The physics of fractionation are largely based on the model COSMOiso (Pfahl et al., 2012) . The first part of this article gives a detailed explanation of the parameterizations that have been implemented in ICON-ART-Iso to simulate the fractionation of water isotopologues.

We first evaluate tagged H_2O tracers of moisture evaporating from land and ocean to investigate the moisture sources of precipitation. This demonstrates the capabilities of ICON-ART-Iso to use tagged water as an additional diagnostic. The latitudinal dependence is similar to that given by other studies (e.g. Risi et al., 2013) . The following three sections then investigate the performance of the model for the simulation of the isotopologues, considering (i) multi annual, (ii) regional and (iii) meso-scale applications.

For a multi annual evaluation, the simulated isotopologues HDO and $H_2{}^{18}O$ from a ~~seven year~~ decadal simulation on a relatively coarse grid (160 km horizontal resolution) are compared to measurements taken from the network of GNIP stations (Terzer et al., 2013; IAEA/WMO, 2017) . The model ~~is shown to simulate~~ simulates δD and $\delta^{18}O$ reasonably well, reproducing the seasonal cycle of $\delta^{18}O$ and the range in d-excess for different stations in the northern and southern hemisphere. ~~The analysis demonstrates the long term stability of the model and~~ This investigation presents a first climatological application.

Regional differences in pairs of $\{H_2O, \delta D\}$ in lower free-tropospheric water vapor are then compared to data retrieved from IASI satellite measurements for a summer and winter case (Schneider and Hase, 2011; Wiegele et al., 2014; Schneider et al., 2016, 2017) .

The latitudinal dependence of these pairs is comparable to those from IASI retrievals. The seasonal cycle over the Pacific ocean and the overall values are reproduced by the model in both seasons. The difference between land and ocean surfaces in the tropics and subtropics in the model is of similar magnitude as in the measurements. However, the daily cycle that is observed in the satellite data is not reproduced in the model. Overall, the performance is similar to that of ECHAM5-wiso ~~(see Schneider et al., 2017)~~ (Werner et al., 2011; Schneider et al., 2017) .

In a meso-scale application, a first comparison with in situ measurements uses δD in upper-tropospheric water vapor from two IAGOS-CARIBIC flights (Brenninkmeijer et al., 2007) transecting the Atlantic and from all tropical IAGOS-CARIBIC ~~measurements~~δD measurements (Dyroff et al., 2010) . ICON-ART-Iso is able to reproduce the general features of the tropical IAGOS-CARIBIC dataset. The characteristics of the samples taken during two flights shortly after Hurricane Igor in September 2010 are also captured by the model. ~~This study is used to discuss differences that appear in the results because of different parameterizations for fractionation during the evaporation of hydrometeors.~~

In all three applications, the tagged evaporation water from the ocean or land surfaces ~~proofs~~ proves to be a valuable tool. It reveals a seasonal cycle in the precipitation water origin or shows the influence of the initialization in case of the comparison with IAGOS-CARIBIC data.

ICON-ART-Iso is a promising tool for future investigations of the atmospheric water cycle. This study demonstrates the flexibility of ~~the model~~ ICON-ART-Iso in terms of the setup for different diagnostics but also in terms of horizontal resolution and time scale. For future applications, it will be interesting to ~~implement~~ use a nudging of ~~meteological~~ meteorological variables towards analysis data to facilitate comparisons with measurements in different case studies. Fractionation will be implemented in different microphysical schemes to make the model numerically more efficient and even better applicable to climatological questions. Due to its flexible setup, ICON-ART-Iso is ready to simulate ~~instances of~~ tracers corresponding to $H_2{}^{17}O$ or to be used as a testbed for new microphysical parameterizations.

Code and data availability. The CARIBIC measurement data analyzed in this paper can be accessed by signing the CARIBIC data protocol to be downloaded at http://www.caribic-atmospheric.com/. The ICON code can be obtained from DWD after signing the license agreement available from icon@dwd.de. The ICON-ART code can be obtained after signing the license agreement available from bernhard.vogel@kit.edu.

Appendix A: Preparing the relative normalized frequency distributions

Sec. 3.3 and 3.4 show and discuss distributions of $\{H_2O, \delta D\}$. The scatter of $\{H_2O, \delta D\}$ is not shown directly as the figures would be too cluttered. Instead, the normalized relative frequency is discussed, isolines of which are shown in the different figures. This method has been adopted from Christner (2015). Fig. A1 shows the scatter and the isolines of normalized relative frequency for the IAGOS-CARIBIC measurements of flights 309-310, which are discussed in Sec. 3.4.

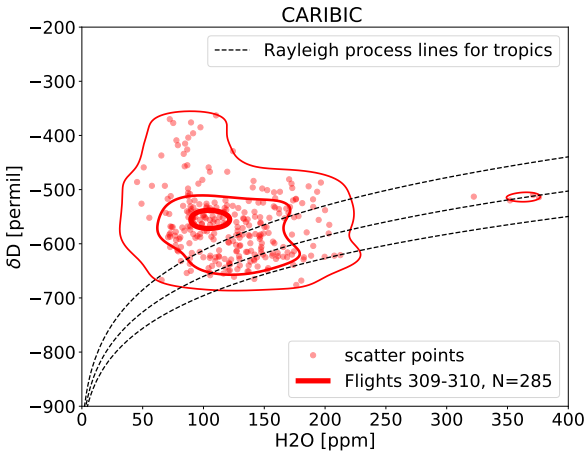

Figure A1. Scatter and isolines of the relative normalized frequency distribution for tropical (latitude $\varphi < 30^\circ N$) measurements of δD and H_2O from IAGOS-CARIBIC flights 309 and 310 (September 2010). The figure demonstrates how the isolines (indicated at 0.1, 0.4 and 0.9) relate to the underlying scatter.

To arrive at the isolines, the data ~~is~~ are binned in H_2O and δD on a grid of $5\,\mathrm{ppm} \times 5‰$. In case of IASI data, the data is binned in $\log_{10} H_2O$ (ppm) $\times$ δD on a grid of 0.05×5. Histogram counts are then interpolated onto a 1000×1000 grid. This is smoothed with a Gaussian filter with a standard deviation of 20 (15 in case of IASI). This smoothed data is then normalized by the sum of all value pairs and then normalized by the maximum value. Within this array of smoothed counts, isolines are drawn at 0.9, 0.4 and ~~0.1~~ 0.05 (0.9, 0.6 and 0.2 in case of IASI).

Appendix B: Fractionation during evaporation of hydrometeors following Blossey et al. (2010)

For evaporation and equilibration of rain and melting hydrometeors, the parameterization following Stewart (1975) has been presented in this paper, see Sec. 2.5 and Eq. 6 therein. As an alternative, we have also implemented the parameterization by Blossey et al. (2010) . For completeness, this parameterization is given in Eq. B1. In order to make a comparison easy, Eq. B2 again states the parameterization by Stewart (1975) . Like above, both are given in the formulation for the evaporation of rain.

The notation is the same as in the main body text.

$$ {}^{h}S_r^{\text{evap, Blossey}} = A \, \frac{{}^{h}f}{{}^{l}f} \frac{{}^{h}D}{{}^{l}D} \left[R_r \alpha_{\text{liq}} \, {}^{l}\rho^*_{l,\infty} - {}^{h}\rho_v \left(1 + B_l \left(1 - \alpha_{\text{liq}} \frac{R_r}{R_v} \right) \right) \right] \tag{B1} $$

$$ {}^{h}S_r^{\text{evap, Stewart}} = A \left(\frac{{}^{h}D}{{}^{l}D} \right)^{n} \left[R_r \alpha_{\text{liq}} \, {}^{l}\rho^*_{l,\infty} - {}^{h}\rho_v \right] \tag{B2} $$

$$ A = \frac{4\pi a^{l} f^{l} D}{1 + B_l} \tag{B3} $$

$$ B_l = \frac{{}^{l}D \, L_e^2 \, {}^{l}e^*_{l,\infty}}{k_a \mathcal{R}_v^2 T_\infty^3} \tag{B4} $$

By the above formulation, the difference of the two parameterizations is easily accessible. While the empirical equation by Stewart (1975) introduces the exponent n, which is determined by measurements, the parameterization by Blossey et al. (2010) modulates the saturation difference by a factor determined by the actual isotopologue ratios in the hydrometeor and the surrounding vapor. The ratio of ventilation factors f is an additional tuning parameter in the parameterization by Blossey et al. (2010) which is set to 1 in standard setup. A detailed comparison to the results of Stewart (1975) is postponed to a later study in order to keep this paper concise.

Author contributions. Johannes Eckstein programmed ICON-ART-Iso as an extension to ICON, performed and evaluated the simulations and prepared the manuscript. This was done with Roland Ruhnke as main and Peter Braesicke as as overall advisor. Stephan Pfahl provided the code of COSMOiso and helped in understanding and implementing the fractionating code. Christopher Diekmann has taken over the work on ICON-ART-Iso and implemented some of the features after submission to GMDD. Daniel Reinert was the main contact person at DWD and helped with the model ICON. Daniel Rieger and Jennifer Schröter aided in the technical development of the ICON-ART part of the model code and helped to solve many technical problems during the development of ICON-ART-Iso. Emanuel Christner provided and discussed data and results of the comparison with IAGOS-CARIBIC. Andreas Zahn is the coordinator of IAGOS-CARIBIC. Christoph Dyroff was responsible for setting up and maintaining the instrument ISOWAT. Matthias Schneider provided data and discussed results of the comparison with IASI satellite data.

Competing interests. There are no competing interests to declare.

Acknowledgements. The authors would like to thank three anonymous reviewers for their helpful comments on the manuscript and A. Lauer for taking over the editorship. We would also like to thank A. Seifert and M. Raschendorfer of DWD for discussions and help with parts of the ICON model code. This work was partly performed on the computational resource ForHLR II funded by the Ministry of Science, Research and the Arts Baden-Württemberg and DFG ("Deutsche Forschungsgemeinschaft"). The MUSICA/IASI data have been produced in

the framework of the projects MUSICA (funded by the European Research Council under the European Community's Seventh Framework Programme (FP7/2007-2013) / ERC Grant agreement number 256961) and MOTIV (funded by ~~the~~ the Deutsche Forschungsgemeinschaft under GZ SCHN 1126/2-1). We thank all the members of the IAGOS-CARIBIC team. The collaboration with Lufthansa and Lufthansa Technik and the financial support from the German Ministry for Education and Science (grant 01LK1301C) are gratefully acknowledged.

References

Bechtold, P., Semane, N., Lopez, P., Chaboureau, J.-P., Beljaars, A., and Bormann, N.: Representing equilibrium and nonequilibrium convection in large-scale models, Journal of the Atmospheric Sciences, 71, 734–753, 2014.

Blossey, P. N., Kuang, Z., and Romps, D. M.: Isotopic composition of water in the tropical tropopause layer in cloud-resolving simulations of an idealized tropical circulation, Journal of Geophysical Research: Atmospheres, 115, 2010.

Bosilovich, M. G. and Schubert, S. D.: Water vapor tracers as diagnostics of the regional hydrologic cycle, Journal of Hydrometeorology, 3, 149–165, 2002.

Brenninkmeijer, C. A. M., Crutzen, P., Boumard, F., Dauer, T., Dix, B., Ebinghaus, R., Filippi, D., Fischer, H., Franke, H., Frieß, U., Heintzenberg, J., Helleis, F., Hermann, M., Kock, H. H., Koeppel, C., Lelieveld, J., Leuenberger, M., Martinsson, B. G., Miemczyk, S., Moret, H. P., Nguyen, H. N., Nyfeler, P., Oram, D., O'Sullivan, D., Penkett, S., Platt, U., Pupek, M., Ramonet, M., Randa, B., Reichelt, M., Rhee, T. S., Rohwer, J., Rosenfeld, K., Scharffe, D., Schlager, H., Schumann, U., Slemr, F., Sprung, D., Stock, P., Thaler, R., Valentino, F., van Velthoven, P., Waibel, A., Wandel, A., Waschitschek, K., Wiedensohler, A., Xueref-Remy, I., Zahn, A., Zech, U., and Ziereis, H.: Civil Aircraft for the Regular Investigation of the Atmosphere Based on an Instrumented Container: The new CARIBIC system, Atmospheric Chemistry and Physics, 7, 4953–4976, https://doi.org/10.5194/acp-7-4953-2007, 2007.

Cappa, C. D., Hendricks, M. B., DePaolo, D. J., and Cohen, R. C.: Isotopic fractionation of water during evaporation, Journal of Geophysical Research: Atmospheres, 108, https://doi.org/10.1029/2003JD003597, 4525, 2003.

Cauquoin, A. and Risi, C.: Importance of the advection scheme for the simulation of water isotopes over Antarctica by general circulation models: a case study with LMDZ-iso (LMDZ5a revision 1750), Geoscientific Model Development Discussions, 2017, 1–10, https://doi.org/10.5194/gmd-2017-178, 2017.

Christner, E.: Messungen von Wasserisotopologen von der planetaren Grenzschicht bis zur oberen Troposphäre zur Untersuchung des hydrologischen Kreislaufs, Ph.D. thesis, KIT, IMK-ASF, H.-v.-Helmholtz-Platz 1, 76344 Leopoldshafen, 2015.

Craig, H.: Isotopic variations in meteoric waters, Science, 133, 1702–1703, 1961.

Craig, H. and Gordon, L.: Deuterium and oxygen 18 variations in the ocean and marine atmospher, in: Stable Isotopes in Oceanographic Studies and Paleotemperatures, edited by Tongiogi, E., pp. 9–130, V. Lishi e F., Pisa, 1965.

Dansgaard, W.: The O18-abundance in fresh water, Geochimica et Cosmochimica Acta, 6, 241–260, 1954.

Dansgaard, W.: Stable isotopes in precipitation, Tellus, 16, 436–468, https://doi.org/10.3402/tellusa.v16i4.8993, 1964.

Dee, D. P., Uppala, S. M., Simmons, A. J., Berrisford, P., Poli, P., Kobayashi, S., Andrae, U., Balmaseda, M. A., Balsamo, G., Bauer, P., Bechtold, P., Beljaars, A. C. M., van de Berg, L., Bidlot, J., Bormann, N., Delsol, C., Dragani, R., Fuentes, M., Geer, A. J., Haimberger, L., Healy, S. B., Hersbach, H., Hólm, E. V., Isaksen, L., Kållberg, P., Köhler, M., Matricardi, M., McNally, A. P., Monge-Sanz, B. M., Morcrette, J.-J., Park, B.-K., Peubey, C., de Rosnay, P., Tavolato, C., Thépaut, J.-N., and Vitart, F.: The ERA-Interim reanalysis: configuration and performance of the data assimilation system, Quarterly Journal of the Royal Meteorological Society, 137, 553–597, https://doi.org/10.1002/qj.828, 2011.

Dyroff, C., Fütterer, D., and Zahn, A.: Compact diode-laser spectrometer ISOWAT for highly sensitive airborne measurements of water-isotope ratios, Applied Physics B, 98, 537–548, https://doi.org/10.1007/s00340-009-3775-6, 2010.

Galewsky, J., Steen-Larsen, H. C., Field, R. D., Worden, J., Risi, C., and Schneider, M.: Stable isotopes in atmospheric water vapor and applications to the hydrologic cycle, Reviews of Geophysics, 54, 809–865, https://doi.org/10.1002/2015RG000512, 2016.

Gat, J. R.: Oxygen and hydrogen isotopes in the hydrologic cycle, Annual Review of Earth and Planetary Sciences, 24, 225–262, 1996.

Gat, J. R.: Isotope hydrology : a study of the water cycle, Series on environmental science and management ; 6, Imperial College Press, London, 2010.

Gimeno, L., Stohl, A., Trigo, R. M., Dominguez, F., Yoshimura, K., Yu, L., Drumond, A., Durán-Quesada, A. M., and Nieto, R.: Oceanic and terrestrial sources of continental precipitation, Reviews of Geophysics, 50, 2012.

Gonfiantini, R., Stichler, W., and Rozanski, K.: Reference and intercomparison materials for stable isotopes of light elements, Tech. Rep. IAEA-TECDOC-825, International Atomic Energy Agency, 1993.

Gunson, M. R., Abbas, M., Abrams, M., Allen, M., Brown, L., Brown, T., Chang, A., Goldman, A., Irion, F., Lowes, L., et al.: The Atmospheric Trace Molecule Spectroscopy (ATMOS) experiment: Deployment on the ATLAS space shuttle missions, Geophysical Research Letters, 23, 2333–2336, 1996.

Heinze, R., Dipankar, A., Henken, C., Moseley, C., Sourdeval, O., Trömel, S., Xie, X., Adamidis, P., Ament, F., Baars, H., Barthlott, C., Behrendt, A., Blahak, U., Bley, S., Brdar, S., Brueck, M., Crewell, S., Deneke, H., Di Girolamo, P., Evaristo, R., Fischer, J., Frank, C., Friederichs, P., Göcke, T., Gorges, K., Hande, L., Hanke, M., Hansen, A., Hege, H.-C., Hoose, C., Jahns, T., Kalthoff, N., Klocke, D., Kneifel, S., Knippertz, P., Kuhn, A., van Laar, T., Macke, A., Maurer, V., Mayer, B., Meyer, C., Muppa, S., Neggers, R. A. J., Orlandi, E., Pantillon, F., Pospichal, B., Röber, N., Scheck, L., Seifert, A., Seifert, P., Senf, F., Siligam, P., Simmer, C., Steinke, S., Stevens, B., Wapler, K., Weniger, M., Wulfmeyer, V., Zängl, G., Zhang, D., and Quaas, J.: Large-eddy simulations over Germany using ICON: a comprehensive evaluation, Quart. J. Roy. Meteorol. Soc., 143, 69–100, https://doi.org/10.1002/qj.2947, 2017.

Holton, J. R. and Hakim, G. J.: An introduction to dynamic meteorology, Elsevier Academic Press, Amsterdam, 5. ed. edn., 2013.

Holton, J. R., Haynes, P. H., McIntyre, M. E., Douglass, A. R., Rood, R. B., and Pfister, L.: Stratosphere-troposphere exchange, Reviews of geophysics, 33, 403–439, 1995.

Horita, J. and Wesolowski, D. J.: Liquid-vapor fractionation of oxygen and hydrogen isotopes of water from the freezing to the critical temperature, Geochimica et Cosmochimica Acta, 58, 3425 – 3437, https://doi.org/http://dx.doi.org/10.1016/0016-7037(94)90096-5, 1994.

IAEA/WMO: Global Network of Isotopes in Precipitation. The GNIP Database., http://www.iaea.org/water, 2017.

Jacob, D. J.: Introduction to atmospheric chemistry, Princeton Univ. Press, Princeton, NJ [u.a.], 1999.

Joussaume, S. and Jouzel, J.: Paleoclimatic tracers: An investigation using an atmospheric general circulation model under ice age conditions: 2. Water isotopes, Journal of Geophysical Research: Atmospheres, 98, 2807–2830, https://doi.org/10.1029/92JD01920, 1993.

Joussaume, S., Sadourny, R., and Jouzel, J.: A general circulation model of water isotope cycles in the atmosphere, Nature, 311, 24–29, 1984.

Jouzel, J. and Merlivat, L.: Deuterium and oxygen 18 in precipitation: Modeling of the isotopic effects during snow formation, Journal of Geophysical Research: Atmospheres, 89, 11 749–11 757, https://doi.org/10.1029/JD089iD07p11749, 1984.

Jouzel, J., Merlivat, L., and Roth, E.: Isotopic study of hail, Journal of Geophysical Research, 80, 5015–5030, https://doi.org/10.1029/JC080i036p05015, 1975.

Klocke, D., Brueck, M., Hohenegger, C., and Stevens, B.: Rediscovery of the doldrums in storm-resolving simulations over the tropical Atlantic, Nature Geoscience, 10, 891, 2017.

Kraus, H.: Die Atmosphäre der Erde : eine Einführung in die Meteorologie, Springer, Berlin, 3 edn., 2004.

Lauritzen, P. H., Ullrich, P. A., Jablonowski, C., Bosler, P. A., Calhoun, D., Conley, A. J., Enomoto, T., Dong, L., Dubey, S., Guba, O., Hansen, A. B., Kaas, E., Kent, J., Lamarque, J.-F., Prather, M. J., Reinert, D., Shashkin, V. V., Skamarock, W. C., Sørensen, B., Taylor, M. A., and Tolstykh, M. A.: A standard test case suite for two-dimensional linear transport on the sphere: results from a collection of state-of-the-art schemes, Geoscientific Model Development, 7, 105–145, https://doi.org/10.5194/gmd-7-105-2014, http://www.geosci-model-dev.net/7/105/2014/, 2014.

Lee, J.-E. and Fung, I.: "Amount effect" of water isotopes and quantitative analysis of post-condensation processes, Hydrological Processes: An International Journal, 22, 1–8, 2008.

Lee, X., Sargent, S., Smith, R., and Tanner, B.: In Situ Measurement of the Water Vapor 18O/16O Isotope Ratio for Atmospheric and Ecological Applications, Journal of Atmospheric and Oceanic Technology, 22, 555–565, https://doi.org/10.1175/JTECH1719.1, 2005.

LeGrande, A. N. and Schmidt, G. A.: Global gridded data set of the oxygen isotopic composition in seawater, Geophysical Research Letters, 33, https://doi.org/10.1029/2006GL026011, 2006.

Majoube, M.: Fractionnement en oxygén 18 et in deutérium entre l'eau et sa vapeur, Journal de Chimie Physique et de Physico-Chimie Biologique, 68, 1423, 1971.

Merlivat, L. and Jouzel, J.: Global climatic interpretation of the deuterium-oxygen 18 relationship for precipitation, Journal of Geophysical Research: Oceans, 84, 5029–5033, 1979.

Merlivat, L. and Nief, G.: Fractionnement isotopique lors des changements d'état solide-vapeur et liquide-vapeur de l'eau à des températures inférieures à 0 C, Tellus, 19, 122–127, 1967.

Mook, W. G.: Environmental isotopes in the hydrological cycle, Principles and Applications, vol. 2, International Atomic Energy Agency, UNESCO, Paris, 2001.

Morrison, H., Jensen, A. A., Harrington, J. Y., and Milbrandt, J. A.: Advection of Coupled Hydrometeor Quantities in Bulk Cloud Microphysics Schemes, Monthly Weather Review, 144, 2809–2829, https://doi.org/10.1175/MWR-D-15-0368.1, 2016.

Numaguti, A.: Origin and recycling processes of precipitating water over the Eurasian continent: Experiments using an atmospheric general circulation model, Journal of Geophysical Research: Atmospheres, 104, 1957–1972, 1999.

Pfahl, S. and Wernli, H.: Lagrangian simulations of stable isotopes in water vapor: An evaluation of nonequilibrium fractionation in the Craig-Gordon model, Journal of Geophysical Research: Atmospheres, 114, 2009.

Pfahl, S., Wernli, H., Yoshimura, K., and Dubey, M.: The isotopic composition of precipitation from a winter storm–a case study with the limited-area model COSMO iso, Atmospheric Chemistry & Physics, 12, 2012.

Pinet, P. R.: Oceanography : an introduction to the planet oceanus, West Publishing, St. Paul, 2. ed. edn., 1993.

Pollock, W., Heidt, L. E., Lueb, R., and Ehhalt, D. H.: Measurement of stratospheric water vapor by cryogenic collection, Journal of Geophysical Research: Oceans, 85, 5555–5568, https://doi.org/10.1029/JC085iC10p05555, 1980.

Pruppacher, H. R. and Klett, J. D.: Microphysics of Clouds and Precipitation: Reprinted 1980, Springer Science & Business Media, 2012.

Randel, W. J., Moyer, E., Park, M., Jensen, E., Bernath, P., Walker, K., and Boone, C.: Global variations of HDO and HDO/H2O ratios in the upper troposphere and lower stratosphere derived from ACE-FTS satellite measurements, Journal of Geophysical Research: Atmospheres, 117, https://doi.org/10.1029/2011JD016632, 2012.

Rieger, D., Bangert, M., Bischoff-Gauss, I., Förstner, J., Lundgren, K., Reinert, D., Schröter, J., Vogel, H., Zängl, G., Ruhnke, R., et al.: ICON–ART 1.0–a new online-coupled model system from the global to regional scale, Geoscientific Model Development, 8, 1659–1676, 2015.

Rieger, D., Steiner, A., Bachmann, V., Gasch, P., Förstner, J., Deetz, K., Vogel, B., and Vogel, H.: Impact of the 4 April 2014 Saharan dust outbreak on the photovoltaic power generation in Germany, Atmos. Chem. Phys. Discuss., 2017, 1–31, https://doi.org/10.5194/acp-2017-441, 2017.

Riese, M., Ploeger, F., Rap, A., Vogel, B., Konopka, P., Dameris, M., and Forster, P.: Impact of uncertainties in atmospheric mixing on simulated UTLS composition and related radiative effects, Journal of Geophysical Research: Atmospheres (1984–2012), 117, 2012.

Risi, C., Bony, S., and Vimeux, F.: Influence of convective processes on the isotopic composition (δ18O and δD) of precipitation and water vapor in the tropics: 2. Physical interpretation of the amount effect, Journal of Geophysical Research: Atmospheres, 113, 2008.

Risi, C., Bony, S., Vimeux, F., and Jouzel, J.: Water-stable isotopes in the LMDZ4 general circulation model: Model evaluation for present-day and past climates and applications to climatic interpretations of tropical isotopic records, Journal of Geophysical Research: Atmospheres, 115, https://doi.org/10.1029/2009JD013255, 2010.

Risi, C., Noone, D., Frankenberg, C., and Worden, J.: Role of continental recycling in intraseasonal variations of continental moisture as deduced from model simulations and water vapor isotopic measurements, Water Resources Research, 49, 4136–4156, 2013.

Schmidt, G. A., Ruedy, R. A., Miller, R. L., and Lacis, A. A.: Attribution of the present-day total greenhouse effect, Journal of Geophysical Research: Atmospheres, 115, https://doi.org/10.1029/2010JD014287, 2010.

Schneider, M. and Hase, F.: Optimal estimation of tropospheric H_2O and δD with IASI/METOP, Atmospheric Chemistry and Physics, 11, 11 207–11 220, https://doi.org/10.5194/acp-11-11207-2011, 2011.

Schneider, M., Wiegele, A., Barthlott, S., González, Y., Christner, E., Dyroff, C., García, O. E., Hase, F., Blumenstock, T., Sepúlveda, E., Mengistu Tsidu, G., Takele Kenea, S., Rodríguez, S., and Andrey, J.: Accomplishments of the MUSICA project to provide accurate, long-term, global and high-resolution observations of tropospheric H_2O,δD pairs – a review, Atmospheric Measurement Techniques, 9, 2845–2875, https://doi.org/10.5194/amt-9-2845-2016, 2016.

Schneider, M., Borger, C., Wiegele, A., Hase, F., García, O. E., Sepúlveda, E., and Werner, M.: MUSICA MetOp/IASI H_2O,δD pair retrieval simulations for validating tropospheric moisture pathways in atmospheric models, Atmospheric Measurement Techniques, 10, 507–525, https://doi.org/10.5194/amt-10-507-2017, 2017.

Schröter, J., Rieger, D., Stassen, C., Vogel, H., Weimer, M., Werchner, S., Förstner, J., Prill, F., Reinert, D., Zängl, G., Giorgetta, M., Ruhnke, R., Vogel, B., and Braesicke, P.: ICON-ART 2.1: a flexible tracer framework and its application for composition studies in numerical weather forecasting and climate simulations, Geoscientific Model Development, 11, 4043–4068, https://doi.org/10.5194/gmd-11-4043-2018, 2018.

Seemann, S. W., Borbas, E. E., Knuteson, R. O., Stephenson, G. R., and Huang, H.-L.: Development of a Global Infrared Land Surface Emissivity Database for Application to Clear Sky Sounding Retrievals from Multispectral Satellite Radiance Measurements, Journal of Applied Meteorology and Climatology, 47, 108–123, https://doi.org/10.1175/2007JAMC1590.1, 2008.

Seifert, A.: On the Parameterization of Evaporation of Raindrops as Simulated by a One-Dimensional Rainshaft Model, Journal of the Atmospheric Sciences, 65, 3608–3619, https://doi.org/10.1175/2008JAS2586.1, 2008.

Seifert, A. and Beheng, K.: A two-moment cloud microphysics parameterization for mixed-phase clouds. Part 1: Model description, Meteorology and atmospheric physics, 92, 45–66, 2006.

Sherwood, S. C., Bony, S., and Dufresne, J.-L.: Spread in model climate sensitivity traced to atmospheric convective mixing, Nature, 505, 37–42, 2014.

Shine, K. P. and Sinha, A.: Sensitivity of the Earth's climate to height-dependent changes in the water vapour mixing ratio, Nature, 354, 382–384, 1991.

Souchez, R. and Jouzel, J.: On the isotopic composition in δD and δ 18 O of water and ice during freezing, Journal of Glaciology, 30, 369–372, 1984.

Souchez, R., Jouzel, J., Lorrain, R., Sleewaegen, S., Stiévenard, M., and Verbeke, V.: A kinetic isotope effect during ice formation by water freezing, Geophysical Research Letters, 27, 1923–1926, 2000.

Steinwagner, J., Milz, M., Clarmann, T. v., Glatthor, N., Grabowski, U., Höpfner, M., Stiller, G., and Röckmann, T.: HDO measurements with MIPAS, Atmospheric chemistry and physics, 7, 2601–2615, 2007.

Stewart, M. K.: Stable isotope fractionation due to evaporation and isotopic exchange of falling waterdrops: Applications to atmospheric processes and evaporation of lakes, Journal of Geophysical Research, 80, 1133–1146, 1975.

Taylor, K. E., Williamson, D., and Zwiers, F.: The sea surface temperature and sea-ice concentration boundary conditions for AMIP II simulations, Program for Climate Model Diagnosis and Intercomparison, Lawrence Livermore National Laboratory, University of California, 2000.

Terzer, S., Wassenaar, L. I., Araguás-Araguás, L. J., and Aggarwal, P. K.: Global isoscapes for δ^{18}O and δ^{2}H in precipitation: improved prediction using regionalized climatic regression models, Hydrology and Earth System Sciences, 17, 4713–4728, https://doi.org/10.5194/hess-17-4713-2013, 2013.

Tiedtke, M.: A comprehensive mass flux scheme for cumulus parameterization in large-scale models, Monthly Weather Review, 117, 1779–1800, 1989.

Van der Ent, R. J., Savenije, H. H., Schaefli, B., and Steele-Dunne, S. C.: Origin and fate of atmospheric moisture over continents, Water Resources Research, 46, 2010.

Werner, M., Langebroek, P. M., Carlsen, T., Herold, M., and Lohmann, G.: Stable water isotopes in the ECHAM5 general circulation model: Toward high-resolution isotope modeling on a global scale, Journal of Geophysical Research: Atmospheres, 116, https://doi.org/10.1029/2011JD015681, 2011.

Wiegele, A., Schneider, M., Hase, F., Barthlott, S., García, O. E., Sepúlveda, E., González, Y., Blumenstock, T., Raffalski, U., Gisi, M., and Kohlhepp, R.: The MUSICA MetOp/IASI H_2O and δD products: characterisation and long-term comparison to NDACC/FTIR data, Atmospheric Measurement Techniques, 7, 2719–2732, https://doi.org/10.5194/amt-7-2719-2014, 2014.

Worden, J., Bowman, K., Noone, D., Beer, R., Clough, S., Eldering, A., Fisher, B., Goldman, A., Gunson, M., Herman, R., Kulawik, S. S., Lampel, M., Luo, M., Osterman, G., Rinsland, C., Rodgers, C., Sander, S., Shephard, M., and Worden, H.: Tropospheric Emission Spectrometer observations of the tropospheric HDO/H2O ratio: Estimation approach and characterization, Journal of Geophysical Research: Atmospheres, 111, https://doi.org/10.1029/2005JD006606, 2006.

Worden, J., Noone, D., Bowman, K., Beer, R., Eldering, A., Fisher, B., Gunson, M., Goldman, A., Herman, R., Kulawik, S. S., et al.: Importance of rain evaporation and continental convection in the tropical water cycle, Nature, 445, 528–533, 2007.

Zängl, G., Reinert, D., Rípodas, P., and Baldauf, M.: The ICON (ICOsahedral Non-hydrostatic) modelling framework of DWD and MPI-M: Description of the non-hydrostatic dynamical core, Quarterly Journal of the Royal Meteorological Society, 141, 563–579, 2015.

From climatological to small scale applications: Simulating water isotopologues with ICON-ART-Iso (version 2.1)

Johannes Eckstein[1], Roland Ruhnke[1], Stephan Pfahl[2,3], Emanuel Christner[1], Christopher Diekmann[1], Christoph Dyroff[1,a], Daniel Reinert[4], Daniel Rieger[4], Matthias Schneider[1], Jennifer Schröter[1], Andreas Zahn[1], and Peter Braesicke[1]

[1]Karlsruhe Institute of Technology (KIT), Institute of Meteorology and Climate Research (IMK), Herrmann-von-Helmholtz-Platz 1, 76344 Eggenstein-Leopoldshafen, Germany
[2]ETH Zürich, Institute for Atmospheric and Climate Science, Universitätstrasse 16, 8092 Zürich, Switzerland
[3]Freie Universität Berlin, Institute of Meteorology, Carl-Heinrich-Becker-Weg 6-10, 12165 Berlin, Germany
[4]Deutscher Wetterdienst, Frankfurter Str. 135, 63067 Offenbach, Germany
[a]now at: Aerodyne Research Inc., 45 Manning Road, Billerica, MA 01821, USA

Correspondence to: Johannes Eckstein (johannes.eckstein@kit.edu)

Abstract. We present the new isotope-enabled model ICON-ART-Iso. The physics package of the global ICOsahedral Non-hydrostatic (ICON) modelling framework has been extended to simulate passive moisture tracers and the stable isotopologues HDO and $H_2{}^{18}O$. The extension builds on the infrastructure provided by ICON-ART, which allows a high flexibility with respect to the number of related water tracers that are simulated. The physics of isotopologue fractionation follow the model COSMOiso. We first present a detailed description of the physics of fractionation that have been implemented in the model. The model is then evaluated on a range of temporal scales by comparing with measurements of precipitation and vapor.

A multi annual simulation is compared to observations of the isotopologues in precipitation taken from the station network GNIP (Global Network for Isotopes in Precipitation). ICON-ART-Iso is able to simulate the main features of the seasonal cycles in δD and δ^{18}O as observed at the GNIP stations. In a comparison with IASI satellite retrievals, the seasonal and daily cycles in the isotopologue content of vapor are examined for different regions in the free troposphere. On a small spatial and temporal scale, ICON-ART-Iso is used to simulate the period of two flights of the IAGOS-CARIBIC aircraft in September 2010, which sampled air in the tropopause region influenced by Hurricane Igor. The general features of this sample as well as those of all tropical data available from IAGOS-CARIBIC are captured by the model.

The study demonstrates that ICON-ART-Iso is a flexible tool to analyze the water cycle of ICON. It is capable of simulating tagged water as well as the isotopologues HDO and $H_2{}^{18}O$.

1 Introduction

Water in gas, liquid and frozen form is an important component of the climate system. The ice caps and snow covered surfaces strongly influence the albedo of the surface (Kraus, 2004), the oceans are unmatched water reservoirs, which dissolve trace substances (Jacob, 1999) and redistribute heat (Pinet, 1993) and all animal and plant life depends on liquid water. The atmosphere is by mass the smallest compartment of the hydrological cycle, but it is this compartment that serves to transfer

water between the spheres of liquid, frozen and biologically bound water on the earth's surface (Gat, 1996). For atmospheric processes themselves, water is also of great importance. It is the strongest green house gas (Schmidt et al., 2010) and distributes energy through the release of latent heat (Holton and Hakim, 2013), while liquid and frozen particles influence the radiative balance (Shine and Sinha, 1991).

A correct description of the atmospheric water cycle is therefore necessary for the understanding and simulation of the atmosphere and the climate system (Riese et al., 2012; Sherwood et al., 2014). The stable isotopologues of water are unique diagnostic tracers that provide a deeper insight into the water cycle (Galewsky et al., 2016). Because of the larger molar mass of the heavy isotopologues, their ratio to (standard) water is changed by phase transitions. This change in the ratio is termed fractionation. Considering the isotopologue ratio of the heavy isotopologues in vapor and precipitation (liquid or ice) provides an opportunity to develop an advanced understanding of the processes that shape the water cycle.

Pioneering research on measuring the heavy isotopologues of water starting in the 1950's first examined the isotopologues in precipitation (Dansgaard, 1954, 1964). First theoretical advances on the microphysics (Jouzel et al., 1975; Jouzel and Merlivat, 1984) and surface evaporation (Craig and Gordon, 1965) enabled the implementation of heavy isotopologues in global climate models (Joussaume et al., 1984; Joussaume and Jouzel, 1993). Since then, measurement techniques and modeling of the isotopologues have advanced. Measurements of the isotopic content of vapor first required cryogenic samplers (Dansgaard, 1954), but in the last 15 years laser absorption spectroscopy has made in situ observations possible (Lee et al., 2005; Dyroff et al., 2010). Today, the isotopologue content in atmospheric vapor can also be derived from satellite measurements (Gunson et al., 1996; Worden et al., 2006; Steinwagner et al., 2007; Schneider and Hase, 2011). Many global and regional circulation models have been equipped to simulate the atmospheric isotopologue distribution, focusing on the global scale (Risi et al., 2010; Werner et al., 2011) or regional phenomena (Blossey et al., 2010; Pfahl et al., 2012, both limited area models). Despite this progress, the potential of isotopologues in improving the understanding and physical description of the single processes "remains largely unexplored" (Galewsky et al., 2016). A more extensive literature overview on the subject is given by Galewsky et al. (2016).

We present ICON-ART-Iso, the newly developed, isotopologue enabled version of the global ICOsahedral Nonhydrostatic (ICON) modelling framework (Zängl et al., 2015). By design, ICON is a flexible model, capable of simulations from climatological down to turbulent scales (Heinze et al., 2017). The advection scheme of ICON has been designed to be mass conserving (Zängl et al., 2015), which is essential for the simulation of water isotopologues (Risi et al., 2010). ICON-ART-Iso builds on the flexible infrastructure provided by the extension ICON-ART (Rieger et al., 2015; Schröter et al., 2018), which has been developed to simulate aerosols and trace gases.

By equipping ICON with the capabilities to simulate the water isotopologues, a first step is made to a deeper understanding of the water cycle. From the multitude of isotopologue enabled global models (see Galewsky et al. (2016) for an overview), ICON-ART-Iso stands out by its non-hydrostatic base model core, enabling simulations with fine horizontal resolution on a global grid. It is flexible in design to simulate diagnostic evaporation tracers as well as the isotopologues HDO and $H_2{}^{18}O$ during a single simulation.

This article first gives some technical details on ICON and ICON-ART. This is followed by a detailed description of the physics special to ICON-ART-Iso, which have been implemented in ICON to simulate the isotopologues (Sec. 2).

The remaining sections describe model results and first validation studies: Section 3.1 looks at passive moisture tracers. Focus is laid on the source regions - ocean or land - of the water that forms precipitation. The next section (Sec. 3.2) compares data from a simulation spanning more than ten years on a coarse grid to measurements from different stations of the GNIP network. A further validation with measurements is performed in Sec. 3.3. Retrievals from IASI satellite measurements are compared with ICON-ART-Iso results for two weeks in winter and summer 2014, considering the seasonal and daily cycle in different regions. Section 3.4 then discusses the comparison with IAGOS-CARIBIC measurements. In situ data from two flights are compared with results of ICON-ART-Iso simulations. Section 4 summarizes and concludes the study.

2 The model ICON-ART-Iso

This section presents the technical and physical background of the model ICON-ART-Iso. First, ICON and the extension ICON-ART are introduced. Next, general thoughts on simulating a diagnostic water cycle are presented. Starting in Sec. 2.3, the main processes that influence the distribution of the isotopologues are discussed in separate sections: surface evaporation, saturation adjustment, cloud microphysics and convection. To close this technical part, Sec. 2.7 discusses the initialization of the model.

2.1 Introduction to the modeling framework ICON-ART

ICON-ART-Iso is the isotope-enabled version of the model ICON. ICON is a new non-hydrostatic general circulation model which is developed and maintained in a joint effort by Deutscher Wetterdienst (DWD) and Max-Planck-Institute for Meteorology (MPI-M). Its horizontally unstructured grid can be refined locally by one-way or two-way nested domains with a higher resolution. The model is applicable from global to turbulent scales: At DWD, ICON is used operationally for global numerical weather prediction (currently $13\,\mathrm{km}$ horizontal resolution, with a nest of $6.5\,\mathrm{km}$ resolution over Europe). Klocke et al. (2017) show the potential of using ICON for convection permitting simulations and it already proved successful as a Large Eddy Simulation (LES) model (Heinze et al., 2017). It is currently also being prepared for climate projections at MPI-M. More details on ICON are given by Zängl et al. (2015).

ICON-ART-Iso builds on the numerical weather prediction physics parameterization package of ICON. The physical parameterizations that have been implemented for the simulation of the isotopologues mainly correspond to those of the model COSMOiso as presented by Pfahl et al. (2012). As the same parameterizations have been described before, the following subsections give only a short summary of each of the different fractionation processes.

In ICON, all tracer constituents are given as mass fractions $q_x = \frac{\rho_x}{\rho}$, where $\rho = \sum_x \rho_x$ is the total density, including all water constituents x. To discriminate values of the heavy isotopologues, these will be denoted by the index h while standard (light) water will be indexed by l. ICON standard water is identified with the light isotopologue $^{1}\mathrm{H}_2{}^{16}\mathrm{O}$, which is a very good assumption also made by Blossey et al. (2010) and Pfahl et al. (2012): Standard water is much more abundant than the lighter

isotopologues, with a ratio of one to $3.1 \cdot 10^{-4}$ for HDO and $2.0 \cdot 10^{-3}$ for $H_2{}^{18}O$ (Gonfiantini et al., 1993). Water in ICON-ART-Iso exists in seven different forms (vapor, cloud water, ice, rain, snow, graupel and hail), each of which is represented by one tracer for standard water and each of the isotopologues. The amount of the isotopologues is expressed relative to standard water by the isotopologue ratio $R = {}^{h}q_x / {}^{l}q_x$. This is referenced to standard ratios of the Vienna Mean Ocean Standard Water (R_{VSMOW}) in the δ notation: $\delta = R_{\mathrm{sample}}/R_{\mathrm{VSMOW}} - 1$, with δ values then given in per mil. If not noted otherwise, δ values are always evaluated for the vapor phase in this paper, which is why this specification is omitted throughout the text.

As in the current version of ICON-ART (Schröter et al., 2018), an XML table is used to define the settings for each of the isotopologues. While this paper mostly discusses realizations of HDO and $H_2{}^{18}O$, this choice is technically arbitrary. The XML table is used to define the tracers at runtime, making a recompilation of the model unnecessary. All tuning parameters can be specified separately for each isotopologue in the XML table and the number of realizations is limited only by the computational resources. Each parameterization describing fractionation can also be turned off separately for each isotopologue, making very different experiments possible during one simulation. This makes the model very flexible and allows using several different water tracers during one model run.

2.2 Simulating a diagnostic water cycle

The isotopologues are affected by all the processes that also influence standard water in ICON: Surface evaporation, saturation adjustment to form clouds, cloud microphysics and convection. Each of these main processes is represented by several parameterizations. Some of these parameterizations include phase changes of or to vapor and in turn lead to a change in the isotopologue ratio - which is termed isotopic fractionation. In addition, advection and turbulent diffusion are non-fractionating processes that change the spatial distribution of all trace substances.

An important prerequisite to a simulation of water isotopologues is a good implementation of advection. ICON-ART makes use of the same numerical methods that are used for advecting the hydrometeors in ICON itself. These assure local mass conservation (Zängl et al., 2015) and mass-consistent transport. The latter is achieved by making use of the same mass flux in the discretized continuity equations for total density and partial densities, respectively (Lauritzen et al., 2014). The advection schemes implemented in ICON conserve linear correlations between tracers and assure the monotonicity of each advected tracer. Note, however, that this does not guarantee monotonicity of the isotopologue ratios (see Morrison et al., 2016).

The parameterizations that influence the water cycle also include processes that do not fractionate. For all non-fractionating processes, the transfer rate ${}^{h}S$ of the heavier isotopologues are defined by Eq. 1.

$$ {}^{h}S = {}^{l}S \cdot R_{\mathrm{source}} \tag{1} $$

Here, ${}^{l}S$ is the transfer rate of ICON standard water, while R_{source} is the isotopologue ratio in the source reservoir of the transfer.

In order to turn any fractionating processes into a non-fractionating one, its respective equation for the transfer rate of the heavy isotopologues can be replaced with Eq. 1. This has been implemented as an option in all processes that describe fractionation, that are explained below. If all processes are set to be non-fractionating in this way, the isotopologue ratio does not change and the species will resemble the standard water of ICON. This is an important feature which can be used to test

the model for self-consistency or to investigate source regions with diagnostic moisture tracers, so called tagged water (e.g. Bosilovich and Schubert, 2002). An application of this will be shown in Sec. 3.1.

Whenever phase changes occur that include the vapor phase, the isotopologue ratio changes because the heavier isotopologues have different diffusion constants and a different saturation vapor pressure compared to standard water. For the diffusion constant ratio, two choices have been implemented for HDO and $H_2{}^{18}O$, making available the values of Merlivat and Jouzel (1979) or Cappa et al. (2003). The differences in saturation pressure are expressed by the equilibrium fractionation factor α, which is the ratio of isotopologue ratios in thermodynamic equilibrium (Mook, 2001), see Eq. 2.

$$\alpha = \frac{R_v}{R_{\text{cond}}} < 1 \tag{2}$$

Here, R_v stands for the isotopologue ratio in the vapor phase, while R_{cond} stands for that in the condensed phase. The ratio α depends on temperature and is different over water and over ice (termed α_{liq} and α_{ice}). The parameterizations by Majoube (1971) and by Horita and Wesolowski (1994) have been implemented for α_{liq} and those by Merlivat and Nief (1967) for α_{ice}. Note the definition for α given in Eq. 2 is also used in COSMOiso (Pfahl et al., 2012), and is the inverse of the definition used by others, e.g. by Blossey et al. (2010).

2.3 Surface evaporation

Surface evaporation is the source for the atmospheric water cycle. In ICON-ART-Iso, the evaporative surface flux is split into evaporation from land and water surfaces, transpiration from plants and dew and rime formation. Transpiration is considered a non-fractionating process (Eq. 1), which is an assumption also made by Werner et al. (2011) or Pfahl et al. (2012). Dew and rime formation (and condensation on the ocean surface) are considered to fractionate according to equilibrium fractionation (Eq. 2). For the evaporation part of the full surface flux, two parameterizations have been implemented (Pfahl and Wernli, 2009; Merlivat and Jouzel, 1979). Both build on the Craig-Gordon model (Craig and Gordon, 1965; Gat, 2010). Equation 3 gives the general expression for R_{evap}.

$$R_{\text{evap}} = k \cdot \frac{\alpha_{\text{liq}} R_{\text{surf}} - h R_v}{1 - h} \tag{3}$$

Here, h is the specific humidity of the lowest model layer relative to the specific humidity at the surface and k is the non-equilibrium fractionation factor. The two parameterization differ in their description of k. While Merlivat and Jouzel (1979) give a parameterization that depends on the surface wind, Pfahl and Wernli (2009) have simplified this to be wind speed independent. In summary, Eq. 4 is used to calculate the surface flux of the isotopologues, ${}^hF^{tot}$.

$${}^hF^{tot} = {}^lF^{\text{evap}} \cdot R_{\text{evap}} + {}^lF^{\text{transp}} \cdot R_{\text{surf}} + {}^lF^{\text{dew}} \cdot \frac{R_v}{\alpha_{\text{liq}}} + {}^lF^{\text{rime}} \cdot \frac{R_v}{\alpha_{\text{ice}}} \tag{4}$$

For transpiration and evaporation, the isotopologue ratio of the surface and ground water (R_{surf}) is necessary. The surface model TERRA (included in ICON) was not extended with isotopologues, so R_{surf} is not available as a prognostic variable. Over land, it is therefore approximated by R_{VSMOW} in Eq. 3 and 4. Of course, this is a simplification that allows testing the atmospheric physics package and will be developed further. Over the ocean, the dataset provided by LeGrande and Schmidt

(2006) has been implemented. Values for HDO are given in this dataset, while those for $H_2{}^{18}O$ are determined from the relationship given by the global meteoritic water line (GMWL), $\delta D = 8 \cdot \delta^{18}O + 10‰$ (Craig, 1961).

2.4 Saturation adjustment

Cloud water is formed by saturation adjustment in ICON. Vapor in excess of saturation vapor pressure is transferred to cloud water and temperature is adjusted accordingly. This is repeated in an iterative procedure. For the isotopologues, the iteration does not have to be repeated. Instead, Eq. 5 is applied directly, using the adjusted values of ICON water. This is the same equation used in COSMOiso (Pfahl et al., 2012) and by Blossey et al. (2010).

$$ {}^{h}q_c = \frac{{}^{h}q_v + {}^{h}q_c}{1 + \alpha_{\mathrm{liq}} \frac{{}^{l}q_v}{{}^{l}q_c}} \tag{5} $$

2.5 Microphysics

Several grid-scale microphysical schemes are available in ICON. ICON-ART-Iso makes use of the two moment scheme by Seifert and Beheng (2006). This scheme computes mass and number densities of vapor, cloud water, rain and four ice classes (ice, snow, graupel and hail) and can be used to simulate aerosol-cloud interaction, see Rieger et al. (2017). As the isotopologues are diagnostic values, the number densities do not have to be simulated separately. The two moment scheme describes more than 60 different processes, but only those processes that include the vapor phase lead to fractionation. All others are described by Eq. 1 in the model. Isotopic effects also occur during freezing of the liquid phase (Souchez and Jouzel, 1984; Souchez et al., 2000), but this is neglected due to the low diffusivities, as in COSMOiso. In accordance with Blossey et al. (2010) and Pfahl et al. (2012), sublimation is also assumed not to fractionate. Condensation to form liquid water happens only during the formation of cloud water and is accounted for by the saturation adjustment. The fractionating processes that remain are ice formation by nucleation, vapor deposition (on all four ice classes) and evaporation of liquid hydrometeors. Besides rain, a fraction of the three larger ice classes (snow, graupel, hail) can evaporate after melting. This liquid water fraction is currently not a prognostic variable.

The two moment scheme by Seifert and Beheng (2006) uses mass densities instead of mass ratios, so we adopt the change in notation here, denoting mass densities by ρ. Vapor pressures are denoted by e. The star (*) indicates values at saturation with respect to liquid (index l) or ice (index i).

For evaporation of rain and melting hydrometeors, the semi-empirical parameterization of Stewart (1975) has been implemented and is discussed in this paper. It allows the exchange of heavy isotopologues with the surroundings in supersaturated as well as subsaturated conditions. The corresponding transfer rate is given in Eq. 6. The equation is given in the formulation for the evaporation of rain, with details on the evaporation of melting ice hydrometeors explained below. In this process, it is

assumed that the whole drop has time to equilibrate, which is a simplification when compared to e.g. Lee and Fung (2008).

$$ {}^{h}S_r^{\text{evap}} = A \left(\frac{{}^{h}D}{{}^{l}D} \right)^{n} \left[R_r \alpha_{\text{liq}} {}^{l}\rho^*_{l,\infty} - {}^{h}\rho_v \right] \tag{6} $$

$$ A = \frac{4\pi a {}^{l}f {}^{l}D}{1 + B_l} \tag{7} $$

$$ B_l = \frac{{}^{l}D \, L_e^2 \, {}^{l}e^*_{l,\infty}}{k_a \mathcal{R}_v^2 T_\infty^3} \tag{8} $$

Here, a is the radius of the hydrometeor, ${}^{l}f$ is the ventilation factor, R_v and R_r are the isotopologue ratios in the vapor and the hydrometeor, $\mathcal{R}_v$ the gas constant of water vapor and L_e and k_a the latent heat of evaporation and the heat conductivity in air. The index ∞ indicates that values are evaluated for the surroundings. The ratio of the diffusion constants D is given by the literature values cited above and can be chosen at the time of simulation for each isotopologue. The tuning parameter n is set to 0.58 by default (Stewart, 1975), but can be changed at runtime.

Note that an alternative parameterization to describe the fractionation of evaporating or equilibrating hydrometeors (that of Blossey et al. (2010)) has also been implemented in the model. For completeness, the physics of this parameterization is briefly explained in App. B in comparison to Stewart (1975). An investigation of this parameterization and the difference to Stewart (1975) will be provided in a later study.

The underlying equation for both parameterizations is derived from fundamentals of cloud microphysics (see Pruppacher and Klett, 2012). It is also used in the microphysical scheme of ICON, where ${}^{l}S_x^{\text{evap}} = A({}^{l}e^*_{l,\infty} - {}^{l}e_v)$. The definitions of a and ${}^{l}f_v$ depend on whether S_x is calculated for rain (Seifert, 2008) or melting ice class hydrometeors (Seifert and Beheng, 2006). For melting ice class hydrometeors, the melting temperature of ice ($T_0 = 273.15\,\text{K}$) is used for the calculation of α_{liq} and in place of T_∞. This implies an additional factor of T_∞ / T_0 for melting ice hydrometeors, as ${}^{l}e^*_{l,\infty}$ is always evaluated at T_∞. Equation 6 otherwise also holds true for the evaporation of melting ice hydrometeors.

Fractionation during nucleation of ice particles or deposition on one of the four ice class hydrometeors is parameterized following Blossey et al. (2010), as in COSMOiso (Pfahl et al., 2012). The flux is assumed to interact only with the outermost layer of the hydrometeor, the isotopologue ratio of which is set to be identical to that of the depositional flux. The transfer rate ${}^{h}S_x^{\text{ice}}$ is then given by Eq. 9 with the fractionation factor α_k as given in Eq. 10. All symbols are used as above, with L_s being the latent heat of sublimation.

$$ {}^{h}S_x^{\text{ice}} = \alpha_k R_v \, {}^{l}S_x^{\text{ice}} \tag{9} $$

$$ \alpha_k = \frac{(1 + B_i) \, {}^{l}\mathcal{S}_i}{\frac{{}^{l}f \, {}^{l}D}{{}^{h}f \, {}^{h}D} ({}^{l}\mathcal{S}_i - 1) + \alpha_{\text{ice}} (1 + B_i \, {}^{l}\mathcal{S}_i)} \tag{10} $$

$$ B_i = \frac{{}^{l}D_v \, L_s^2 \, {}^{l}e^*_{i,\infty}}{k_a \mathcal{R}_v^2 \, T_\infty^3} \tag{11} $$

2.6 Convection

ICON uses the Tiedtke-Bechtold scheme for simulating convective processes (Tiedtke, 1989; Bechtold et al., 2014). The scheme uses a simple cloud model considering a liquid fraction in cloud water (denoted here by ω) and the remaining solid

fraction $(1-\omega)$. Fractionation happens during convective saturation adjustment (during initialization of convection and in updrafts), in saturated downdrafts and in evaporation below cloud base. The parameterizations are the same that have been implemented by Pfahl et al. (2012) in COSMOiso.

Convective saturation adjustment calculates equilibration between vapor and the total condensed water (liquid and ice). The parameterization used for grid scale adjustment therefore has to be expanded in order to be used in convection if the liquid water fraction is smaller than one. The isotopologue ratio is determined over liquid and ice particles separately. A closed system approach (Gat, 1996) is used for the liquid fraction ($R_v^{\text{by liq}}$ of Eq. 12). The underlying assumption for Eq. 13 used for the ice fraction is a Rayleigh process with the kinetic fractionation factor α_{eff} following Jouzel and Merlivat (1984). The two are then recombined according to the fraction of liquid water, following Eq. 14. This procedure has been adopted from COSMOiso (Pfahl et al., 2012).

$$R_v^{\text{by liq}} = R_v^{\text{old}} \frac{\alpha_{\text{liq}}}{1 + \frac{{}^{l}q_v^{\text{new}}}{{}^{l}q_v^{\text{old}}}(\alpha_{\text{liq}} - 1)} \tag{12}$$

$$R_v^{\text{by ice}} = R_v^{\text{old}} \left(\frac{{}^{l}q_v^{\text{new}}}{{}^{l}q_v^{\text{old}}} \right)^{\alpha_{\text{eff}}-1} \tag{13}$$

$$R_v = (1-\omega) \cdot R_v^{\text{by ice}} + \omega \cdot R_v^{\text{by liq}} \tag{14}$$

Here, the indices `old` and `new` denote the values of the respective variables before and after the convective saturation adjustment. The factor α_{eff} which appears in Eq. 13 is determined by Eq. 15. The supersaturation with respect to ice, ξ_{ice}, is calculated from Eq. 16, where $T_0 = 273.15\,\text{K}$ is used. The tuning parameter λ is set to 0.004 in the standard setup, following Pfahl et al. (2012) and Risi et al. (2010).

$$\alpha_{\text{eff}} = \frac{\xi_{\text{ice}}\zeta}{\xi_{\text{ice}} - 1 + \alpha_{\text{ice}}\zeta} \tag{15}$$

$$\xi_{\text{ice}} = 1 - \lambda(T - T_0) \tag{16}$$

Convective downdrafts are assumed to remain saturated by continuously evaporating precipitation (Tiedtke, 1989). In these saturated downdrafts, equilibrium fractionation is applied for the liquid fraction, while the ice fraction is assumed to sublimate without fractionation.

Evaporation of precipitation below cloud base is an important process for several reasons: it leads to a drop in the temperature and therefore influences dynamics, but is also important for the isotopic composition (Risi et al., 2008). To describe fractionation here, the parameterization by Stewart (1975) is again applied to the liquid fraction. Different to Eq. 6 for evaporation during microphysics, the integrated form is now applied. In following Stewart (1975), the ratio in the liquid part of the general hydrometeor after evaporation $R_{\text{adj}}^{\text{liq}}$ is given with Eq. 17. Here, f is the fraction of remaining condensate. $R_{\text{hyd}}^{\text{old}}$ is the isotopologue ratio in the hydrometeor before adjustment and rH is the relative humidity calculated as the vapor pressure over

saturation vapor pressure.

$$R_{\text{adj}}^{\text{liq}} = \gamma R_v + f^{\beta}\left(R_{\text{hyd}}^{\text{old}} - \gamma R_v\right) \tag{17}$$

$$\gamma = \frac{\text{rH}}{\alpha_{\text{liq}} - \mu} \tag{18}$$

$$\beta = \frac{\alpha_{\text{liq}} - \mu}{\mu} \tag{19}$$

$$\mu = (1 - \text{rH})\left(\frac{{}^{h}D}{{}^{l}D}\right)^{-n} \tag{20}$$

Using Eq. 17, the isotopologue ratio in the adjusted hydrometeor is given with Eq. 21. The ice fraction is assumed to sublimate without fractionation, maintaining its isotopologue ratio.

$$R_{\text{adj}} = (1-\omega)R_{\text{hyd}}^{\text{old}} + \omega R_{\text{adj}}^{\text{liq}} \tag{21}$$

Following Pfahl et al. (2012), an additional equilibration has been implemented to determine the final isotopologue ratio of the hydrometeors, which is given in Eq. 22. The parameter ξ_{add} is a tuning parameter that is set to 0.5 in the standard setup.

$$R_{\text{adj}}^{\text{final}} = R_{\text{adj}} + \xi_{\text{add}} \cdot \omega \left(\frac{R_v}{\alpha_{\text{liq}}} - R_{\text{adj}}\right) \tag{22}$$

2.7 Initialization of the isotopologues

A meaningful initialization is an important prerequisite for any simulation, also of the isotopologues. In addition to an initialization with a constant ratio to standard water, the isotopologues can be initialized with the help of mean measured δ values. Values at the lowest model level, the tropopause level (WMO definition, see Holton et al., 1995) and model top are prescribed for vapor and linear and log-linear interpolation is applied below and above the tropopause, respectively. Values for the tropopause level and the model top are taken from MIPAS measurements (Steinwagner et al., 2007), the value at the lowest level is a standard value taken from Gat (2010). All values are given in Table 1. By using the local tropopause height, an adaptation to the local meteorological situation is assured. To calculate the δ value of the hydrometeors, a constant offset is applied to the local δ value of vapor. The literature provides values for HDO, while those for $H_2{}^{18}O$ are determined from the relationship given by the global meteoritic water line (GMWL, Craig, 1961).

	literature	HDO	$H_2{}^{18}O$
δ_{bottom}	Gat (2010)	-50	-5
$\delta_{\text{tropopause}}$	Steinwagner et al. (2007)	-650	-80
δ_{top}	Steinwagner et al. (2007)	-400	-48.75
δ_{offset}	Gat (2010)	-100	-11.25

Table 1. Values for the initialization with mean measured δ values. Literature provides the values for HDO, values for $H_2{}^{18}O$ have been determined from GMWL (Craig, 1961).

3 Model evaluation results

In the following sections, we present first results and comparisons of model simulations with measurements spanning several spatio-temporal scales: Sec. 3.1 shows how the model simulated diagnostic H_2O can be used to investigate source regions of the (modeled) water cycle. Sec. 3.2 compares results for precipitation from the same long model integration with measurements taken from the GNIP network (Terzer et al., 2013; IAEA/WMO, 2017). Sec. 3.3 looks at seasonal and regional differences by comparing model output with pairs of $\{H_2O, \delta D\}$ derived from IASI satellite measurements (Schneider et al., 2016). Finally, Sec. 3.4 presents a first case study, in which simulated values of δD are compared with measurements from the IAGOS-CARIBIC project (Brenninkmeijer et al., 2007). All simulations discussed here are free-running.

In the following sections, we focus on H_2O (ICON standard water) and of HDO and $H_2{}^{18}O$. The settings for each isotopologue are defined at runtime, which is why the specifications for the simulations are given here. The diffusion constant ratio is set to the values of Merlivat and Jouzel (1979) and the equilibrium fractionation is parameterized following Majoube (1971) over liquid water and following Merlivat and Nief (1967) over ice. Surface evaporation is described by the parameterization of Pfahl and Wernli (2009). The parameterization by Merlivat and Jouzel (1979) has little influence on the values in the free troposphere and is not discussed further. The dataset by LeGrande and Schmidt (2006) for the isotopic content of the ocean surface is used for all isotopologues. Grid scale evaporation of hydrometeors is described by the parameterization by Stewart (1975) if not noted differently.

In addition to ICON standard water, three diagnostic sets of water tracers are simulated. All fractionation is turned off, so they resemble H_2O. But the evaporation and initialization is different: water indexed by `init` (as in q^{init}) is set to ICON water at initialization, but evaporation is turned off. In the course of the simulation, the water of this type precipitates out of the model atmosphere. Water indexed by `ocn` and `lnd` are initialized with zero and evaporate from the ocean (q^{ocn}) and land areas (q^{lnd}), respectively. The sum of q^{init}, $q^{\text{ocn}}$and q^{lnd}always equals the mass mixing ratio of ICON standard water, indexed as q^{ICON}. These tracers allow us to infer the relative importance of ocean and land evaporation - essentially the source of water in the model atmosphere - at all times. In addition to case studies, this is interesting because of the simplified implementation of isotopic processes during land evaporation in the current version of ICON-ART-Iso, see Sec. 2.3. The tracers of q^{init} provide information on the importance of the initialization at a certain time in the simulation.

3.1 An application of diagnostic water tracers: Precipitation source regions

This section examines the moisture source regions of precipitation over ocean and land. Gimeno et al. (2012) give a review of the subject, while e.g. Numaguti (1999), Van der Ent et al. (2010) and Risi et al. (2013) study this question by use of other models and in more detail.

Here, we use a decadal model integration. The simulation was initialized with ECMWF (European Centre for Medium-Range Weather Forecast) Integrated Forecast System (IFS) operational analysis data on January 1, 2007, 0UTC, to simulate 11 years on an R2B04 grid ($\approx 160\,\mathrm{km}$ horizontal resolution). The time step was set to $240\,\mathrm{s}$ (convection called every second step) and output was saved on a regular $1^\circ \times 1^\circ$ grid every $10\,\mathrm{h}$ in order to obtain values from all times of the day. Sea surface

temperatures and sea ice cover were updated daily, by linearly interpolating monthly data provided by the AMIP II project (Taylor et al., 2000). The first year is not considered as spin-up time of the model and the simulation is evaluated up to the end of 2017.

We look at the total precipitation P in northern hemisphere winter (December, January and February, denoted by DJF) and summer (June, July, August, denoted by JJA). Figure 1 displays zonal sums of P^{init}, P^{ocn} and P^{lnd} relative to standard water precipitation P^{ICON} as a function of latitude. The sum of precipitation that originates from convection is also given for each water species. The top panels give winter values while the bottom panels display the results for summer months.

The area covered by ocean is not equally distributed over different latitudinal bands, which is the reason why ocean and land points are considered separately. The center panels show the fraction of precipitation that has fallen over the ocean relative to the total precipitation and the area fraction of the ocean in each latitudinal band. Despite the characteristics of the different seasons, which will be discussed in the following paragraphs, the latitudinal distribution of the ocean area fraction largely determines the overall fraction of rain that falls over the ocean or over land. This is why the other panels display values of P relative to the sum over each compartment, not to the total sum.

To evaluate the model simulation, we use values starting in the second year. At this time, the tropospheric moisture has been completely replaced by water that has evaporated during the model run. This is demonstrated by the values of P^{init} close to zero in all four panels in Fig. 1. Technically, this means that the ternary solution of q^{init}, q^{ocean} and q^{land} that makes up q^{ICON} is practically reduced to a binary solution of only q^{ocean} and q^{land}. Other experiments show that this is already true after a few weeks (not shown).

During northern hemisphere winter over the ocean (top left panel of Fig. 1), the precipitation is strongly dominated by water that has evaporated from the ocean. Water from the land surface hardly reaches the ocean. Over land areas, the ocean is also the dominant source for precipitation, reaching more than 50% at almost all latitudes. In the northern hemisphere mid latitude land areas, more than 70% of the precipitated water originates from the ocean. The tropical and southern hemisphere land areas (in DJF) receive up to 40% of precipitation from land evaporation. Most precipitation at tropical and subtropical latitudes over the ocean originates from convection (indicated by dashed lines). The role of convection is much smaller over land areas and again stronger in the southern hemisphere. Note that in a simulation with very high horizontal resolution (for an example using ICON, see Klocke et al., 2017), more convective processes could have been directly resolved. In this specific case of a resolution close to 160 km, practically no convection is directly resolved by the model. It should therefore be considered that the amount of precipitation from convection only shows the importance of this parameterization in the simulations at this resolution.

The distribution of precipitation water sources is different in northern hemisphere summer (bottom row of Fig. 1). In summer, the northern hemisphere land areas (bottom right) supply themselves a substantial fraction of the moisture that then precipitates. The importance of convection is increased in northern hemisphere summer with its maximum influence shifted into northern mid-latitudes. Despite the larger moisture availability over the ocean, the far northern hemisphere land areas also supply the larger part of moisture that precipitates over the ocean in summer, see the lower left hand panel.

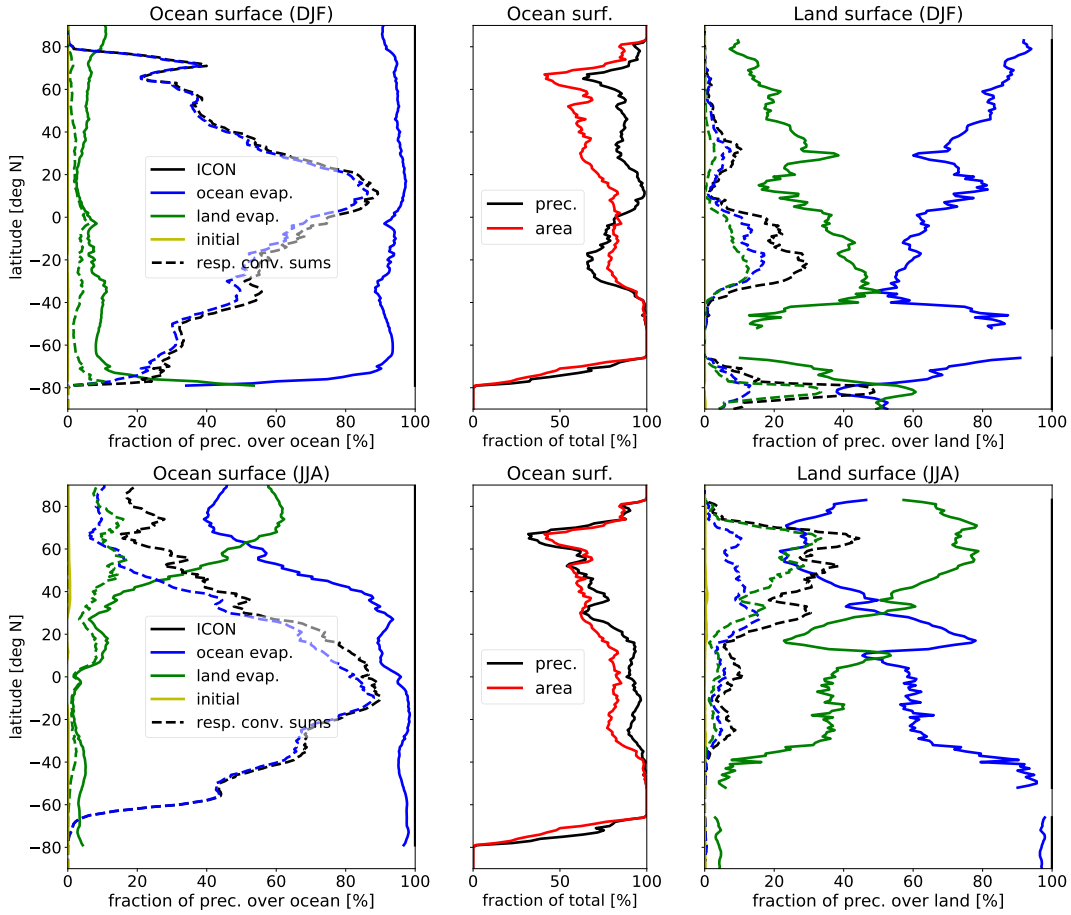

Figure 1. Fractional contributions of P^{ICON}, P^{init}, P^{ocn} and P^{lnd} to zonal sums of total precipitation for northern hemisphere winter (DJF, top) and summer (JJA, bottom), as a function of latitude. Left and right panels show sums over the ocean and land grid points, respectively. Dashed lines indicate the contribution of convective precipitation for each source of atmospheric water. Center panels display the fraction of precipitation over the ocean relative to total precipitation (over land plus ocean) and the fraction of the area covered by ocean.

These results are comparable to the studies by Numaguti (1999), Van der Ent et al. (2010) and Risi et al. (2013). While these studies look at regional differences, the latitudinal dependence is similar to the results presented here. This first application of ICON-ART-Iso - while no isotopologues are used - shows how diagnostic moisture tracers can be applied to better understand specific aspects of the atmospheric water cycle.

3.2 The multi annual simulation compared to GNIP data

For a first validation of δD and δ^{18}O values, we use the decadal ICON-ART-Iso model integration of the previous section and compare results to data taken from the GNIP network (Global Network for Isotopes in Precipitation, see Terzer et al., 2013; IAEA/WMO, 2017). In this section, we analyze δ values in total precipitation.

Five GNIP stations were chosen for their good data availability in the respective years, sampling different climate zones: Vienna in eastern Austria ($48.2°N$,$16.3°E$) in central Europe, Ankara in central Anatolia ($40.0°N$,$32.9°E$), Bangkok in tropical southern Asia ($13.7°N$,$100.5°E$), Puerto Montt in central Chile ($41.5°S$,$72.9°W$) and Halley station in Antarctica ($75.6°S$,$20.6°W$). The closest grid point to each of these stations was taken from the model output and the multi-year mean of each calender month was calculated for δD, δ^{18}O and d-excess (d-excess $= \delta\mathrm{D} - 8\,\delta^{18}\mathrm{O}$) in precipitation, total precipitation P and two meter temperature T_{2m}. The corresponding values are available from GNIP. Results are displayed in Fig. 2. The panels for total precipitation also include the mean values of precipitation from ocean and land evaporation (see previous section). All panels (except for the precipitation amount) show the 1σ standard deviation range for model and measurement data.

For most stations, the seasonal cycle of precipitation is reproduced by the model. This includes the summer minimum for Ankara and the strong winter precipitation in Puerto Montt. Precipitation is underestimated for Bangkok, especially in northern hemisphere spring. For all stations, the influence of land evaporation is strongest in their respective summer. Vienna and Ankara show a decreasing influence of the ocean in winter, typical for a more continental climate. For Puerto Montt, located between the Pacific and the Andean mountain range, and for Bangkok, almost all precipitating water originates from the ocean.

The seasonal cycle of temperature is reproduced for all stations. Winter temperatures are too cold in this model configuration for all stations. This temperature bias can partly be explained by the fact that the altitude of all stations is higher in the model because of the coarse grid, e.g. 550 m for the grid point identified with Vienna versus 198 m for the GNIP station. Also, the measured temperatures are slightly higher than mean monthly ERA-Interim (Dee et al., 2011) two meter temperatures for the corresponding grid points (not shown).

Despite some biases, the mean values of δD and δ^{18}O are well reproduced by ICON-ART-Iso for all five stations. The seasonal cycle is captured correctly on the northern as well as on the southern hemisphere. Values of d-excess are also of similar magnitude. Model data is more variable than the measurements. However, the model data is mostly within the standard deviation range of measurements. This demonstrates the capability of ICON-ART-Iso to simulate climatological patterns. The seasonal cycle and regional differences in δD and δ^{18}O are correctly reproduced in this climatological integration.

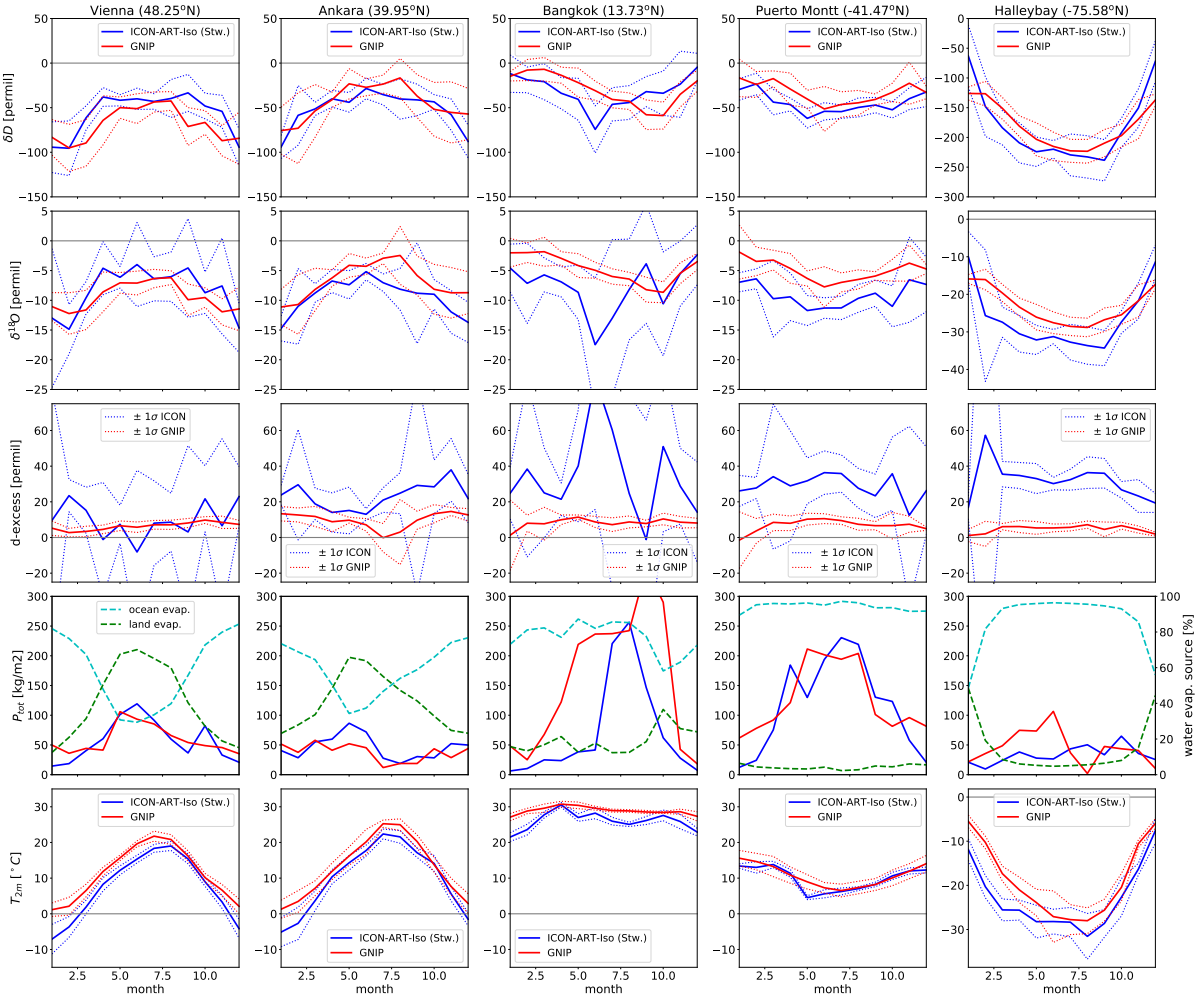

Figure 2. Monthly mean data for five GNIP stations (left to right: Vienna, Ankara, Bangkok, Puerto Montt and Halley station). Variables listed from top to bottom: δD, δ^{18}O, d-excess ($\delta\mathrm{D} - 8\,\delta^{18}\mathrm{O}$), total precipitation P_{tot} and two meter temperature (T_{2m}). Plots showing P_{tot} also include the percentage of land and ocean evaporation in precipitation. The 1σ standard deviation interval is indicated by dashed lines (except P for readability).

3.3 Comparison with IASI satellite data for a seasonal perspective

Here, we compare pairs of $\{H_2O, \delta D\}$ retrieved from MetOp/IASI remote sensing measurements with data from two simulations. The section closely follows the case studies presented by Schneider et al. (2017), who compared IASI retrievals and data from the global, hydrostatic model ECHAM5-wiso (Werner et al., 2011).

3.3.1 IASI satellite data and model postprocessing

IASI (Infrared Atmospheric Sounding Interferometer) A and B are instruments on board the MetOp-A and MetOp-B satellites (Schneider et al., 2016). They measure thermal infrared spectra in nadir view from which free tropospheric $\{H_2O, \delta D\}$ pair data are derived. As the satellites circle the earth in polar, sunsynchronous orbit, each IASI instrument takes measurements twice a day at local morning (approximately 9:30) and evening (approximately 21:30) hours. The measurements are most sensitive at a height of approximately 4.9 km. An IASI $\{H_2O, \delta D\}$ pair retrieval method has been developed and validated in the framework of the project MUSICA (MUlti-platform remote Sensing of Isotopologues for investigating the Cycle of Atmospheric water). The MUSICA retrieval method is presented by Schneider and Hase (2011) and Wiegele et al. (2014) with updates given in Schneider et al. (2016).

Schneider et al. (2017) present guidelines for comparing model data to the remote sensing data. First, a Retrieval Simulator software is used for simulating the MUSICA averaging kernel, using the atmospheric state of the model atmosphere. The simulated kernel is than applied to the original model state ($\boldsymbol{x}$) in order to calculate the state that would be reported by the satellite retrieval product ($\hat{\boldsymbol{x}}$, see Eq. 23).

$$\hat{\boldsymbol{x}} = \boldsymbol{A}(\boldsymbol{x} - \boldsymbol{x}_\mathrm{a}) + \boldsymbol{x}_\mathrm{a} \tag{23}$$

Here, $\boldsymbol{A}$ is the simulated averaging kernel and $\boldsymbol{x}_\mathrm{a}$ the a priori state. The a priori value used in the retrieval process for 4.9 km is at $\{1780\,\mathrm{ppm}, -217.4‰\}$. This value represents the climatological state of the atmosphere. In the retrieval process, the satellite radiance measurements are used for estimating the deviation of the actual atmospheric state from the a priori assumed state, where it is important to note that the remote sensing retrieval product is not independent from the a priori assumptions (see Schneider et al. (2016) for more details). In Schneider et al. (2017), these guidelines have been followed for comparison of IASI data with ECHAM5-wiso model data. We use the same approach for comparisons to ICON-ART-Iso and our results can be directly compared to the results from the hydrostatic, global model ECHAM5-wiso.

In order to compare ICON-ART-Iso measurements with IASI data, a simulation of twelve months is used, which was initialized on November 5, 2013. This simulation uses a finer resolution of R2B06, corresponding to roughly 40 km. Again, we use varying ocean surface temperatures and sea ice cover, see the specifications in Sec. 3.1. As in Schneider et al. (2017), two target time periods are investigated from February 12-18 and August 12-18, respectively. As has been pointed out in Sec. 3.1, the amount of water remaining in the troposphere from initialization is negligible by using lead times of three months. For this study, model output was interpolated to a regular $0.36^\circ \times 0.36^\circ$ grid, which is close to the 40 km resolution of the numerical ICON grid in the tropics. Output was written for every hour of simulation.

IASI observations are only available at cloud free conditions. In order to exclude cloud affected grid points in the ICON data, the total cloud cover simulated by ICON was used, denoted by C_{clct}. All points with $C_{\text{clct}} > 90\%$ were excluded. The parameter C_{clct} goes into saturation quickly and 90% is reached even for thin clouds. Surface emissivity E_{srf} is a necessary input parameter for the Retrieval Simulator. In this first study, E_{srf} was set to 0.96 over land and 0.975 over the ocean. This is in accordance with the mean values as given by Seemann et al. (2008). In addition, Schneider et al. (2017) show in a sensitivity study that errors on the order of 10% in this value have only a limited influence on the averaging kernels as simulated by the Retrieval Simulator. We follow the method outlined by Schneider et al. (2017) and use values only where the sensitivity metric $s_{\text{err}} < 0.05$.

We examine results for different areas over ocean and over land, using all data from the satellite and the model in the respective areas. The scatter of $\{\mathrm{H_2O}, \delta\mathrm{D}\}$ is not shown directly. Instead, the figures show the isolines of relative normalized frequency, which is explained in App. A. In addition, Rayleigh fractionation curves are indicated in all figures. These are the same as those given by Schneider et al. (2017).

3.3.2 Seasonal and daily cycle

Seasonal and daily cycle are investigated in $\{\mathrm{H_2O}, \delta\mathrm{D}\}$ space. The seasonal cycle is discussed for different regions over the central Pacific Ocean. The daily cycle is considered in the tropics and subtropics, also investigating differences between land and ocean areas.

First, the seasonal cycle over the Pacific Ocean is examined by comparing the two target periods in different areas ($\lambda < 140°W$ or $\lambda > 140°E$ longitude and different latitudinal bins). Results are presented in Fig. 3, that incluedes the exact latitudes. IASI data (bottom panels) show specific characteristics of the different regions. $\mathrm{H_2O}$ content is highest for tropical air masses and lowest for the highest latitudes in February and August. At the same time, tropical air is least depleted in HDO, while the highest latitudes show the lowest values of δD, i.e. are more depleted. When comparing February and August values at each latitude, a clear seasonal signal appears everywhere except for the tropics: During summer of the corresponding hemisphere, the air is more humid and more depleted in HDO. The distributions seem to shift from season to season along a line perpendicular to those of the Rayleigh model. The distribution in the tropics shows a broadened shape in August.

The results of ICON-ART-Iso are shown in the top panels of Fig. 3. The latitudinal dependence is similar to IASI: high $\mathrm{H_2O}$ and δD in the tropics and the lower values for mid-latitudes. The range of values is also very similar. The seasonal cycle in $\mathrm{H_2O}$ and δD is also reproduced to some degree, especially in the subtropical latitudes. The most obvious differences to IASI results occur in the northern hemisphere mid-latitudes in summer, which show less negative values of δD in the model than in the satellite data, especially for humid situations. In winter, this may also be the case, but there are only few humid values simulated at all or available in the satellite dataset. In general, the model shows a similar behavior as ECHAM5-wiso, the results of which are presented by Schneider et al. (2017).

For the daily cycle in the tropics and subtropics, land and ocean points are considered separately (Fig. 4, see caption for exact definition of the bins). IASI shows a clear signal of the daily cycle for both the tropics and subtropics over land (bottom panels of Fig. 4). There is no such signal over the ocean, where morning and evening distributions are almost identical. Over

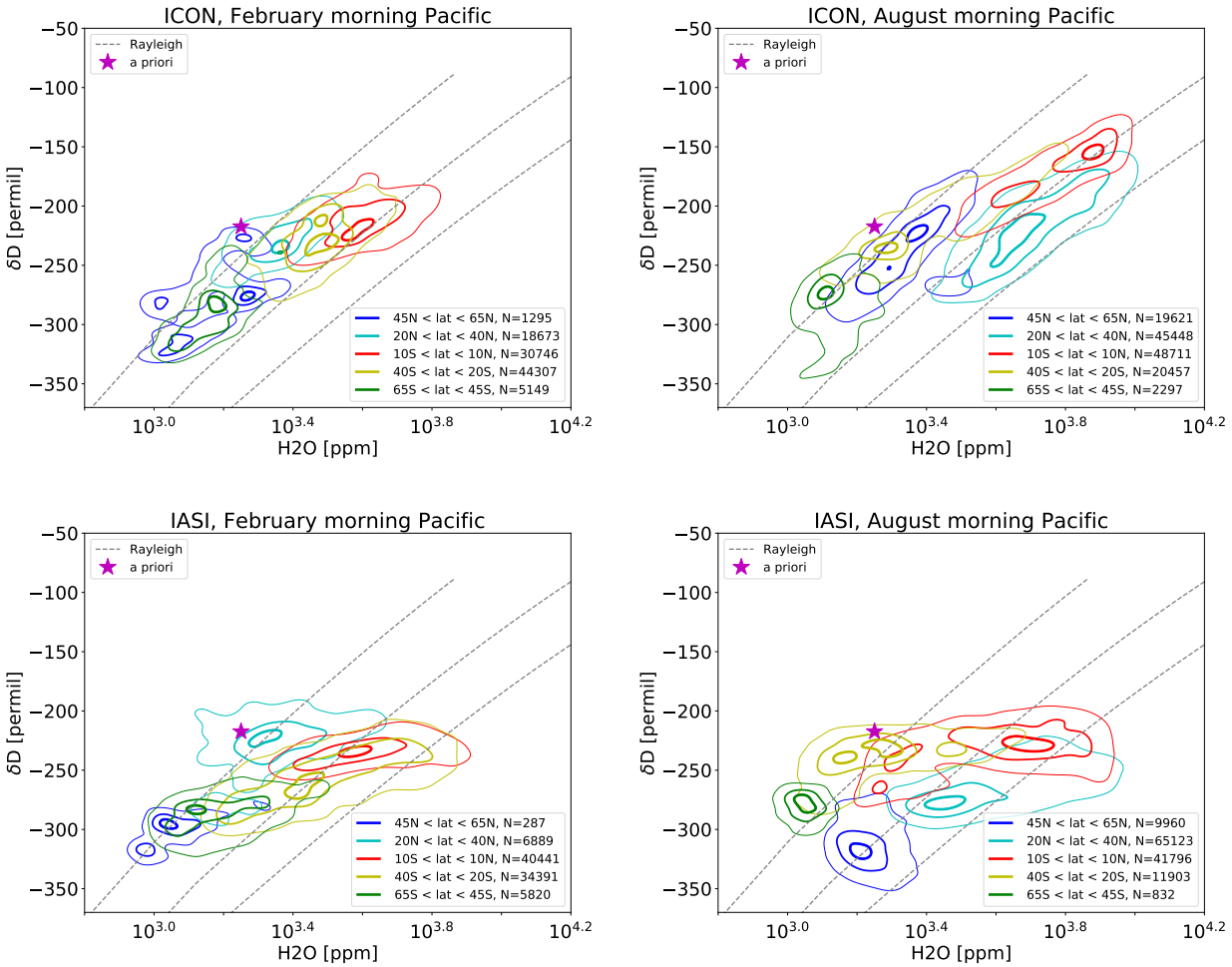

Figure 3. Isolines of the relative normalized frequency distribution for pairs of δD and H_2O (see App. A for the method) after processing ICON-ART-Iso data with the IASI Retrieval Simulator of Schneider et al. (2017) (top) and IASI data for the same time (bottom). Data from morning overpasses are shown for 12 to 18 February (left) and 12 to 18 August (right), 2014, for different latitudinal bands over the Pacific Ocean (longitude $\lambda < 140°W$ or $\lambda > 140°E$). Contour lines are indicated at 0.2, 0.6 and 0.9 of the normalized distribution.

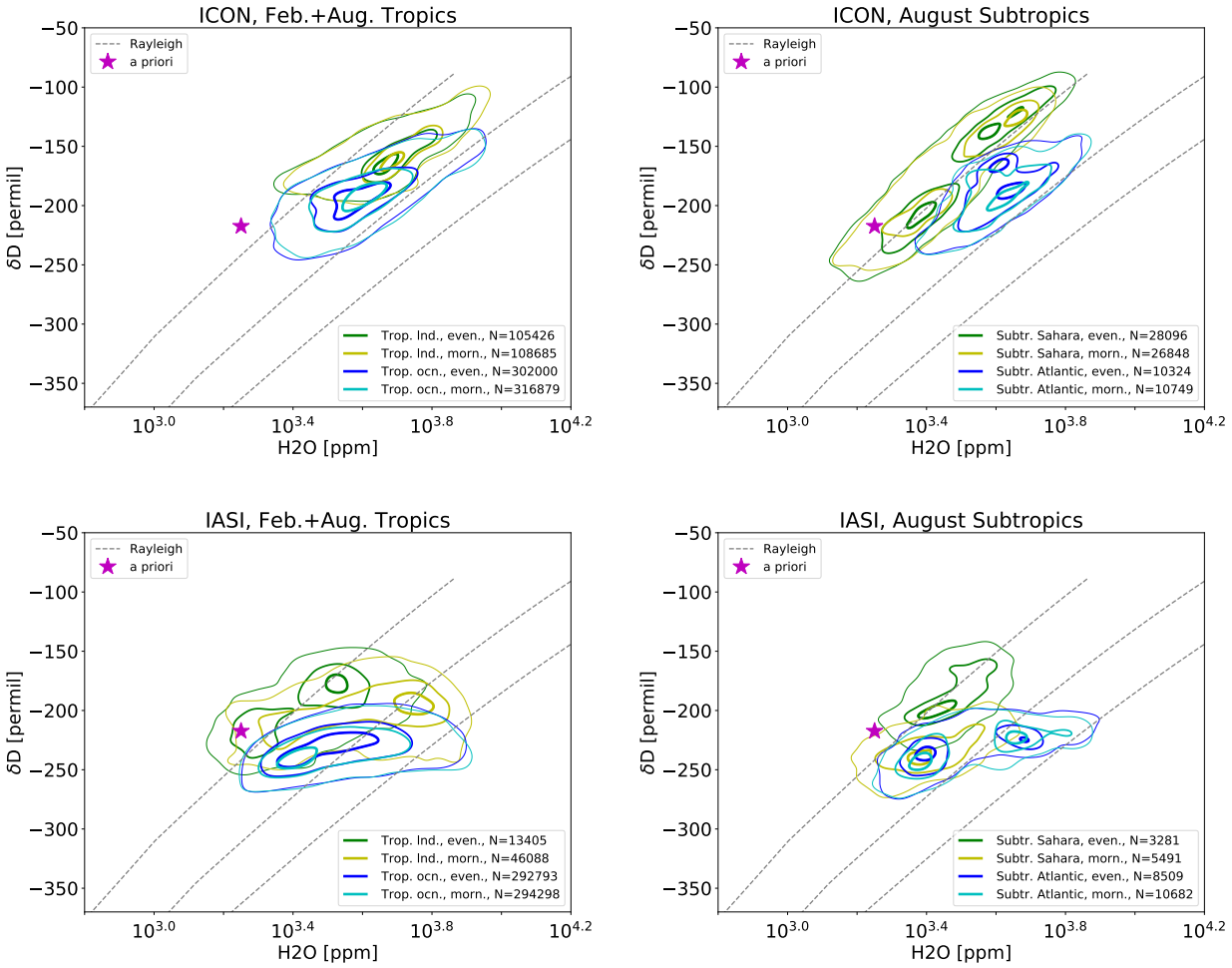

Figure 4. Isolines of the relative normalized frequency distribution for pairs of δD and H_2O (see App. A for the method) after processing ICON-ART-Iso data with the IASI Retrieval Simulator of Schneider et al. (2017) (top) and IASI data for the same time (bottom). Left: Data corresponding to morning and evening overpasses for the tropics ($10^\circ S < \varphi < 10^\circ N$, all longitudes, summer and winter simulation) over land and over the ocean. Right: Morning and evening overpasses for the subtropics ($22.5^\circ S < \varphi < 35^\circ N$, summer simulation) over land (Saharan desert region, $10^\circ W < \varphi < 50^\circ E$) and Atlantic Ocean ($50^\circ W < \varphi < 30^\circ W$). Contour lines are indicated at 0.2, 0.6 and 0.9 of the normalized distribution.

land, the water vapor in the tropics and subtropics is more depleted of HDO in the morning. There is also a daily cycle in H_2O in the tropics: During morning overpasses, H_2O values are higher than in the evening. Schneider et al. (2017) argue that this is due to the cloud filter, which removes areas of heavy convection in the evening. In the morning, the clouds have disappeared, but high humidity remains, especially in the lower troposphere. This may partly be due to evaporation of rain drops, which explains the enhanced depletion in HDO (Worden et al., 2007). Over the Sahara (the subtropical land area considered), the daily cycle is different: While mixing ratios of H_2O rise only slightly during the day, there is a strong increase in the HDO content in the evening. This behavior can be attributed to vertical mixing (Schneider et al., 2017, and references therein).

The data retrieved from ICON-ART-Iso model simulations is shown in the top panels of Fig. 4. Tropical air (top left) over the land shows slightly lower mixing ratios for H_2O than IASI. The humidity of tropical ocean points is better reproduced. The difference in δD is stronger for both areas, with δD values being too high in the model. There is no daily cycle in the tropics for ICON-ART-Iso. The subtropical mixing ratios (top right) of H_2O over the ocean are similar to those in the tropics but cover a smaller range than those retrieved from IASI. The very humid and very dry parts of the IASI distribution are not reproduced by the model. δD values in ICON-ART-Iso are larger than in the IASI retrievals. As pointed out by Schneider et al. (2017), the daily cycle in IASI also manifests itself in the number of samples passing the IASI cloud filter and quality control. The IASI cloud filter removes much more evening observations than morning observations, meaning more cloud coverage in the evening than in the morning. In contrast, the ICON-ART-Iso cloud filter removes a similar number of data for morning and evening, i.e. in the model morning and evening cloud coverage is rather similar. This may also influence the results.

To further analyze the influence of ocean and land areas, the analysis of the daily cycle is repeated, making use of the humidity tracers q^{ocn} and q^{lnd}. As has been pointed out in Sec. 3.1, q^{init} is negligible three months after initialization. To distinguish between grid points mostly influenced by ocean or land evaporation, we additionally use the following criteria to define ocean and land points: $q^{\mathrm{ocn}}/q^{\mathrm{ICON}} > 0.9$ for grid points over the ocean, $q^{\mathrm{lnd}}/q^{\mathrm{ICON}} > 0.5$ for land grid points predominantly affected by land evaporation. This investigation serves to showcase how the ocean and land evaporation tracers can be used and the threshold values are therefore arbitrary to some degree. The tracer fields of water evaporating from ocean and land have not been processed with the retrieval simulator, instead values interpolated to $4.9\,\mathrm{km}$ are directly used.

The result is shown in Fig. 5 for tropics and subtropics, using the same method as for Fig. 4. The characteristics of the different regions show up much more clearly with the additional criteria. For the tropical ocean, the distribution of H_2O is similar, but the values are slightly more depleted in HDO. The distribution of pairs attributed to the land surface is reduced to values with relatively high humidity and enriched in HDO. The latter might be due to the signal of plant evapotranspiration, which is considered a non-fractionation process.

In the subtropics, the distributions over land change their shape completely and are separated from those over the ocean. The distribution for the subtropical ocean remains largely unchanged, becoming slightly more elongated with lower values in δD. For the land surface, the additional criterion strongly reduces the number of values that are considered. This implies that over the Saharan desert, air mostly influenced by land evaporation (50% or more) is very dry and highly processed (low δD).

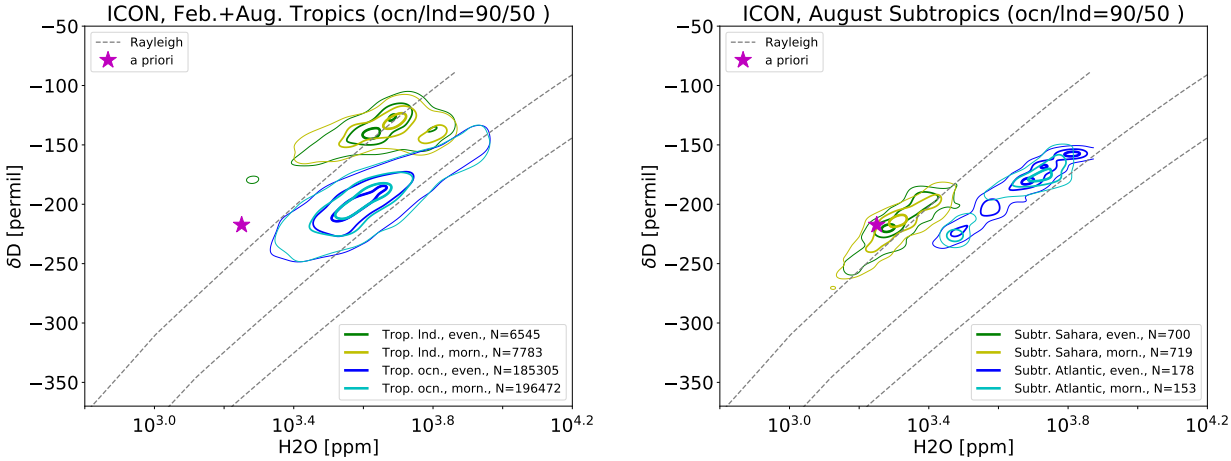

Figure 5. As Fig. 4 for ICON-ART-Iso. In addition to the land-ocean mask, land data must pass the condition $q_v^{\mathrm{lnd}}/q_v > 0.5$ and ocean data must pass $q_v^{\mathrm{ocn}}/q_v > 0.9$.

This section shows that ICON-ART-Iso is able to reproduce regional differences and the seasonal cycle of $\{\mathrm{H_2O}, \delta\mathrm{D}\}$ of vapor in the lower troposphere. The additional water diagnostics are used to study the behavior of the model in more detail and will help in investigating the measured distributions in future studies.

3.4 Comparing with in situ IAGOS-CARIBIC measurements

In this section, we present a first case study, in which results of ICON-ART-Iso are compared to in situ measurements of δD taken by the IAGOS-CARIBIC passenger aircraft at 9-12 km altitude. Two flights in September 2010 are considered, which took place a few days after the passage of the tropical cyclone Igor over the Atlantic ocean. The full dataset of all δD measurements taken by IAGOS-CARIBIC in the tropics is also used as reference.

3.4.1 IAGOS-CARIBIC data and model postprocessing

In the European research infrastructure IAGOS-CARIBIC, a laboratory equipped with 15 instruments is deployed on board a Lufthansa A340-600 for four intercontinental flights per month. Measurements of up to 100 trace gases and aerosol parameters are taken in situ and in air samples (Brenninkmeijer et al., 2007). δD is measured using the instrument ISOWAT (Dyroff et al., 2010). It is a tunable diode-laser absorption spectrometer that simultaneously measures HDO and $\mathrm{H_2O}$ at wave numbers near $3765\,\mathrm{cm^{-1}}$ to derive δD in vapor. The instrument is calibrated based on regular calibration measurements (each 30 min) of a water vapor standard with 500 ppm $\mathrm{H_2O}$ and $\delta\mathrm{D} = -109‰$. The δD offset is derived by considering the data of the driest 5% of the air masses sampled during each flight, which is typically 4-8 ppm $\mathrm{H_2O}$. At the flight altitude of 10-12 km, this is without exception lowermost stratospheric air (LMS), for which a δD of -600‰ is assumed (Pollock et al., 1980; Randel et al., 2012). An assumed uncertainty of this LMS value of 400‰ translates to a relevant uncertainty of 20‰ at 100 ppm $\mathrm{H_2O}$. Due

to further sources of measurement uncertainty, the data has a total flight specific systematic uncertainty up to 100‰. The total uncertainty is humidity dependent, decreasing towards higher humidity (e.g. 100‰ at 80 ppm H_2O versus less than 20‰ at 500 ppm H_2O, see Christner (2015) for more details).

The in-situ IAGOS-CARIBIC data is suitable for the analysis of processes on small scales. δD measurements are available one minute means, which translates to a spatial scale of approximately 15 km. This horizontal resolution is finer than the chosen ICON-ART-Iso configuration (R2B06 corresp. to 40 km) and is therefore suitable for a case study validation. Unfortunately, the uncertainty of δD data at humidity below approximately 40 ppm H_2O is too high to be used for analysis. Because of the systematic total uncertainty (see above), we use mean δD values from two flights through similar conditions.

In this section, measurements from a return flight from Frankfurt to Caracas on September 22, 2010 are analyzed (IAGOS-CARIBIC flight nrs. 309 and 310, taking off at 10:16 UTC in Frankfurt and 22:12 UTC in Caracas, respectively). The two flights crossed the Atlantic approximately two days after Hurricane Igor had passed the flight track. The storm caused large-scale lofting of tropospheric air masses and a moistening at flight level. The high humidity at flight level (9-12 km) allowed many accurate δD-measurements to be taken.

An ICON-ART-Iso simulation was initialized with ECMWF IFS analysis data from September 12, 2010 and with the isotope values initialized as explained in Sec. 2.7. This corresponds to a ten day forecast for the time of the two flights. In this case, not all tropospheric water from the initialization has been replaced by water evaporated during the simulation at the time of analysis. However, the δD values adjust to local meteorology within a few days, developing realistic horizontal and vertical gradients. The simulation was set up on an R2B06 grid (≈ 40 km) with a time step of 240 s (convection called every second step). The output with a frequency of one snapshot per 15 minutes was examined on a 0.5° regular grid and interpolated linearly to the position of the aircraft. Fig. 6 shows δD in water vapor in the upper troposphere roughly 24 hours before the flights cross the Atlantic. The vortex signal of the hurricane clearly shows up in the δD field. The flight paths are also indicated in Fig. 6.

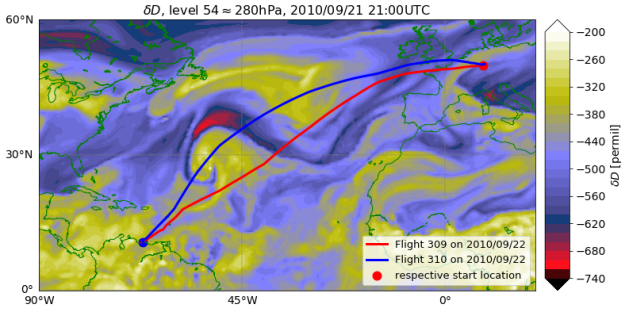

Figure 6. δD in water vapor on model level 54 (≈ 260 hPa) on September 21, 21UTC, the date prior to that of the IAGOS-CARIBIC flights. The storm is visible in the western half of the plotted area (center approximately at $30^\circ N, 50^\circ W$). The flight paths of IAGOS-CARIBIC flights 309 and 310 are also indicated by two lines, where the departure locations are emphasized.

3.4.2 Results for flights in tropical regions

In order to compare values influenced by hurricane Igor, model and measurement data from flights 309 and 310 are considered in latitudes around the storm track only ($0°N < \varphi < 30°N$). For reference, all tropical δD values from the IAGOS-CARIBIC database are also examined. To create a comparable dataset from model data, the results of the decadal simulation presented in Sec. 3.1 were interpolated to the location of these measurements and are treated in the same manner. As in Sec. 3.3, the distribution of pairs of $\{H_2O, \delta D\}$ are examined. The results are shown in Fig. 7.

The distribution of IAGOS-CARIBIC δD-measurements is shown in the left panel of Fig. 7. The tropical measurement sample (blue contours) consists of all relevant measurements ($23.5°S < \varphi < 23.5°N$). While most tropical values are centered around -500‰ in δD and 100 ppm to 150 ppm H_2O, there is also a tail towards more humid pairs in the distribution. The lower limit in δD follows the curves of Rayleigh fractionation. The measurement data from flights 309 and 310 (red contours) show different characteristics. The range in H_2O is similar to the maximum density values of all tropical values, but the samples are more depleted in HDO. The humid branch is not continuous and the area of high humidity is sparsely populated. In general, both distributions are limited by the detection limit of 40 ppm in H_2O, while contour lines may reach slightly lower values because of the smoothing that is applied in processing the data (see App. A).

Model results are shown in the right panel of Fig. 7. For this figure, model data along the flight tracks is used only where accurate δD-measurements are available. A limit of 40 ppm is also applied to the model data. The isolines stretching to lower value pairs again result from smoothing the data.

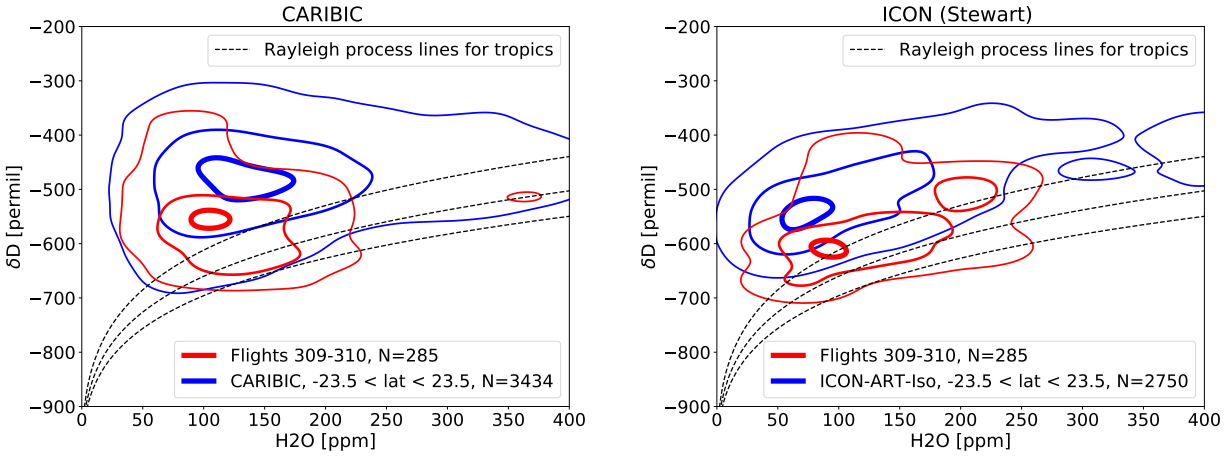

Figure 7. Isolines of the relative normalized frequency distribution (contours at 0.05, 0.4 and 0.9, see App. A for the method) of IAGOS-CARIBIC measurements (left) and ICON-ART-Iso model simulations for tropical samples, interpolated onto the paths of two IAGOS-CARIBIC flights 309-310 (right). The total number of datapoints in each distribution is given by the value N. Model data is considered only in locations with measurements and the H_2O measurement limit of 40 ppm is also considered in model data.

The distribution from the tropical model sample is in some ways similar to the one by all tropical IAGOS-CARIBIC measurements (comparing the blue contours of the two panels): There is a tail towards high humidities and the upper limit of δD is roughly at -400‰, while the lower limit is given by the second Rayleigh curve. The model sample is 4% lower in δD on average (H_2O reduced by 18%). The mean for all values within the lowest density contour in $\{H_2O, \delta D\}$ is at $\{193.5\,\mathrm{ppm}, -478.0‰\}$ for measurements, while it is at $\{175.4\,\mathrm{ppm}, -482.0‰\}$ for the model sample ($\{131.7\,\mathrm{ppm}, -481.6‰\}$ for measurements versus $\{72.7\,\mathrm{ppm}, -543.6‰\}$ in case of the highest density contour).

The main characteristics of the distribution for the two flights following Hurricane Igor is captured by the model ICON-ART-Iso (comparing the red contours of the two panels) and the center of the distribution is below the full tropical sample. The model sample is slightly reduced in δD (1.1%) when comparing to the full tropical sample, but 12.3% more humid. From this simulation and these measurements alone, it is difficult to say if these discrepancies result from errors in the meteorological representation of the hurricane or in the physical parameterizations of the model. The good agreement between model and measurements in general is promising, while details will need to be examined in future studies.

By using the other three diagnostic moisture tracers (initialization water q^{init} and water evaporating from the ocean and land, q^{ocn} and q^{lnd}), the model results are examined further. The two transatlantic flights spent little time over land areas. Accordingly, q_v^{lnd} only reaches an average of 2.8% for both flights, 19.9% at maximum. An average of 47.2% of the sampled water originates from the initialization (59.6% maximum), while the remainder has evaporated from the ocean in the course of the simulation. Part of the discrepancies between model and measurements may thus result from the simplified representation of δD in the initial vapor field, while the influence of the approximated land surface isotope values remains limited.

This is analyzed in more detail in Fig. 8. Values of δD and H_2O along the flight paths are combined with information on the origin of the water that is sampled in the model. W stands for the ratio of vapor that originates from land or ocean evaporation or initialization, e.g. $W^{\mathrm{init}} = q_v^{\mathrm{init}}/q_v$. In Fig. 8, the scatter is colorcoded by W^{ocn}. Because W^{lnd} is very low during most parts of the flights and especially so over the ocean, $W^{\mathrm{ocn}} = 1 - W^{\mathrm{init}}$ is a good approximation. In Fig. 8, green colors indicate $W^{\mathrm{lnd}} > 10\%$, where the approximation of a binary solution is not valid.

Fig. 8 shows the strong influence of the ocean. More than 50% of the sampled vapor originates from ocean evaporation for long parts of the flights. Those values with the highest values of W^{init} (low W^{ocn}) mostly follow the course of the Rayleigh fractionation lines. The lowest and highest values in δD are reached where W^{ocn} is high (low values of W^{init}), indicating that the isotopologues in the model have seen many fractionating and transport processes. This includes air mass mixing, but also the microphysical and convective processes that are imprinted on the isotopologue ratio. The exact nature of these processes remain to be investigated in future studies.

4 Conclusions

We present ICON-ART-Iso, the isotope-enabled version of the global atmospheric model ICON (Zängl et al., 2015). We describe the model formulation as well as a set of evaluation studies. By using parts of the ICON-ART infrastructure (Schröter et al., 2018), the model is very flexible in terms of the simulated moisture tracers. These can be set to resemble either H_2O

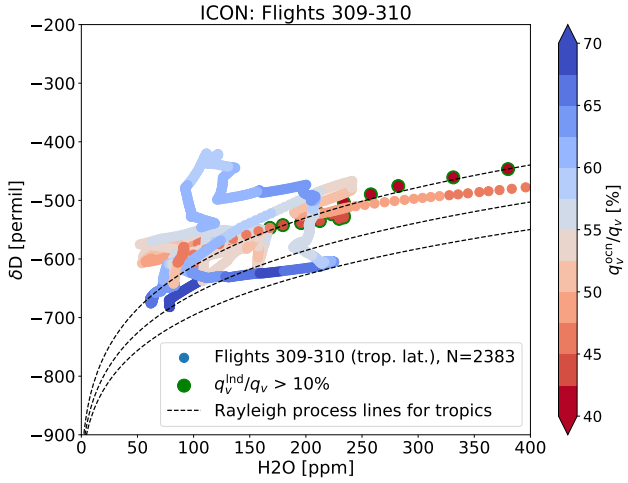

Figure 8. Scatter of δD against H_2O from ICON-ART-Iso interpolated to the flight paths of IAGOS-CARIBIC flights 309 and 310. Color coding indicates the ratio of $W^{\text{init}} \approx 1 - W^{\text{ocn}}$ in percent. Locations with $W^{\text{lnd}} > 10\%$ are marked in green. Values are considered where $p < 280\,\text{hPa}$.

(tagged water) or the stable isotopologues HDO or $H_2{}^{18}O$ if fractionation is turned on. The physics of fractionation are largely based on the model COSMOiso (Pfahl et al., 2012). The first part of this article gives a detailed explanation of the parameterizations that have been implemented in ICON-ART-Iso to simulate the fractionation of water isotopologues.

We first evaluate tagged H_2O tracers of moisture evaporating from land and ocean to investigate the moisture sources of precipitation. This demonstrates the capabilities of ICON-ART-Iso to use tagged water as an additional diagnostic. The latitudinal dependence is similar to that given by other studies (e.g. Risi et al., 2013). The following three sections then investigate the performance of the model for the simulation of the isotopologues, considering (i) multi annual, (ii) regional and (iii) meso-scale applications.

For a multi annual evaluation, the simulated isotopologues HDO and $H_2{}^{18}O$ from a decadal simulation on a relatively coarse grid (160 km horizontal resolution) are compared to measurements taken from the network of GNIP stations (Terzer et al., 2013; IAEA/WMO, 2017). The model simulates δD and δ^{18}O reasonably well, reproducing the seasonal cycle of δ^{18}O and the range in d-excess for different stations in the northern and southern hemisphere. This investigation presents a first climatological application.

Regional differences in pairs of $\{H_2O, \delta D\}$ in lower free-tropospheric water vapor are then compared to data retrieved from IASI satellite measurements for a summer and winter case (Schneider and Hase, 2011; Wiegele et al., 2014; Schneider et al., 2016, 2017). The latitudinal dependence of these pairs is comparable to those from IASI retrievals. The seasonal cycle over the Pacific ocean and the overall values are reproduced by the model in both seasons. The difference between land and ocean surfaces in the tropics and subtropics in the model is of similar magnitude as in the measurements. However, the daily cycle that

is observed in the satellite data is not reproduced in the model. Overall, the performance is similar to that of ECHAM5-wiso (Werner et al., 2011; Schneider et al., 2017).

In a meso-scale application, a first comparison with in situ measurements uses δD in upper-tropospheric water vapor from two IAGOS-CARIBIC flights (Brenninkmeijer et al., 2007) transecting the Atlantic and from all tropical IAGOS-CARIBIC δD measurements (Dyroff et al., 2010). ICON-ART-Iso is able to reproduce the general features of the tropical IAGOS-CARIBIC dataset. The characteristics of the samples taken during two flights shortly after Hurricane Igor in September 2010 are also captured by the model.

In all three applications, the tagged evaporation water from the ocean or land surfaces proves to be a valuable tool. It reveals a seasonal cycle in the precipitation water origin or shows the influence of the initialization in case of the comparison with IAGOS-CARIBIC data.

ICON-ART-Iso is a promising tool for future investigations of the atmospheric water cycle. This study demonstrates the flexibility of ICON-ART-Iso in terms of the setup for different diagnostics but also in terms of horizontal resolution and time scale. For future applications, it will be interesting to use a nudging of meteorological variables towards analysis data to facilitate comparisons with measurements in different case studies. Fractionation will be implemented in different microphysical schemes to make the model numerically more efficient and even better applicable to climatological questions. Due to its flexible setup, ICON-ART-Iso is ready to simulate tracers corresponding to $\mathrm{H_2{}^{17}O}$ or to be used as a testbed for new microphysical parameterizations.

Code and data availability. The CARIBIC measurement data analyzed in this paper can be accessed by signing the CARIBIC data protocol to be downloaded at http://www.caribic-atmospheric.com/. The ICON code can be obtained from DWD after signing the license agreement available from icon@dwd.de. The ICON-ART code can be obtained after signing the license agreement available from bernhard.vogel@kit.edu.

Appendix A: Preparing the relative normalized frequency distributions

Sec. 3.3 and 3.4 show and discuss distributions of $\{\mathrm{H_2O}, \delta\mathrm{D}\}$. The scatter of $\{\mathrm{H_2O}, \delta\mathrm{D}\}$ is not shown directly as the figures would be too cluttered. Instead, the normalized relative frequency is discussed, isolines of which are shown in the different figures. This method has been adopted from Christner (2015). Fig. A1 shows the scatter and the isolines of normalized relative frequency for the IAGOS-CARIBIC measurements of flights 309-310, which are discussed in Sec. 3.4.

To arrive at the isolines, the data are binned in $\mathrm{H_2O}$ and δD on a grid of $5\,\mathrm{ppm} \times 5‰$. In case of IASI data, the data is binned in $\log_{10}\mathrm{H_2O}$ (ppm) $\times$ δD on a grid of 0.05×5. Histogram counts are then interpolated onto a 1000×1000 grid. This is smoothed with a Gaussian filter with a standard deviation of 20 (15 in case of IASI). This smoothed data is then normalized by the sum of all value pairs and then normalized by the maximum value. Within this array of smoothed counts, isolines are drawn at 0.9, 0.4 and 0.05 (0.9, 0.6 and 0.2 in case of IASI).

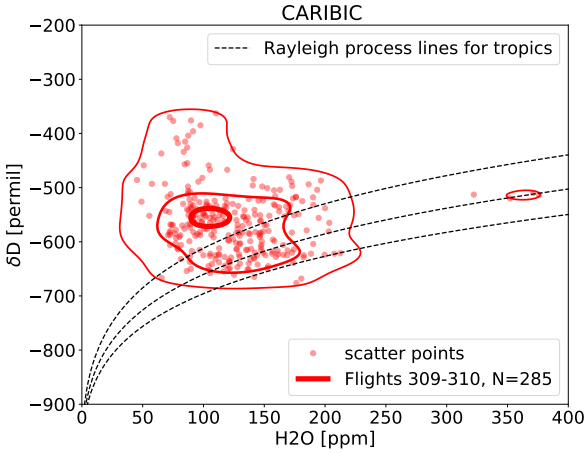

Figure A1. Scatter and isolines of the relative normalized frequency distribution for tropical (latitude $\varphi < 30^\circ N$) measurements of δD and H_2O from IAGOS-CARIBIC flights 309 and 310 (September 2010). The figure demonstrates how the isolines (indicated at 0.1, 0.4 and 0.9) relate to the underlying scatter.

Appendix B: Fractionation during evaporation of hydrometeors following Blossey et al. (2010)

For evaporation and equilibration of rain and melting hydrometeors, the parameterization following Stewart (1975) has been presented in this paper, see Sec. 2.5 and Eq. 6 therein. As an alternative, we have also implemented the parameterization by Blossey et al. (2010). For completeness, this parameterization is given in Eq. B1. In order to make a comparison easy, Eq. B2 again states the parameterization by Stewart (1975). Like above, both are given in the formulation for the evaporation of rain. The notation is the same as in the main body text.

$$ {}^{h}S_r^{\text{evap, Blossey}} = A \, \frac{{}^{h}f}{{}^{l}f} \frac{{}^{h}D}{{}^{l}D} \quad \left[R_r \alpha_{\text{liq}} \, {}^{l}\rho^*_{l,\infty} - {}^{h}\rho_v \left(1 + B_l \left(1 - \alpha_{\text{liq}} \frac{R_r}{R_v} \right) \right) \right] \tag{B1} $$

$$ {}^{h}S_r^{\text{evap, Stewart}} = A \left(\frac{{}^{h}D}{{}^{l}D} \right)^n \left[R_r \alpha_{\text{liq}} \, {}^{l}\rho^*_{l,\infty} - {}^{h}\rho_v \right] \tag{B2} $$

$$ A = \frac{4\pi a \, {}^{l}f \, {}^{l}D}{1 + B_l} \tag{B3} $$

$$ B_l = \frac{{}^{l}D \, L_e^2 \, {}^{l}e^*_{l,\infty}}{k_a \mathcal{R}_v^2 T_\infty^3} \tag{B4} $$

By the above formulation, the difference of the two parameterizations is easily accessible. While the empirical equation by Stewart (1975) introduces the exponent n, which is determined by measurements, the parameterization by Blossey et al. (2010) modulates the saturation difference by a factor determined by the actual isotopologue ratios in the hydrometeor and the surrounding vapor. The ratio of ventilation factors f is an additional tuning parameter in the parameterization by Blossey et al.

(2010) which is set to 1 in standard setup. A detailed comparison to the results of Stewart (1975) is postponed to a later study in order to keep this paper concise.

Author contributions. Johannes Eckstein programmed ICON-ART-Iso as an extension to ICON, performed and evaluated the simulations and prepared the manuscript. This was done with Roland Ruhnke as main and Peter Braesicke as as overall advisor. Stephan Pfahl provided the code of COSMOiso and helped in understanding and implementing the fractionating code. Christopher Diekmann has taken over the work on ICON-ART-Iso and implemented some of the features after submission to GMDD. Daniel Reinert was the main contact person at DWD and helped with the model ICON. Daniel Rieger and Jennifer Schröter aided in the technical development of the ICON-ART part of the model code and helped to solve many technical problems during the development of ICON-ART-Iso. Emanuel Christner provided and discussed data and results of the comparison with IAGOS-CARIBIC. Andreas Zahn is the coordinator of IAGOS-CARIBIC. Christoph Dyroff was responsible for setting up and maintaining the instrument ISOWAT. Matthias Schneider provided data and discussed results of the comparison with IASI satellite data.

Competing interests. There are no competing interests to declare.

Acknowledgements. The authors would like to thank three anonymous reviewers for their helpful comments on the manuscript and A. Lauer for taking over the editorship. We would also like to thank A. Seifert and M. Raschendorfer of DWD for discussions and help with parts of the ICON model code. This work was partly performed on the computational resource ForHLR II funded by the Ministry of Science, Research and the Arts Baden-Württemberg and DFG ("Deutsche Forschungsgemeinschaft"). The MUSICA/IASI data have been produced in the framework of the projects MUSICA (funded by the European Research Council under the European Community's Seventh Framework Programme (FP7/2007-2013) / ERC Grant agreement number 256961) and MOTIV (funded by the Deutsche Forschungsgemeinschaft under GZ SCHN 1126/2-1). We thank all the members of the IAGOS-CARIBIC team. The collaboration with Lufthansa and Lufthansa Technik and the financial support from the German Ministry for Education and Science (grant 01LK1301C) are gratefully acknowledged.

References

Bechtold, P., Semane, N., Lopez, P., Chaboureau, J.-P., Beljaars, A., and Bormann, N.: Representing equilibrium and nonequilibrium convection in large-scale models, Journal of the Atmospheric Sciences, 71, 734–753, 2014.

Blossey, P. N., Kuang, Z., and Romps, D. M.: Isotopic composition of water in the tropical tropopause layer in cloud-resolving simulations of an idealized tropical circulation, Journal of Geophysical Research: Atmospheres, 115, 2010.

Bosilovich, M. G. and Schubert, S. D.: Water vapor tracers as diagnostics of the regional hydrologic cycle, Journal of Hydrometeorology, 3, 149–165, 2002.

Brenninkmeijer, C. A. M., Crutzen, P., Boumard, F., Dauer, T., Dix, B., Ebinghaus, R., Filippi, D., Fischer, H., Franke, H., Frieß, U., Heintzenberg, J., Helleis, F., Hermann, M., Kock, H. H., Koeppel, C., Lelieveld, J., Leuenberger, M., Martinsson, B. G., Miemczyk, S., Moret, H. P., Nguyen, H. N., Nyfeler, P., Oram, D., O'Sullivan, D., Penkett, S., Platt, U., Pupek, M., Ramonet, M., Randa, B., Reichelt, M., Rhee, T. S., Rohwer, J., Rosenfeld, K., Scharffe, D., Schlager, H., Schumann, U., Slemr, F., Sprung, D., Stock, P., Thaler, R., Valentino, F., van Velthoven, P., Waibel, A., Wandel, A., Waschitschek, K., Wiedensohler, A., Xueref-Remy, I., Zahn, A., Zech, U., and Ziereis, H.: Civil Aircraft for the Regular Investigation of the Atmosphere Based on an Instrumented Container: The new CARIBIC system, Atmospheric Chemistry and Physics, 7, 4953–4976, https://doi.org/10.5194/acp-7-4953-2007, 2007.

Cappa, C. D., Hendricks, M. B., DePaolo, D. J., and Cohen, R. C.: Isotopic fractionation of water during evaporation, Journal of Geophysical Research: Atmospheres, 108, https://doi.org/10.1029/2003JD003597, 4525, 2003.

Christner, E.: Messungen von Wasserisotopologen von der planetaren Grenzschicht bis zur oberen Troposphäre zur Untersuchung des hydrologischen Kreislaufs, Ph.D. thesis, KIT, IMK-ASF, H.-v.-Helmholtz-Platz 1, 76344 Leopoldshafen, 2015.

Craig, H.: Isotopic variations in meteoric waters, Science, 133, 1702–1703, 1961.

Craig, H. and Gordon, L.: Deuterium and oxygen 18 variations in the ocean and marine atmospher, in: Stable Isotopes in Oceanographic Studies and Paleotemperatures, edited by Tongiogi, E., pp. 9–130, V. Lishi e F., Pisa, 1965.

Dansgaard, W.: The O18-abundance in fresh water, Geochimica et Cosmochimica Acta, 6, 241–260, 1954.

Dansgaard, W.: Stable isotopes in precipitation, Tellus, 16, 436–468, https://doi.org/10.3402/tellusa.v16i4.8993, 1964.

Dee, D. P., Uppala, S. M., Simmons, A. J., Berrisford, P., Poli, P., Kobayashi, S., Andrae, U., Balmaseda, M. A., Balsamo, G., Bauer, P., Bechtold, P., Beljaars, A. C. M., van de Berg, L., Bidlot, J., Bormann, N., Delsol, C., Dragani, R., Fuentes, M., Geer, A. J., Haimberger, L., Healy, S. B., Hersbach, H., Hólm, E. V., Isaksen, L., Kållberg, P., Köhler, M., Matricardi, M., McNally, A. P., Monge-Sanz, B. M., Morcrette, J.-J., Park, B.-K., Peubey, C., de Rosnay, P., Tavolato, C., Thépaut, J.-N., and Vitart, F.: The ERA-Interim reanalysis: configuration and performance of the data assimilation system, Quarterly Journal of the Royal Meteorological Society, 137, 553–597, https://doi.org/10.1002/qj.828, 2011.

Dyroff, C., Fütterer, D., and Zahn, A.: Compact diode-laser spectrometer ISOWAT for highly sensitive airborne measurements of water-isotope ratios, Applied Physics B, 98, 537–548, https://doi.org/10.1007/s00340-009-3775-6, 2010.

Galewsky, J., Steen-Larsen, H. C., Field, R. D., Worden, J., Risi, C., and Schneider, M.: Stable isotopes in atmospheric water vapor and applications to the hydrologic cycle, Reviews of Geophysics, 54, 809–865, https://doi.org/10.1002/2015RG000512, 2016.

Gat, J. R.: Oxygen and hydrogen isotopes in the hydrologic cycle, Annual Review of Earth and Planetary Sciences, 24, 225–262, 1996.

Gat, J. R.: Isotope hydrology : a study of the water cycle, Series on environmental science and management ; 6, Imperial College Press, London, 2010.

Gimeno, L., Stohl, A., Trigo, R. M., Dominguez, F., Yoshimura, K., Yu, L., Drumond, A., Durán-Quesada, A. M., and Nieto, R.: Oceanic and terrestrial sources of continental precipitation, Reviews of Geophysics, 50, 2012.

Gonfiantini, R., Stichler, W., and Rozanski, K.: Reference and intercomparison materials for stable isotopes of light elements, Tech. Rep. IAEA-TECDOC-825, International Atomic Energy Agency, 1993.

Gunson, M. R., Abbas, M., Abrams, M., Allen, M., Brown, L., Brown, T., Chang, A., Goldman, A., Irion, F., Lowes, L., et al.: The Atmospheric Trace Molecule Spectroscopy (ATMOS) experiment: Deployment on the ATLAS space shuttle missions, Geophysical Research Letters, 23, 2333–2336, 1996.

Heinze, R., Dipankar, A., Henken, C., Moseley, C., Sourdeval, O., Trömel, S., Xie, X., Adamidis, P., Ament, F., Baars, H., Barthlott, C., Behrendt, A., Blahak, U., Bley, S., Brdar, S., Brueck, M., Crewell, S., Deneke, H., Di Girolamo, P., Evaristo, R., Fischer, J., Frank, C., Friederichs, P., Göcke, T., Gorges, K., Hande, L., Hanke, M., Hansen, A., Hege, H.-C., Hoose, C., Jahns, T., Kalthoff, N., Klocke, D., Kneifel, S., Knippertz, P., Kuhn, A., van Laar, T., Macke, A., Maurer, V., Mayer, B., Meyer, C., Muppa, S., Neggers, R. A. J., Orlandi, E., Pantillon, F., Pospichal, B., Röber, N., Scheck, L., Seifert, A., Seifert, P., Senf, F., Siligam, P., Simmer, C., Steinke, S., Stevens, B., Wapler, K., Weniger, M., Wulfmeyer, V., Zängl, G., Zhang, D., and Quaas, J.: Large-eddy simulations over Germany using ICON: a comprehensive evaluation, Quart. J. Roy. Meteorol. Soc., 143, 69–100, https://doi.org/10.1002/qj.2947, 2017.

Holton, J. R. and Hakim, G. J.: An introduction to dynamic meteorology, Elsevier Academic Press, Amsterdam, 5. ed. edn., 2013.

Holton, J. R., Haynes, P. H., McIntyre, M. E., Douglass, A. R., Rood, R. B., and Pfister, L.: Stratosphere-troposphere exchange, Reviews of geophysics, 33, 403–439, 1995.

Horita, J. and Wesolowski, D. J.: Liquid-vapor fractionation of oxygen and hydrogen isotopes of water from the freezing to the critical temperature, Geochimica et Cosmochimica Acta, 58, 3425 – 3437, https://doi.org/http://dx.doi.org/10.1016/0016-7037(94)90096-5, 1994.

IAEA/WMO: Global Network of Isotopes in Precipitation. The GNIP Database., http://www.iaea.org/water, 2017.

Jacob, D. J.: Introduction to atmospheric chemistry, Princeton Univ. Press, Princeton, NJ [u.a.], 1999.

Joussaume, S. and Jouzel, J.: Paleoclimatic tracers: An investigation using an atmospheric general circulation model under ice age conditions: 2. Water isotopes, Journal of Geophysical Research: Atmospheres, 98, 2807–2830, https://doi.org/10.1029/92JD01920, 1993.

Joussaume, S., Sadourny, R., and Jouzel, J.: A general circulation model of water isotope cycles in the atmosphere, Nature, 311, 24–29, 1984.

Jouzel, J. and Merlivat, L.: Deuterium and oxygen 18 in precipitation: Modeling of the isotopic effects during snow formation, Journal of Geophysical Research: Atmospheres, 89, 11 749–11 757, https://doi.org/10.1029/JD089iD07p11749, 1984.

Jouzel, J., Merlivat, L., and Roth, E.: Isotopic study of hail, Journal of Geophysical Research, 80, 5015–5030, https://doi.org/10.1029/JC080i036p05015, 1975.

Klocke, D., Brueck, M., Hohenegger, C., and Stevens, B.: Rediscovery of the doldrums in storm-resolving simulations over the tropical Atlantic, Nature Geoscience, 10, 891, 2017.

Kraus, H.: Die Atmosphäre der Erde : eine Einführung in die Meteorologie, Springer, Berlin, 3 edn., 2004.

Lauritzen, P. H., Ullrich, P. A., Jablonowski, C., Bosler, P. A., Calhoun, D., Conley, A. J., Enomoto, T., Dong, L., Dubey, S., Guba, O., Hansen, A. B., Kaas, E., Kent, J., Lamarque, J.-F., Prather, M. J., Reinert, D., Shashkin, V. V., Skamarock, W. C., Sørensen, B., Taylor, M. A., and Tolstykh, M. A.: A standard test case suite for two-dimensional linear transport on the sphere: results from a collection of state-of-the-art schemes, Geoscientific Model Development, 7, 105–145, https://doi.org/10.5194/gmd-7-105-2014, http://www.geosci-model-dev.net/7/105/2014/, 2014.

Lee, J.-E. and Fung, I.: "Amount effect" of water isotopes and quantitative analysis of post-condensation processes, Hydrological Processes: An International Journal, 22, 1–8, 2008.

Lee, X., Sargent, S., Smith, R., and Tanner, B.: In Situ Measurement of the Water Vapor 18O/16O Isotope Ratio for Atmospheric and Ecological Applications, Journal of Atmospheric and Oceanic Technology, 22, 555–565, https://doi.org/10.1175/JTECH1719.1, 2005.

LeGrande, A. N. and Schmidt, G. A.: Global gridded data set of the oxygen isotopic composition in seawater, Geophysical Research Letters, 33, https://doi.org/10.1029/2006GL026011, 2006.

Majoube, M.: Fractionnement en oxygén 18 et in deutérium entre l'eau et sa vapeur, Journal de Chimie Physique et de Physico-Chimie Biologique, 68, 1423, 1971.

Merlivat, L. and Jouzel, J.: Global climatic interpretation of the deuterium-oxygen 18 relationship for precipitation, Journal of Geophysical Research: Oceans, 84, 5029–5033, 1979.

Merlivat, L. and Nief, G.: Fractionnement isotopique lors des changements d'état solide-vapeur et liquide-vapeur de l'eau à des températures inférieures à 0 C, Tellus, 19, 122–127, 1967.

Mook, W. G.: Environmental isotopes in the hydrological cycle, Principles and Applications, vol. 2, International Atomic Energy Agency, UNESCO, Paris, 2001.

Morrison, H., Jensen, A. A., Harrington, J. Y., and Milbrandt, J. A.: Advection of Coupled Hydrometeor Quantities in Bulk Cloud Microphysics Schemes, Monthly Weather Review, 144, 2809–2829, https://doi.org/10.1175/MWR-D-15-0368.1, 2016.

Numaguti, A.: Origin and recycling processes of precipitating water over the Eurasian continent: Experiments using an atmospheric general circulation model, Journal of Geophysical Research: Atmospheres, 104, 1957–1972, 1999.

Pfahl, S. and Wernli, H.: Lagrangian simulations of stable isotopes in water vapor: An evaluation of nonequilibrium fractionation in the Craig-Gordon model, Journal of Geophysical Research: Atmospheres, 114, 2009.

Pfahl, S., Wernli, H., Yoshimura, K., and Dubey, M.: The isotopic composition of precipitation from a winter storm–a case study with the limited-area model COSMO iso, Atmospheric Chemistry & Physics, 12, 2012.

Pinet, P. R.: Oceanography : an introduction to the planet oceanus, West Publishing, St. Paul, 2. ed. edn., 1993.

Pollock, W., Heidt, L. E., Lueb, R., and Ehhalt, D. H.: Measurement of stratospheric water vapor by cryogenic collection, Journal of Geophysical Research: Oceans, 85, 5555–5568, https://doi.org/10.1029/JC085iC10p05555, 1980.

Pruppacher, H. R. and Klett, J. D.: Microphysics of Clouds and Precipitation: Reprinted 1980, Springer Science & Business Media, 2012.

Randel, W. J., Moyer, E., Park, M., Jensen, E., Bernath, P., Walker, K., and Boone, C.: Global variations of HDO and HDO/H2O ratios in the upper troposphere and lower stratosphere derived from ACE-FTS satellite measurements, Journal of Geophysical Research: Atmospheres, 117, https://doi.org/10.1029/2011JD016632, 2012.

Rieger, D., Bangert, M., Bischoff-Gauss, I., Förstner, J., Lundgren, K., Reinert, D., Schröter, J., Vogel, H., Zängl, G., Ruhnke, R., et al.: ICON–ART 1.0–a new online-coupled model system from the global to regional scale, Geoscientific Model Development, 8, 1659–1676, 2015.

Rieger, D., Steiner, A., Bachmann, V., Gasch, P., Förstner, J., Deetz, K., Vogel, B., and Vogel, H.: Impact of the 4 April 2014 Saharan dust outbreak on the photovoltaic power generation in Germany, Atmos. Chem. Phys. Discuss., 2017, 1–31, https://doi.org/10.5194/acp-2017-441, 2017.

Riese, M., Ploeger, F., Rap, A., Vogel, B., Konopka, P., Dameris, M., and Forster, P.: Impact of uncertainties in atmospheric mixing on simulated UTLS composition and related radiative effects, Journal of Geophysical Research: Atmospheres (1984–2012), 117, 2012.

Risi, C., Bony, S., and Vimeux, F.: Influence of convective processes on the isotopic composition (δ18O and δD) of precipitation and water vapor in the tropics: 2. Physical interpretation of the amount effect, Journal of Geophysical Research: Atmospheres, 113, 2008.

Risi, C., Bony, S., Vimeux, F., and Jouzel, J.: Water-stable isotopes in the LMDZ4 general circulation model: Model evaluation for present-day and past climates and applications to climatic interpretations of tropical isotopic records, Journal of Geophysical Research: Atmospheres, 115, https://doi.org/10.1029/2009JD013255, 2010.

Risi, C., Noone, D., Frankenberg, C., and Worden, J.: Role of continental recycling in intraseasonal variations of continental moisture as deduced from model simulations and water vapor isotopic measurements, Water Resources Research, 49, 4136–4156, 2013.

Schmidt, G. A., Ruedy, R. A., Miller, R. L., and Lacis, A. A.: Attribution of the present-day total greenhouse effect, Journal of Geophysical Research: Atmospheres, 115, https://doi.org/10.1029/2010JD014287, 2010.

Schneider, M. and Hase, F.: Optimal estimation of tropospheric H_2O and δD with IASI/METOP, Atmospheric Chemistry and Physics, 11, 11 207–11 220, https://doi.org/10.5194/acp-11-11207-2011, 2011.

Schneider, M., Wiegele, A., Barthlott, S., González, Y., Christner, E., Dyroff, C., García, O. E., Hase, F., Blumenstock, T., Sepúlveda, E., Mengistu Tsidu, G., Takele Kenea, S., Rodríguez, S., and Andrey, J.: Accomplishments of the MUSICA project to provide accurate, long-term, global and high-resolution observations of tropospheric H_2O,δD pairs – a review, Atmospheric Measurement Techniques, 9, 2845–2875, https://doi.org/10.5194/amt-9-2845-2016, 2016.

Schneider, M., Borger, C., Wiegele, A., Hase, F., García, O. E., Sepúlveda, E., and Werner, M.: MUSICA MetOp/IASI H_2O,δD pair retrieval simulations for validating tropospheric moisture pathways in atmospheric models, Atmospheric Measurement Techniques, 10, 507–525, https://doi.org/10.5194/amt-10-507-2017, 2017.

Schröter, J., Rieger, D., Stassen, C., Vogel, H., Weimer, M., Werchner, S., Förstner, J., Prill, F., Reinert, D., Zängl, G., Giorgetta, M., Ruhnke, R., Vogel, B., and Braesicke, P.: ICON-ART 2.1: a flexible tracer framework and its application for composition studies in numerical weather forecasting and climate simulations, Geoscientific Model Development, 11, 4043–4068, https://doi.org/10.5194/gmd-11-4043-2018, 2018.

Seemann, S. W., Borbas, E. E., Knuteson, R. O., Stephenson, G. R., and Huang, H.-L.: Development of a Global Infrared Land Surface Emissivity Database for Application to Clear Sky Sounding Retrievals from Multispectral Satellite Radiance Measurements, Journal of Applied Meteorology and Climatology, 47, 108–123, https://doi.org/10.1175/2007JAMC1590.1, 2008.

Seifert, A.: On the Parameterization of Evaporation of Raindrops as Simulated by a One-Dimensional Rainshaft Model, Journal of the Atmospheric Sciences, 65, 3608–3619, https://doi.org/10.1175/2008JAS2586.1, 2008.

Seifert, A. and Beheng, K.: A two-moment cloud microphysics parameterization for mixed-phase clouds. Part 1: Model description, Meteorology and atmospheric physics, 92, 45–66, 2006.

Sherwood, S. C., Bony, S., and Dufresne, J.-L.: Spread in model climate sensitivity traced to atmospheric convective mixing, Nature, 505, 37–42, 2014.

Shine, K. P. and Sinha, A.: Sensitivity of the Earth's climate to height-dependent changes in the water vapour mixing ratio, Nature, 354, 382–384, 1991.

Souchez, R. and Jouzel, J.: On the isotopic composition in δD and δ 18 O of water and ice during freezing, Journal of Glaciology, 30, 369–372, 1984.

Souchez, R., Jouzel, J., Lorrain, R., Sleewaegen, S., Stiévenard, M., and Verbeke, V.: A kinetic isotope effect during ice formation by water freezing, Geophysical Research Letters, 27, 1923–1926, 2000.

Steinwagner, J., Milz, M., Clarmann, T. v., Glatthor, N., Grabowski, U., Höpfner, M., Stiller, G., and Röckmann, T.: HDO measurements with MIPAS, Atmospheric chemistry and physics, 7, 2601–2615, 2007.

Stewart, M. K.: Stable isotope fractionation due to evaporation and isotopic exchange of falling waterdrops: Applications to atmospheric processes and evaporation of lakes, Journal of Geophysical Research, 80, 1133–1146, 1975.

Taylor, K. E., Williamson, D., and Zwiers, F.: The sea surface temperature and sea-ice concentration boundary conditions for AMIP II simulations, Program for Climate Model Diagnosis and Intercomparison, Lawrence Livermore National Laboratory, University of California, 2000.

Terzer, S., Wassenaar, L. I., Araguás-Araguás, L. J., and Aggarwal, P. K.: Global isoscapes for δ^{18}O and δ^{2}H in precipitation: improved prediction using regionalized climatic regression models, Hydrology and Earth System Sciences, 17, 4713–4728, https://doi.org/10.5194/hess-17-4713-2013, 2013.

Tiedtke, M.: A comprehensive mass flux scheme for cumulus parameterization in large-scale models, Monthly Weather Review, 117, 1779–1800, 1989.

Van der Ent, R. J., Savenije, H. H., Schaefli, B., and Steele-Dunne, S. C.: Origin and fate of atmospheric moisture over continents, Water Resources Research, 46, 2010.

Werner, M., Langebroek, P. M., Carlsen, T., Herold, M., and Lohmann, G.: Stable water isotopes in the ECHAM5 general circulation model: Toward high-resolution isotope modeling on a global scale, Journal of Geophysical Research: Atmospheres, 116, https://doi.org/10.1029/2011JD015681, 2011.

Wiegele, A., Schneider, M., Hase, F., Barthlott, S., García, O. E., Sepúlveda, E., González, Y., Blumenstock, T., Raffalski, U., Gisi, M., and Kohlhepp, R.: The MUSICA MetOp/IASI H_2O and δD products: characterisation and long-term comparison to NDACC/FTIR data, Atmospheric Measurement Techniques, 7, 2719–2732, https://doi.org/10.5194/amt-7-2719-2014, 2014.

Worden, J., Bowman, K., Noone, D., Beer, R., Clough, S., Eldering, A., Fisher, B., Goldman, A., Gunson, M., Herman, R., Kulawik, S. S., Lampel, M., Luo, M., Osterman, G., Rinsland, C., Rodgers, C., Sander, S., Shephard, M., and Worden, H.: Tropospheric Emission Spectrometer observations of the tropospheric HDO/H2O ratio: Estimation approach and characterization, Journal of Geophysical Research: Atmospheres, 111, https://doi.org/10.1029/2005JD006606, 2006.

Worden, J., Noone, D., Bowman, K., Beer, R., Eldering, A., Fisher, B., Gunson, M., Goldman, A., Herman, R., Kulawik, S. S., et al.: Importance of rain evaporation and continental convection in the tropical water cycle, Nature, 445, 528–533, 2007.

Zängl, G., Reinert, D., Rípodas, P., and Baldauf, M.: The ICON (ICOsahedral Non-hydrostatic) modelling framework of DWD and MPI-M: Description of the non-hydrostatic dynamical core, Quarterly Journal of the Royal Meteorological Society, 141, 563–579, 2015.